JGR Atmospheres

RESEARCH ARTICLE
10.1029/2022JD037758

Fire Influence on Regional to Global Environments and Air Quality (FIREX-AQ)

Carsten Warneke[1], Joshua P. Schwarz[1], Jack Dibb[2], Olga Kalashnikova[3], Gregory Frost[1], Jassim Al-Saad[4], Steven S. Brown[1], Wm. Alan Brewer[1], Amber Soja[4,5], Felix C. Seidel[3,6], Rebecca A. Washenfelder[1], Elizabeth B. Wiggins[4], Richard H. Moore[4], Bruce E. Anderson[4], Carolyn Jordan[4,5], Tara I. Yacovitch[7], Scott C. Herndon[7], Shang Liu[8], Toshihiro Kuwayama[8], Daniel Jaffe[9], Nancy Johnston[10], Vanessa Selimovic[11], Robert Yokelson[11], David M. Giles[12,13], Brent N. Holben[12], Philippe Goloub[14], Ioana Popovici[14,15], Michael Trainer[1,16], Aditya Kumar[17], R. Bradley Pierce[17], David Fahey[1], James Roberts[1], Emily M. Gargulinski[5], David A. Peterson[18], Xinxin Ye[19], Laura H. Thapa[19], Pablo E. Saide[19,20], Charles H. Fite[21], Christopher D. Holmes[21], Siyuan Wang[1,16], Matthew M. Coggon[1,16], Zachary C. J. Decker[1,16,22,23], Chelsea E. Stockwell[1,16], Lu Xu[1,16], Georgios Gkatzelis[1,16,24], Kenneth Aikin[1,16], Barry Lefer[6], Jackson Kaspari[25], Debora Griffin[26], Linghan Zeng[27], Rodney Weber[27], Meredith Hastings[28], Jiajue Chai[28], Glenn M. Wolfe[12], Thomas F. Hanisco[12], Jin Liao[12,29], Pedro Campuzano Jost[16], Hongyu Guo[16], Jose L. Jimenez[16], James Crawford[4], and The FIREX-AQ Science Team[30]

[1]Chemical Sciences Laboratory, National Oceanic and Atmospheric Administration NOAA, Boulder, CO, USA, [2]Earth Systems Research Center, University of New Hampshire, Durham, NH, USA, [3]NASA, Jet Propulsion Laboratory, California Institute of Technology, Pasadena, CA, USA, [4]NASA Langley Research Center, Hampton, VA, USA, [5]National Institute of Aerospace, Hampton, VA, USA, [6]Earth Sciences Division, NASA Headquarters, Washington, DC, USA, [7]Aerodyne Research Inc., Billerica, MA, USA, [8]Research Division, California Air Resource Board, Sacramento, CA, USA, [9]Physical Sciences Division, University of Washington, Seattle, WA, USA, [10]Lewis-Clark State College, Lewiston, ID, USA, [11]Department of Chemistry and Biochemistry, University of Montana, Missoula, MT, USA, [12]NASA Goddard Space Flight Center, Greenbelt, MD, USA, [13]Science Systems and Applications, Inc. (SSAI), Lanham, MD, USA, [14]Laboratoire d'Optique Atmosphérique, Lille University, Villeneuve d'Ascq Cedex, France, [15]Research & Development Department, Cimel Electronique, Paris, France, [16]Cooperative Institute for Research in Environmental Sciences, University of Colorado Boulder, Boulder, CO, USA, [17]Space Science and Engineering Center, Madison, WI, USA, [18]Naval Research Laboratory, Monterey, CA, USA, [19]Department of Atmospheric and Oceanic Sciences, University of California Los Angeles, Los Angeles, CA, USA, [20]Institute of the Environment and Sustainability, University of California Los Angeles, Los Angeles, CA, USA, [21]Earth, Ocean, and Atmospheric Science, Florida State University, Tallahassee, FL, USA, [22]Now at Paul Scherrer Institute (PSI), Villigen, Switzerland, [23]Department of Chemistry, University of Colorado Boulder, Boulder, CO, USA, [24]Now at: Forschungszentrum Jülich, IEK 8: Troposphäre, Jülich, Germany, [25]Department of Chemistry, University of New Hampshire, Durham, NH, USA, [26]Air Quality Research Division, Environment and Climate Change Canada, Toronto, ON, Canada, [27]School of Earth and Atmospheric Sciences, Georgia Institute of Technology, Atlanta, GA, USA, [28]Department of Earth, Environment and Planetary Science, Brown University, Providence, RI, USA, [29]Goddard Earth Sciences Technology and Research (GESTAR) II, University of Maryland, College Park, MD, USA, [30]See Appendix A

Abstract The NOAA/NASA Fire Influence on Regional to Global Environments and Air Quality (FIREX-AQ) experiment was a multi-agency, inter-disciplinary research effort to: (a) obtain detailed measurements of trace gas and aerosol emissions from wildfires and prescribed fires using aircraft, satellites and ground-based instruments, (b) make extensive suborbital remote sensing measurements of fire dynamics, (c) assess local, regional, and global modeling of fires, and (d) strengthen connections to observables on the ground such as fuels and fuel consumption and satellite products such as burned area and fire radiative power. From Boise, ID western wildfires were studied with the NASA DC-8 and two NOAA Twin Otter aircraft. The high-altitude NASA ER-2 was deployed from Palmdale, CA to observe some of these fires in conjunction with satellite overpasses and the other aircraft. Further research was conducted on three mobile laboratories and ground sites, and 17 different modeling forecast and analyses products for fire, fuels and air quality and climate implications. From Salina, KS the DC-8 investigated 87 smaller fires in the Southeast with remote and in-situ data collection. Sampling by all platforms was designed to measure emissions of trace gases and aerosols with multiple transects to capture the chemical transformation of these emissions and perform remote sensing observations of fire and smoke plumes under day and night conditions. The emissions were linked to fuels

Key Points:

- This work is an overview of the NOAA/NASA Fire Influence on Regional to Global Environments and Air Quality (FIREX-AQ) field experiment
- FIREX-AQ investigated biomass burning emissions and chemistry and smoke transport
- FIREX-AQ was a multi-platform mission that also utilized fire modeling and satellite detections and validation

Supporting Information:

Supporting Information may be found in the online version of this article.

Correspondence to:

C. Warneke,
carsten.warneke@noaa.gov

Citation:

Warneke, C., Schwarz, J. P., Dibb, J., Kalashnikova, O., Frost, G., Al-Saad, J., et al. (2023). Fire influence on regional to global environments and air quality (FIREX-AQ). *Journal of Geophysical Research: Atmospheres*, *128*, e2022JD037758. https://doi.org/10.1029/2022JD037758

Received 29 AUG 2022
Accepted 2 DEC 2022

consumed and fire radiative power using orbital and suborbital remote sensing observations collected during overflights of the fires and smoke plumes and ground sampling of fuels.

Plain Language Summary The NOAA/NASA Fire Influence on Regional to Global Environments and Air Quality (FIREX-AQ) experiment was aimed at understanding how fuel and fire conditions at the point of emission influence the chemistry of smoke, what conditions and processes control the rise of smoke plumes, what happens to smoke as it is distributed in the atmosphere, and how chemical transformation of smoke impacts air quality, weather, and climate downwind. Lessons learned from FIREX-AQ will also be used to assess and improve the effectiveness of satellites for estimating the emissions from wildfires and prescribed burns and to reduce uncertainties associated with modeling and forecasting of smoke. Here we present an overview of the FIREX-AQ effort, its motivation and design, with detailed descriptions of the measurements and analyses carried out, their connections to FIREX-AQ science goals, and the early findings of this exceptionally broad effort to understand fire and its many impacts on the atmosphere.

1. Rationale and Motivation

The combination of a warmer, drier climate with fire-control practices applied over the last century has led to more intense fires, larger burned areas, and longer fire seasons in the U.S., Canada, and around the world. The 20th century saw fire suppression become the standard response to wildfires, especially in the western U.S. and southwest Canada; this has led to a buildup of fuels in forested areas, a breakdown in the natural ecology of forests. In addition, risks to life and property associated with the expansion of the Wildland Urban Interface (WUI) have increased (Radeloff et al., 2018). Climate change causes increased temperatures, drought, higher fuel aridity and tree death further increasing the fire intensity (Abatzoglou, Battisti, et al., 2021; Kitzberger et al., 2007; Westerling, 2016). Prescribed fires and allowing some naturally occurring fires to burn are some of the management practices that address the above problem (Mutch, 1994; Schoennagel et al., 2017).

Fire is important for many ecosystems (Mutch, 1994), but it also poses costly risks to human health and property. These risks have increased in recent decades due in part to population growth in the WUI (Westerling et al., 2006). Extreme fire seasons attract mounting attention due to the increasing number of costly extreme wildfires that include: the 2018 Camp Fire, which was the deadliest and most destructive wildfire in California's history and burned 62,053 ha and cost 16.65 billion dollars. The 2016 fires that burned across eight states in the southeast (48,158 ha); the 2016 Anderson Creek prairie fire that was the largest in Kansas history (161,874 ha); the 2016 Fort McMurray fire, which is the costliest fire in Canadian history ($2.7 B, 589,552 ha, 2400 structures destroyed); the 2004 Alaskan fire season (2.74 M ha), the largest in almost 80 years of Alaskan fire history and the extreme 2015 unusually-early-season Alaskan fires (2.07 M ha) (Abatzoglou, Rupp, et al., 2021; Wentworth et al., 2018) and the extreme fires in North America in 2020 and 2021 (https://www.nifc.gov/fire-information/statistics). Coupled with the direct threats to life and property, wildland fires have demonstrable detrimental air quality related health impacts including aggravated asthma, chronic bronchitis, decreased lung function, congestive heart failure, and premature death (Adetona et al., 2016; Doubleday et al., 2020; Rappold et al., 2011; Reid et al., 2016; Thelen et al., 2013).

Prescribed fires in the United States have ranged from 3.3 to 4.8 million ha (M ha) annually over the last decade, well above the typical wildfire area (Melvin, 2020). The majority of this area (80%) is in forests and rangeland (wildland) and agricultural use makes up about 20% of prescribed fire area (Melvin, 2018). Prescribed fires can reduce the risk of dangerous wildfires and usually have low direct risk to people and property, but they still generate smoke and air quality impacts (Addington et al., 2015; Fernandes & Botelho, 2003; Nowell et al., 2018; Stephens et al., 2012).

Fire impacts occur over wide time and distance scales, from local to global (Ansmann et al., 2018; Schill et al., 2020), via complex, interdependent, and poorly understood processes. For example, primary fire emissions are affected by a wide variety of factors including fuel conditions (type, structure, quantity, and moisture content), fire intensity, and fire weather (cumulative temperature, relative humidity (RH), wind speed, and precipitation), which in turn can be rapidly and heterogeneously modified by fires as they burn. Wildfire initiation can be natural (by lightning) or human caused, and prescribed fires are a frequent tool for land management (e.g., reducing fuels, land clearing and agriculture). Human ignition is currently the dominant ignition source in the United States (Balch et al., 2017). Over the life cycle of a fire, combinations of flaming and smoldering combustion

lead to different emissions at different times and at different locations within a fire (Bertschi et al., 2003; Saide et al., 2015; Yates et al., 2016). These variables also influence plume rise and the subsequent transport and chemical evolution of fire emissions (Herron-Thorpe et al., 2014), which determines secondary products (e.g., evolved gases and aerosol species) (Akagi et al., 2012). Fire growth is driven by weather conditions, and forecasts are subject to the limitations of weather-based prediction (Potter, 2020). Fire activity varies on a broad seasonal scale, but climatology is inadequate to provide the detailed information needed to understand and predict fire impacts. This is especially true for impacts related to air quality, which depend on the intersection of fire emissions with populations and are sensitive to chemical transformations that can result when emissions from fires and anthropogenic sources combine (Selimovic et al., 2020).

The importance of biomass burning (BB) on a global scale is well-known (Akagi et al., 2011; Bond et al., 2004, 2013; Crutzen & Andreae, 1990; Crutzen et al., 1979; Schill et al., 2020). Previous BB studies have focused on: the tropics, documenting both the near field environment (Andreae et al., 1994; Kaufman et al., 1998; Swap et al., 2002; Ward et al., 1992; Yokelson et al., 2011) and the widespread impacts across remote oceanic regions (Fishman et al., 1996; Hoell et al., 1999), boreal/Arctic regions (Goode et al., 2000; Jacob et al., 2010; Lefer et al., 1994; Nance et al., 1993; Palmer et al., 2013; Soja et al., 2004) where the relative importance of BB to fossil fuel and other air pollution sources is great, and temperate BB field measurements, which can also target prescribed fires (Akagi et al., 2013; Baker et al., 2018; Burling et al., 2011; May et al., 2014; Yokelson et al., 1999, 2013).

The ubiquity of fire emissions is also evident from previous airborne field studies in North America that were not focused solely on BB but sampled smoke frequently. Following are examples from some of the more recent missions that observed BB atmospheric impacts. The international ICARTT study 2004 (International Consortium for Atmospheric Research on Transport and Transformation) found a strong BB influence from Canadian and Alaskan fires in the northeast U.S. (Clarke et al., 2007; Warneke et al., 2006), and NOAA's TEXAQS 2006 (Texas Air Quality Study) identified systematic differences in particle morphology between urban and BB sources (Schwarz et al., 2008). The international POLARCAT study 2008 (Polar Study using Aircraft, Remote Sensing, Surface Measurements and Models, of Climate, Chemistry, Aerosols, and Transport) focused on Arctic measurements, where arctic haze over Alaska was attributed to spring fires burning in Asia (Warneke et al., 2009, 2010). While sampling local Canadian fire emissions during the summer was intentional, sampling fires in California in the spring during ARCTAS-CARB 2008 (Arctic Research of the Composition of the Troposphere from Aircraft and Satellites) was unexpected (Sahu et al., 2012), but these campaigns provided a broad cross section of fire emissions and impacts (Hecobian et al., 2011; Singh et al., 2012). Canadian fire emissions and their downwind impacts were the focus of the BORTAS (quantifying the impact of BOReal forest fires on Tropospheric oxidants over the Atlantic using Aircraft and Satellites) (Palmer et al., 2013) campaigns in 2011. NOAA's SENEX 2013 (Southeast Nexus) acquired data on the relative contribution of BB to organic aerosols and gases in the southeast U.S. in summertime and provided the first airborne measurements of nighttime smoke (Zarzana et al., 2017), while the NASA/NSF DC3 (2012) campaign fortuitously encountered a smoke plume interacting with a deep convective cloud (Apel et al., 2015) and evidence for the broad influence of convection on the ventilation of fire emissions (Huntrieser et al., 2016). Most recently, the NASA Atmospheric Tomography (ATom) project revisited the widespread BB products that are transported across the remote ocean atmosphere (Bourgeois et al., 2021; Schill et al., 2020).

Large scale atmospheric campaigns in temperate regions began specifying wildfires as targets during NASA's ARCTAS 2008 and SEAC^{4}RS 2013 (Studies of Emissions and Atmospheric Composition, Clouds, and Climate Coupling by Regional Surveys) (Toon et al., 2016). The latter included detailed evaluation of the plume from the Rim Fire, which was one of the largest known wildfires in California at the time (Forrister et al., 2015; Peterson et al., 2015; Saide et al., 2015; Yates et al., 2016; Yu et al., 2016). SEAC^{4}RS also measured emissions and smoke evolution from 15 small agricultural fires in the Mississippi River Valley (MRV) (Liu et al., 2016).

The DOE BBOP 2013 (Department of Energy BB Observation Project) mission was the first airborne campaign to focus primarily on western US wildfires and detailed smoke optical properties. BBOP identified evidence for evolving brown carbon (BrC) materials in fire plumes (Kleinman et al., 2020; Sedlacek et al., 2018; Zhou et al., 2017). By combining all the wildfire data from BBOP and SEAC^{4}RS, Liu et al. (2017) calculated wildfire emission factors (EFs) for about 80 species based on three fires. Parallel to the above field measurements, the University of Montana and others led laboratory studies including FLAME-3 and 4 that produced numerous

fuel-specific EFs and smoke aging simulations for laboratory fires (Ahern et al., 2019; Hatch et al., 2015, 2017; May et al., 2013; McMeeking et al., 2009; Stockwell et al., 2014, 2015).

The Western wildfire Experiment for Cloud chemistry, Aerosol absorption and Nitrogen 2018 (WE-CAN 2018) (https://www.eol.ucar.edu/field_projects/we-can) was originally planned to coincide with the NASA/NOAA 2019 field campaign as a complement to FIREX-AQ, but aircraft schedules could not be aligned. WE-CAN systematically characterized the emissions and early evolution of western U.S. wildfire plumes and focused on three sets of scientific questions related to fixed nitrogen, absorbing aerosols, cloud activation, and chemistry in wildfire plumes (Lindaas et al., 2021; Palm et al., 2020; Permar et al., 2021). The data were collected from the NCAR/NSF C-130 research aircraft stationed in Boise, ID in the summer of 2018. The main focus was on the first day of processing, which is a major driver of the eventual air quality and climate significance of wildfire smoke, because the chemistry and micro-physics occurring during this time determine the partitioning of reactive nitrogen, alters cloud chemistry and nucleation, and determines aerosol scattering and absorption (Hodshire et al., 2019). Several WE-CAN results have been published (https://www.eol.ucar.edu/node/12743/publications).

Due in large part to the variability and complexity of wildfires and agricultural burning, and due to their evolving emission trends, there remains a need to enhance the understanding of emissions, smoke evolution, and AQ impacts across a greater range of conditions, while taking advantage of the most recent advances in atmospheric chemistry instrumentation. FIREX-AQ was planned to advance these critical research needs to better characterize BB impacts on air quality and climate impacts.

1.1. FIREX-AQ Science Objectives

The overarching objective of FIREX-AQ was to provide an unprecedented combination of fire science covering: (a) measurements of trace gas and aerosol emissions for not only wildfires but also prescribed fires in great detail, (b) relate them to fuel and fire conditions at the point of emission, (c) characterize the conditions relating to plume rise, (d) follow plumes downwind to understand chemical transformation and air quality impacts, (e) assess the efficacy of satellite detections for estimating the emissions from sampled fires, (f) connecting remote sensing and in-situ with satellite data, and (g) improve air quality and climate models.

The NOAA FIREX research effort was designed as a five-year research project and later merged into the comprehensive NOAA/NASA FIREX-AQ research effort to target critical unknowns about BB with state-of-the-art technologies and collaborative laboratory and field studies, culminating in the 2019 field campaign that deployed multiple aircraft, mobile laboratories and fixed ground sites coupled with satellite measurements and intensive modeling studies. The diverse activities included in FIREX-AQ 2019 range from scientists collecting fuels on the ground to multiple aircraft measurements of smoke plumes from wildfires and prescribed burning to global 3D fire and health impacts modeling.

Wildfires tend to be seasonal and generally result in large pollution concentrations over wide areas and can cause both local and regional air quality impacts. Their emissions are often transported thousands of kilometers and can impact large regions of the U.S. at a time (Park et al., 2007; Rogers et al., 2020; Selimovic et al., 2019; Warneke et al., 2006). Prescribed fires are usually smaller and less intense than wildfires but are much greater in number and occur throughout the whole year. They may be ignited during periods that minimize population exposure and air quality impacts, but can cause regional backgrounds to increase, are generally in closer proximity to populations, and are responsible for a large fraction of the U.S. $PM_{2.5}$ emissions (Washenfelder et al., 2015). Prescribed burning associated with agricultural fire outputs is still poorly represented in emission inventories (McCarty et al., 2009; Nowell et al., 2018; Pouliot et al., 2017; Ramo et al., 2021). The field experiments in FIREX-AQ investigated both wild and prescribed fires, but did not include residential or trash burning. Subsequent sections discuss the coordination of prescribed and wildfire sampling, including the resulting benefits to stakeholders.

1.2. FIREX-AQ Science Questions

A summary of the FIREX-AQ science questions is provided here and the topics include questions about emissions, chemical transformations, local air quality effects, regional and long-term impacts, climate relevant properties, and satellite measurements of wildfires and prescribed fires in North America.

1. What are the emissions of gases and aerosols from North American fires?
2. What chemical transformations affect those emissions?
3. What are the local air quality impacts of North American fires?
4. What are the regional and long-term impacts of North American fires?
5. What are the climate-relevant properties of BB aerosols?
6. How can satellite measurements help with #1–5?

1.3. FIREX FireLab 2016 Campaign

The NOAA FIREX FireLab Experiment was conducted at the USDA Fire Sciences Laboratory in Missoula, Montana in 2016, in preparation for FIREX-AQ. The goal of these experiments was to apply the most technically up-to-date methods to measure emissions, optical properties, and aging of smoke from laboratory fires. The focus was to burn fuels under combustion conditions that are characteristic of the western U.S. and other fuels that are under-sampled by the fire research community. Three main areas of research were conducted: quantifying the emissions of gases and particles, understanding chemical and physical processing of smoke emissions, and measuring optical properties of smoke. A very comprehensive set of EFs for various fire conditions was measured and is available for trace gases and aerosol from fuels typical in the Western and some limited fuels from the Southeastern U.S. The Fire Lab Experiment also provided a better understanding of the mechanisms of trace gas emissions for different fire conditions, such as high and low temperature combustion (Sekimoto et al., 2018). In addition, a large number of photochemical products of smoke aging were determined and used to update chemical mechanisms in various models (Coggon et al., 2019). Several new methods were applied to the measurement of optical properties of smoke particles, and new results were obtained on the relationships between particle chemistry and optical properties. There have been a substantial number of publications from the 2016 FireLab study that describe a variety of research products (Table S1 in Supporting Information S1).

The Missoula FireLab facility has been featured in a number of previous publications (Burling et al., 2010; Christian et al., 2003) so is not described here. A website with substantial detail can be found here (https://csl.noaa.gov/projects/firex/firelab/). The details of the fuels burned, quantities, and elemental compositions can be found in Selimovic et al. (2018). For the most part, the fuels burned during the study were characteristic of western North America, since one main goal of FIREX-AQ was a better understanding of how wildfires impact air quality in this region. The fuels were often burned as realistic mixtures of canopy, litter, and duff material from a particular species, for example, Engelmann Spruce, and some fires were conducted with only one of those classes of materials, for example, duff (the partially decayed material right above the soil surface). It should be recognized that there are limitations inherent in the simulation of fires in the laboratory: fuel moisture is often lower than in the natural setting: the soil boundary and its associated moisture and heat capacity is absent. Nevertheless, laboratory studies have provided essential information with which to begin analyzing and interpreting measurements of actual wildfires.

Considerable progress was made during the FireLab experiment on understanding emissions from North American fuels. This has resulted in more detailed ways to categorize volatile organic compounds (VOC), reactive N, and POC (particulate organic carbon) emissions according to fire regime (Koss et al., 2018; Roberts et al., 2020). In addition, the application of new analytical techniques has led to refinements in the identification of VOC species responsible for oxidant and SOA (secondary organic aerosol) formation, and the absorption properties of primary and secondary organic aerosol particles (BrC). The FireLab study also provided an opportunity to compare multiple measurement methods for gas phase species, and for black carbon (BC) particles in particular. Many of these features of primary wildfire emissions are being examined and refined using the results of the FIREX-AQ measurements.

A number of experiments at the FireLab involved capturing the emissions from the Stack Burns and subjecting them to short-term (hours to a few days) simulated atmospheric processing, either under photochemical (e.g., OH reaction) or nighttime (e.g., NO_3 and O_3 reaction) conditions. These efforts yielded valuable information of which compounds were important in oxidant, SOA, and BrC formation, and what product species could be expected from these processes. Several experiments also encompassed liquid and particle condensed phase photochemical processing to examine the potential of that chemistry to produce and destroy BrC chromophores (Adler et al., 2019; Fleming et al., 2020).

Table 1
List of the Platforms and Their Location and Timing During FIREX-AQ

Platform/Site	Location	Deployment date	Number of flights/drives
Aircraft			
NASA DC-8	Boise, ID	24 July–16 August 2019	13
	Salina, KS	19 August–03 September 2019	7
NOAA Chem Twin Otter	Boise, ID	03 August–05 September 2019	33
	Cedar City, UT		6
NOAA Met Twin Otter	Boise, ID	21 July–13 August 2019	23
NASA ER-2	Palmdale, CA	01–21 August 2019	12
Mobile Laboratories			
AML	McCall, ID	05–30 August 2019	12
MACH-2	McCall, ID	21 July–27 August 2019	8
	Boise, ID		
CARB	CA	15–30 August, 1–4 November 2019	4
DRAGON-Mobile 1 and 2	McCall, ID	29 July–28 August 2019	11
	Boise, ID		
	Missoula, MT		
Ground sites			
DRAGON	Multiple sites	23 July–3 September 2019	
McCall, ID	44.871 N, 116.115 W	25–30 June 2019	
Missoula, MT	46.86 N, 113.985 W	2017–2021	
Lewiston, ID	46.413 N, 117.027 W	18 June–08 September 2019	
Boise, ID	43.60 N, 116.351 W	25 June–10 September 2019	
Mt. Bachelor, WA	43.979 N, 121.687 W	05 August–15 September 2019	

The final goal of the FireLab experiment can be broadly categorized as the application of new and improved analytical methods to measure the optical properties of smoke. Much of this work was performed during the Room Burns, as many of these methods needed a consistent smoke source that lasted for a sufficient time (10 min to over an hour). The instrumentation used in this work measured both the light scattering and absorption properties of smoke, as well as BC and BrC properties. Several of the optical experiments have direct application to refining the detection and characterization of smoke plumes by satellites (Manfred et al., 2018).

2. Assets Deployed During FIREX-AQ 2019

2.1. Platform Summary

The FIREX-AQ campaign was a large-scale coordinated effort in summer 2019. The deployment dates and locations of the various platforms for FIREX-AQ science are listed in Table 1, a schematic of the deployed platforms is shown in Figure 1, and each platform is then discussed in detail. The FIREX-AQ field campaign was conducted in two phases, focusing first on western wildfires and then targeting smaller fires in the south east. All of the platforms and the forecasting team described below deployed to the western region in late July 2019. Boise, ID was the main operations base. When the DC-8 relocated to Salina, KS on 19 August to conduct the small fire sampling, several of the other platforms and ground sites continued to sample smoke from western wildfires until early September. The forecasting team moved to Salina with the DC-8 but continued to provide daily briefings for the team members that remained in the west.

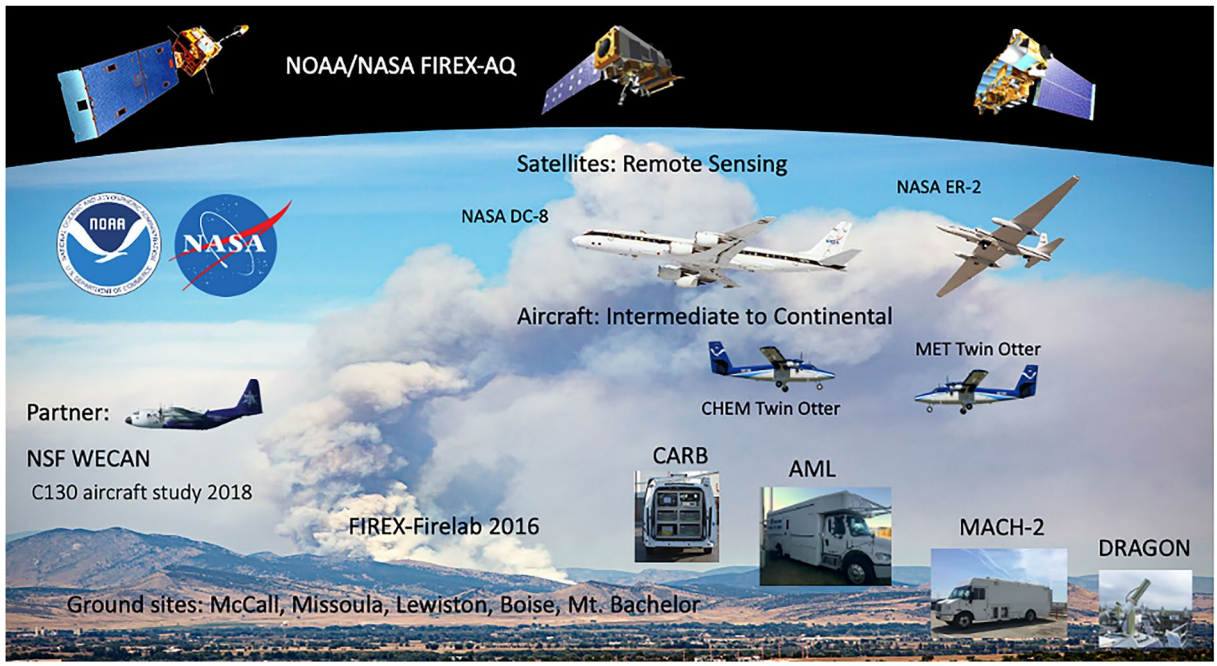

Figure 1. The platforms used for the coordinated sampling of the western wildfires during FIREX-AQ.

2.2. Fires Investigated

All the western wildfires that were investigated during the FIREX-AQ campaign are listed in Table 2 and locations are shown in Figure 2. Table 2 also includes information of the platforms and dates that each fire was sampled and total burned area and fuels burned.

2.3. Aircraft Platforms

2.3.1. NASA DC-8

The NASA DC-8 instrument payload for FIREX-AQ 2019 is described in Table 3 and was designed to provide the most detailed characterization of fire plumes from any aircraft platform to date. The DC-8 had a very complete package of gas- and aerosol-phase measurements as well as extensive remote sensing capabilities. Several of the in-situ measurements had a time resolution of up to 10 Hz, which was essential when sampling small fires with plume penetrations shorter than 5 s (Liu et al., 2016). The value of sampling with a sub-second time resolution has been demonstrated by Müller et al. (2016). The NASA DC-8 flights are shown in Figure 3 and the intercepted fires are included in Table 2. The specific flight tracks of the NASA DC-8 for the western wildfires are shown in Figure S1 in Supporting Information S1 color coded with CO.

2.3.2. NOAA Chem Twin Otter

The NOAA Chem Twin Otter completed 39 science flights during 3 August 2019–5 September 2019 and sampled 10 regional wildfires near Boise, ID and Cedar City, UT. The payload weight limited the aircraft to flight durations of 2.5–3.0 hr. The aircraft typically completed two or three individual flights per day, for a total daily flight time of 5–9 hr. The NOAA Chem Twin Otter was stationed in Boise, ID and Cedar City, UT, but regularly refueled at small regional airports to access fires throughout Idaho, Oregon, Montana, Nevada, and Utah. The flight duration allowed the NOAA Chem Twin Otter to follow wildfire plumes approximately 200 km downwind, corresponding to plume ages near 10 hr.

The NOAA Chem Twin Otter payload during FIREX-AQ 2019 was selected for detailed measurements of emissions, BrC evolution, and fast chemistry during both day and night. The payload is listed in Table 4. The NOAA Chem Twin Otter flights are shown in Figure 2 and the 10 intercepted fires are included in Table 2. The specific

Journal of Geophysical Research: Atmospheres

10.1029/2022JD037758

Table 2
List of Western US Fires Investigated During FIREX-AQ

Fire name	State	Ignition lat	Ignition lon	Date	DC-8	Chem-otter	ER-2	Met-otter	LARGE	DRAGON	AML	MMP	Final burned area (acres)	Fuels (FCCS 2014) 30 m
204 Cow	OR	44.29	−118.46	8/23/19						X			9,602	Douglas-fir-Pacific ponderosa pine/oceanspray forest
				8/24/19		X				X				
				8/25/19		X				X	X			
				8/26/19					X	X	X			
				8/27/19		X			X	X				
				8/28/19		X				X				
				9/3/19		X								
				9/4/19		X								
Barren Hills	ID	46.24	−114.98	7/29/19				X					1,306	Grand fir-Douglas fir forest
				7/30/19				X						
				8/1/19				X						
Beeskove	MT	46.96	−113.87	7/30/19				X					430	Douglas-fir-Pacific ponderosa pine/oceanspray forest
Black Diamond	MT	46.95	−112.43	8/2/19					X				31	Subalpine fir-lodgepole pine-whitebark pine-Engelmann spruce forest
Boulin	AZ	35.39	−112.01	8/15/19			X						4,095	Ponderosa pine-two-needle pinyon-Utah juniper forest
Canyon 66	OR	44.42	−120.39	9/4/19		X							4,451	Douglas-fir-Pacific ponderosa pine/oceanspray forest
Castle	AZ	36.53	−112.23	8/12/19	X								19,378	Ponderosa pine-two-needle pinyon-Utah juniper forest
				8/13/19	X									
				8/15/19			X							
				8/16/19			X							
				8/20/19		X	X				X			
				8/21/19		X	X				X			
				8/22/19					X		X			
				8/23/19					X					
CCC Fire	ID	47.57	−116.32	8/8/19						X			450	Douglas-fir-Pacific ponderosa pine/oceanspray forest
Crab	ID	46.5	−114.57	7/29/19				X					214	Subalpine fir-lodgepole pine-whitebark pine-Engelmann spruce forest
				7/30/19				X						
Dixon	CA	38.57	−119.74	8/2/19			X						9	Red fir forest
Goose	NV	41.87	−114.2	8/5/19		X		X					6,857	Sagebrush shrubland - post prescribed burn

Journal of Geophysical Research: Atmospheres

10.1029/2022JD037758

Table 2
Continued

Fire name	State	Ignition lat	Ignition lon	Date	DC-8	Chem-otter	ER-2	Met-otter	LARGE	DRAGON	AML	MMP	Final burned area (acres)	Fuels (FCCS 2014) 30 m
Granite Gulch	OR	45.18	−117.43	8/7/19				X					5,559	Whitebark pine/subalpine fir forest and Douglas-fir-Pacific ponderosa pine/oceanspray forest
				8/9/19		X								
				8/16/19		X								
				8/17/19		X								
				8/20/19						X				
				8/21/19						X				
HK163	OR	45.05	−119.46	8/9/19		X		X					2,666	Douglas-fir-Pacific ponderosa pine/oceanspray forest and Ponderosa pine savanna
Horsefly	MT	46.96	−112.44	8/6/19	X								1,352	Subalpine fir-lodgepole pine-whitebark pine-Engelmann spruce forest
Ikes	AZ	36.35	−112.29	8/16/19			X						16,424	Ponderosa pine-two-needle pinyon-Utah juniper forest
				8/20/19			X				X			
				8/21/19			X				X			
				8/22/19							X			
Left Hand Fire	WA	46.93	−120.99	7/30/19	X								3,463	Grand fir-Douglas-fir forest and ponderosa pine/oceanspray forest
Lick Creek	ID	47.16	−115.91	8/2/19	X								178	Grand fir-Douglas-fir forest
Little Bear	UT	37.59	−112.32	8/20/19		X	X		X				2,651	White fir-gamble oak forest and Ponderosa pine savanna
	UT			8/21/19		X	X		X					
Lizzy	ID	44.26	−115.17	8/3/19				X					13	Pasture/Barren
Mica Creek	ID	47.23	−116.17	8/2/19	X								40	Grand fir-Douglas-fir forest
Milepost 97	OR	42.91	−123.27	7/27/19				X					13,097	Douglas-fir-madrone-tanoak forest
Mill	CA	36.01	−121.47	8/2/19			X						322	Scrub oak chaparral shrubland and California black oak woodland

Journal of Geophysical Research: Atmospheres

10.1029/2022JD037758

Table 2
Continued

Fire name	State	Ignition lat	Ignition lon	Date	DC-8	Chem-otter	ER-2	Met-otter	LARGE	DRAGON	AML	MMP	Final burned area (acres)	Fuels (FCCS 2014) 30 m
Nethker	ID	45.25	−115.93	8/9/19		X		X	X		X		2,369	Douglas-fir-Pacific ponderosa pine/oceanspray forest and Subalpine fir-lodgepole pine-whitebark pine-Engelmann spruce forest
				8/10/19				X	X	X				
				8/11/19				X	X	X				
				8/12/19					X	X				
				8/13/19						X				
				8/14/19					X	X				
				8/15/19					X	X				
				8/16/19					X	X				
				8/17/19						X				
				8/19/19						X				
				8/22/19						X				
				8/23/19						X				
				8/24/19						X				
				8/28/19							X			
Nevada Mountain	MT	46.83	−112.57	8/1/19				X					57	Douglas-fir-Pacific ponderosa pine/oceanspray forest
				8/2/19				X						
North Hills	MT	46.75	−111.96	7/29/19	X								5,009	Idaho fescue-bluebunch wheatgrass grassland, Ponderosa pine savanna, and Douglas-fir-Pacific ponderosa pine/oceanspray forest
Pipeline	WA	46.83	−120.52	7/25/19						X			6,516	Sagebrush shrubland - exotic species
				7/26/19						X				
				7/27/19						X				
Prescribed	ID	44.956	−116.18	8/27/19							X		151	Prescibed understory burn, Litter primarily from Douglas-fir-Pacific ponderosa pine/oceanspray forest
				8/28/19							X			
Ridgetop	MT	47.5	−108.23	8/2/19	X								11,128	Bluebunch wheatgrass-bluegrass grassland
Saber	AZ	35.01	−112.90	8/15/19	X								3,280	Understory grass and litter primarily from Ponderosa pine-two-needle pinyon-Utah juniper forest

Journal of Geophysical Research: Atmospheres

10.1029/2022JD037758

Table 2
Continued

Fire name	State	Ignition lat	Ignition lon	Date	DC-8	Chem-otter	ER-2	Met-otter	LARGE	DRAGON	AML	MMP	Final burned area (acres)	Fuels (FCCS 2014) 30 m
Shady	ID	44.52	−115.02	7/24/19	X								6,091	Timber litter and shrubs under Douglas-fir, Pacific ponderosa-lodgepole pine/oceanspray forest
				7/25/19	X									
				7/26/19				X						
				7/28/19					X					
				7/29/19				X	X	X				
				8/1/19				X						
				8/2/19				X						
				8/3/19				X						
Sheep	ID	43.56	−112.88	7/24/19	X			X					112,168	Sagebrush shrubland with grasses
Sheridan	AZ	34.68	−112.89	8/15/19	X		X						21,483	Pinyon-Utah juniper forest
				8/16/19	X		X							
				8/21/19			X							
Smith Knob	ID	45.3	−115.54	9/5/19		X							874	Showy sedge-black alpine sedge grassland and Douglas-fir-Pacific ponderosa pine/oceanspray forest
Springs	CA	37.83	−118.87	8/12/19	X								4,841	Ponderosa pine-Jeffrey pine forest
				8/13/19			X							
				8/15/19								X		
				8/30/19								X		
Trumbull	AZ	36.41	−113.14	8/15/19			X						3,027	Pinyon-Utah juniper and Ponderosa pine forest with timber and grass understory
Tucker	CA	41.73	−121.24	7/30/19	X								14,154	Sagebrush-greasewood shrubland with open grasses
Vader	ID	44.36	−115.14	7/21/19					X				443	Timber litter from primarily Mature lodgepole pine forest
				7/22/19					X					
				7/25/19					X					
Williams Flats	WA	47.94	−118.62	8/3/19	X				X				44,360	Ignited in primarily Idaho fescue-bluebunch wheatgrass grassland and expanded to primarily Douglas-fir-Pacific ponderosa pine/oceanspray forest
				8/4/19					X	X				
				8/5/19					X	X				
				8/6/19	X		X		X	X				
				8/7/19	X		X		X	X				
				8/8/19	X		X			X				

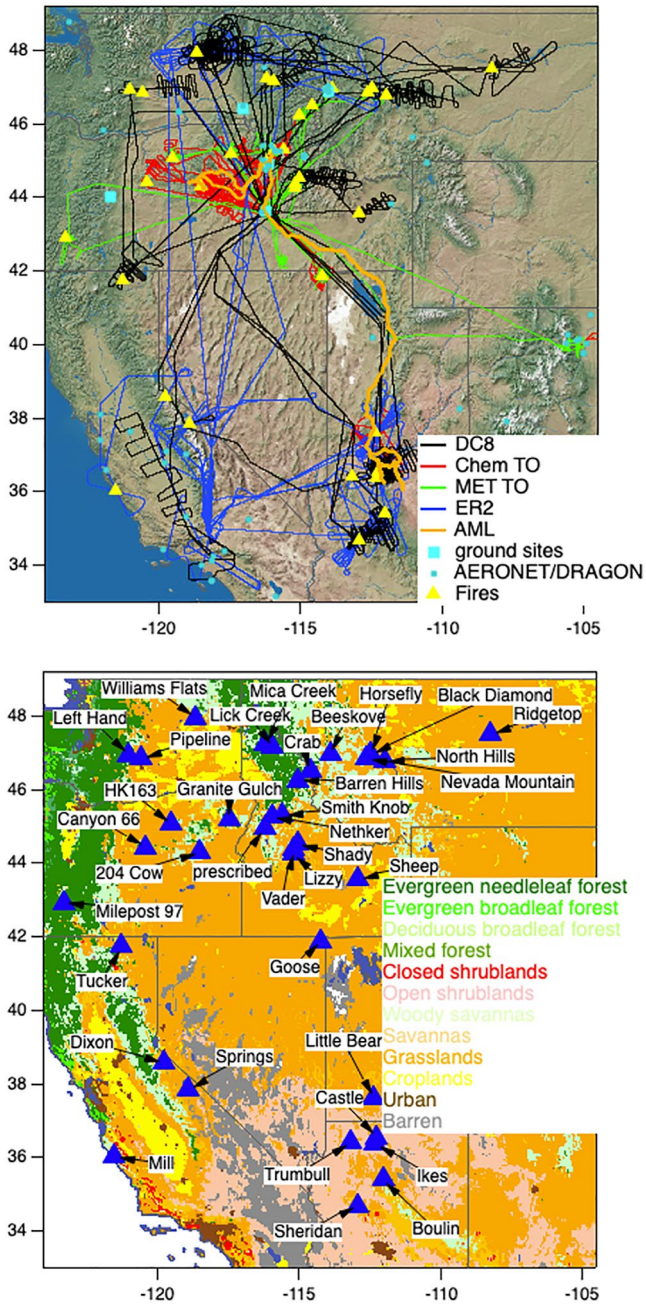

Figure 2. Maps showing the western portion of the campaign. (left) The flight tracks of the FIREX-AQ aircraft, the drive tracks of the mobile laboratories, the locations of the ground sites, and the locations of the investigated fires. (right) The investigated fires on top of a land cover map.

flight tracks color coded with CO of the NOAA Chem Twin Otter for the western wildfires are shown in Figure S2 in Supporting Information S1.

The NOAA Chem Twin Otter was the only aircraft to observe significant nighttime processing of a smoke plume and an example is described in Figure 3 for the 204 Cow Fire.

The NOAA Chem Twin Otter was the only platform where a main science goal was to focus on nighttime smoke. Several flights targeted the transition between photochemistry and dark chemistry and intercepted nighttime smoke, which was usually aged daytime smoke. Figure 3 shows results from smoke sampled after sunset on 28 August 2019 from the 204 Cow fire. Plume age estimates suggest the youngest smoke was emitted between 0 and 2.25 hr before sunset with a best estimate of 1.0 hr before sunset. The time series shows that the production rate of NO_3, $P(NO_3)$, is significant due to enhanced NO_2 within the plume and the smoke sampled contained <100 pptv of NO. The left panel shows a positive correlation of O_3 with CO from O_3 production for smoke emitted >5 hr before sunset, but a negative correlation with CO for smoke emitted <5 hr before sunset suggesting a strong potential for NO_3 chemistry.

2.3.3. NASA ER-2

NASA's high-altitude ER-2 research aircraft flew seven satellite simulator instruments with the goal to serve as a bridge between in-situ and satellite datasets. An airborne remote sensing instrument suite was used to help characterize fire development, emission processes, plume evolution, and downwind impacts on air quality. The primary objective for addressing broad FIREX-AQ science goals was to provide large-scale high-resolution observational constraints for fire behavior, plume rise, and smoke emission models, while the specific objectives of this platform were to: (a) Establish observational links between atmospheric conditions, fire temperature, smoke plume heights, and downwind smoke dispersion; (b) Characterize regional aerosol properties and trace gases profiles/amounts downwind from fires; (c) Evaluate multi-instrument synergy for fire process characterization. The payload of the NASA ER-2 was designed to achieve those goals and is listed in Table 5. The NASA ER-2 flights are shown in Figure 2 and the 10 observed fires are included in Table 2. The specific flight tracks of the NASA ER-2 for the western wildfires are shown in Figure S3 in Supporting Information S1.

All NASA ER-2 flights were coordinated with satellites in a variety of smoke conditions to evaluate how well satellite retrievals can handle small-scale sub-pixel variabilities. The satellite coordination included NASA ER-2 flight legs on and parallel to satellite tracks to evaluate viewing angle uncertainties in satellite retrievals. Ground monitors (including mobile AERONET, and California Air Resources Board (CARB) mobile platforms) were routinely targeted during the campaign primarily for NASA ER-2 instrument algorithm validation purposes.

An example of how the ER-2 connects to satellite data is shown in Figure 4. The NASA ER-2 investigated the Williams Flats fire in coordination with the NASA DC-8 aircraft on 06 August 2019, where the eMAS instrument measured high aerosol optical depth (AOD) with a very high spatial resolution at center of the MODIS-Aqua swath, where the collocation of MODIS and eMAS aligned nicely. The comparison shows that eMAS and MODIS 10 km data are in good agreement. The NASA DC-8 aircraft sampled the plume in-situ at roughly the same time.

Table 3
Payload of the NASA DC-8 for FIREX-AQ

Species measured	Technique	Frequency (Hz)	Investigator	Institution	References
Gas phase measurements (tracers and reactive nitrogen)					
O_3, NO, NO_2, NO_y	Chemiluminescence	1	Tom Ryerson	NOAA CSL	Ryerson et al. (2000)
CO_2, CO, CH_4, H_2O	Laser absorption spectroscopy	1–5	Glenn Diskin	NASA LaRC	Sachse et al. (1991)
NH_3, Speciated hydrocarbons, and OVOCs[a]	PTR-ToF-MS	1–5	Armin Wisthaler	U Innsbruck and U Oslo	Müller et al. (2014), Tomsche et al. (2022)
PAN, PPN, other PANs	Chemical ionization mass spectrometry (CIMS)	1–10	Greg Huey	Georgia Tech	Zheng et al. (2011)
HONO, HCN, HNCO, HCOOH, N_2O_5, hydroperoxymethyl thioformate (HPMTF), halogenated compounds	Iodide ToF-CIMS	1	Patrick Veres	NOAA CSL	Veres et al. (2020)
CH_3CN	H3O+ ToF-CIMS	1–5	Carsten Warneke	NOAA CSL	Yuan et al. (2017)
CO, N_2O, H_2O	Cavity enhanced absorption	1	Jeff Peischl	NOAA CSL	Eilerman et al. (2016)
SO_2	Laser induced fluorescence	1	Andrew Rollins	NOAA CSL	Rollins et al. (2016)
NO	Laser induced fluorescence	1	Andrew Rollins	NOAA CSL	Rollins et al. (2020)
HCN	CIMS	1–10	Paul Wennberg	CalTech	Crounse et al. (2006)
NO_2	CANOE, nonresonant laser-induced fluorescence	1	Jason St. Clair	NASA GSFC	St. Clair et al. (2019)
NO_2, HONO	Airborne cavity enhanced spectrometer	1	Caroline Womack	NOAA CSL	Min et al. (2016)
HNO_3	Mist chamber	0.0066	Jack Dibb	UNH	Scheuer et al. (2010)
O_3	ROZE, cavity enhanced absorption	1–10	Tom Hanisco	NASA GSFC	Hannun et al. (2020)
Gas phase measurements (Hydrocarbons and Oxidation Products)					
CH_2O, C_2H_6	Laser absorption spectroscopy	1	Alan Fried	CU Boulder	Weibring et al. (2007)
C_2-C_{11} Alkanes, $C_{2\text{-}10}$ Alkenes, C_6-C_9 Aromatics, C_1-C_5 Alkylnitrates, etc.	Whole air sampling	Up to 168/flight	Don Blake	UC Irvine	Simpson et al. (2020)
Speciated hydrocarbons and OVOCs	H3O+ ToF-CIMS	1–5	Carsten Warneke	NOAA CSL	Yuan et al. (2017)
C_2-C_{10} Alkanes, C_2-C_4 Alkenes, C_6-C_9 Aromatics, C_1-C_5 Alkylnitrates, etc.	Whole air sampling	Up to 72/flight	Jessica Gilman	NOAA CSL	Lerner et al. (2017)
C_3-C_{10} hydrocarbons, C_1-C_7 OVOCs, HCN, CH_3CN, C_1-C_2 halocarbons, etc.	HR-ToF-GC/MS	0.0095	Eric Apel	NCAR ACOM	Apel et al. (2010)
CH_2O	Laser induced fluorescence	1–10	Tom Hanisco	NASA GSFC	Cazorla et al. (2015)
H_2O_2, organic peroxides, organic acids, isoprene oxidations products, etc.	CIMS	1	Paul Wennberg	CalTech	Crounse et al. (2006)
glyoxal, methylglyoxal	Airborne cavity enhanced spectrometer	1	Caroline Womack	NOAA CSL	Min et al. (2016)
Aerosol measurements (physical/optical/chemical)					
bulk aerosol composition	Filter sampling (FS) and mist chamber (MC)	0.0066	Jack Dibb	UNH	Heim et al. (2020)

Table 3
Continued

Species measured	Technique	Frequency (Hz)	Investigator	Institution	References
BrC absorption	FS and MC with spectro-photometer	0.0066	Rodney Weber	Georgia Tech	Forrister et al. (2015), Zeng et al. (2021)
Aerosol absorption and extinction at multiple wavelengths and RH	Cavity ringdown extinction and photoacoustic absorption spectrometers	1	Nick Wagner	NOAA CSL	Lack et al. (2012)
Aerosol scattering phase function at UV and visible (blue) wavelengths	Laser imaging nephelometer	1	Adam Ahern	NOAA CSL	Manfred et al. (2018)
Aerosol number concentration	TSI CPC	1	Richard Moore	NASA LaRC	Sinclair & Hoopes (1975)
	BMI mCPC	~5–10			Agarwal & Sem (1980)
Cloud and supermicron aerosol size distribution	DMT CDP DMT CPSPD	1	Richard Moore	NASA LaRC	Baumgardner et al. (2014), Lance et al. (2010)
Aerosol number size distribution	TSI SMPS (mobility), TSI LAS (optical)	0.016 1	Richard Moore	NASA LaRC	Moore et al. (2021)
Non-volatile aerosol number concentration and size distribution (350°C)	Thermally-denuded CPC and LAS	1	Richard Moore	NASA LaRC	
Cloud condensation nuclei (0.34%SS)	DMT CCN Counter	1	Richard Moore	NASA LaRC	Roberts & Nenes (2005)
Aerosol absorption and scattering at multiple wavelengths and RH	TSI nephelometer, radiance research PSAP BMI TAP	1	Richard Moore	NASA LaRC	Bodhaine et al. (1991), Bond et al. (1999), Lin et al. (1973), and Ogren (2010)
BC concentration, size, mixing state	SP2	1	Joshua Schwarz	NOAA CSL	Schwarz et al. (2008)
Submicron aerosol bulk and size segregated composition	HR-ToF-AMS	1–10	Jose Jimenez	CU Boulder	Canagaratna et al. (2007), Guo et al. (2021)
Molecular aerosol composition	EESI-MS (ESI offline filters)	1 (2e−4)	Jose Jimenez (Alexander Laskin)	CU Boulder (Purdue U)	Pagonis et al. (2021)
Cloud and coarse mode size distribution	Optical wing probe detectors	1	Bernadett Weinzierl	U Vienna	Baumgardner et al. (2001)
mixing state, shape, composition of single particles	transmission electron microscopy	24/flight	Adachi Kouji	Meteorological Research Institute, Japan	Adachi et al. (2020)
Remote sensing measurements (active and passive)					
Zenith/nadir solar actinic flux and photolysis frequencies	4π-sr spectroradiometry	1	Sam Hall	NCAR ACOM	Hall et al. (2018)
Active fires ($T \leq 850$ K) and burn scars at 10–20 m resolution	MODIS/ASTER airborne simulator (MASTER) scanning spectrometer		Jeff Myers	NASA ARC	Hook et al. (2001)
Zenith/nadir profiles of O_3, aerosol backscatter, extinction, depolarization., etc.	Differential absorption lidar-high spectral resolution lidar (DIAL-HSRL)	0.1	John Hair	NASA LaRC	Hair et al. (2008)
Meteorological measurements					

Table 3
Continued

Species measured	Technique	Frequency (Hz)	Investigator	Institution	References
3D winds, turbulence, Reynolds number	Meteorological measurement system	1–20	Paul Bui	NASA ARC	
Meteorological and navigation parameters	Various	1–5	Melissa Yang	NASA NSRC	

[a]The VOCs from this instrument were only archived for one flight to cover unavailable data from the primary H_3O^+-ToF CIMS.

2.3.4. NOAA Met Twin Otter

The NOAA Met Twin Otter (MET-TO), based in Boise, ID, completed 14 science flights (57 hr) and sampled 12 different fires. The MET-TO had a typical endurance of 4 hr and, for more distant fires, would land and refuel at nearby airfields to extend its sampling time on station. Four of the flights were coordinated with the NOAA Chem Twin Otter.

The MET-TO was deployed to characterize the spatial structure of the horizontal wind fields surrounding the fire, the fire strength and progression, and to investigate the vertical motions over the fire and the transport and geometry of the downwind plume. This was accomplished using remote sensing instrumentation (a scanning Doppler lidar, optical imager, and infrared radiometer) and a meteorological package to profile thermodynamic variables when the aircraft was changing altitudes and measuring conditions at flight altitude. The payload listed in Table 6 for this platform was purposely kept light in order to maximize the endurance of the aircraft. The NOAA Met Twin Otter flights are shown in Figure 2 and the intercepted fires are included in Table 2. The specific flight tracks of the NOAA Met Twin Otter for the western wildfires are shown in Figure S4 in Supporting Information S1.

The NOAA MET Twin Otter aircraft flew above the plume, when possible, in order to provide complete vertical coverage of dynamics and aerosol concentration throughout the plume. The aerosol backscatter measured with the Micro-pulse Doppler Lidar of the NOAA MET-TO is shown in Figure 5. The backscatter data together with the measured wind field structure can be used to determine fire weather dynamics. For example, the plume rise and the injection height can be measured as a function of the fire strength and boundary layer conditions.

2.4. Mobile Laboratories

2.4.1. NASA MACH-2

The NASA Langley Aerosol Research Group (LARGE; https://science-data.larc.nasa.gov/large/) deployed the NASA Mobile Aerosol Characterization laboratory (MACH-2) with Boise, ID as a home base. The MACH-2 was driven to the fires as listed in Table 1 to investigate smoke for up to 5 days like in the case of the Williams Flats fire. The MACH-2 coordinated with other research platforms, including the NOAA Twin Otters, the Aerodyne Mobile Laboratory (AML), the Mobile Dragons, and the NASA DC-8. The MACH-2 traveled 13,300 miles in 51 days, sampled eight fires in six different states, and recorded 10.5 days of 1-s data.

The payload of the MACH-2 is listed in Table 7 and was focused on characterizing aerosol optical, microphysical and compositional properties. Most instruments sampled during the drive, but filter samples were only collected during stationary measurements. The MACH-2 conducted detailed measurements of gaseous and particulate nitrogen species including the isotopic composition of NO_x, HONO, HNO_3 and aerosol nitrate to examine reactive nitrogen budgets in fresh and aged smoke plumes. In addition, quartz-fiber and Teflon filter samples were collected and analyzed for EC/OC, BrC, toxicity, organic functional groups, and isotopes. Samples were drawn from a common inlet on the top rear of the vehicle to minimize generator exhaust contamination and enable temporal correlation between measured species. Ancillary measurements of CO, CO_2, NO_2, NO_x, H_2O, temperature, pressure, vertical aerosol backscattering and navigational parameters were made to establish plume characteristics and vehicle location relative to emission sources. The MACH-2 drives are shown in Figure 2 and the intercepted fires are included in Table 2. The specific drive tracks color coded with CO of the MACH-2 for the western wildfires are shown in Figure S5 in Supporting Information S1.

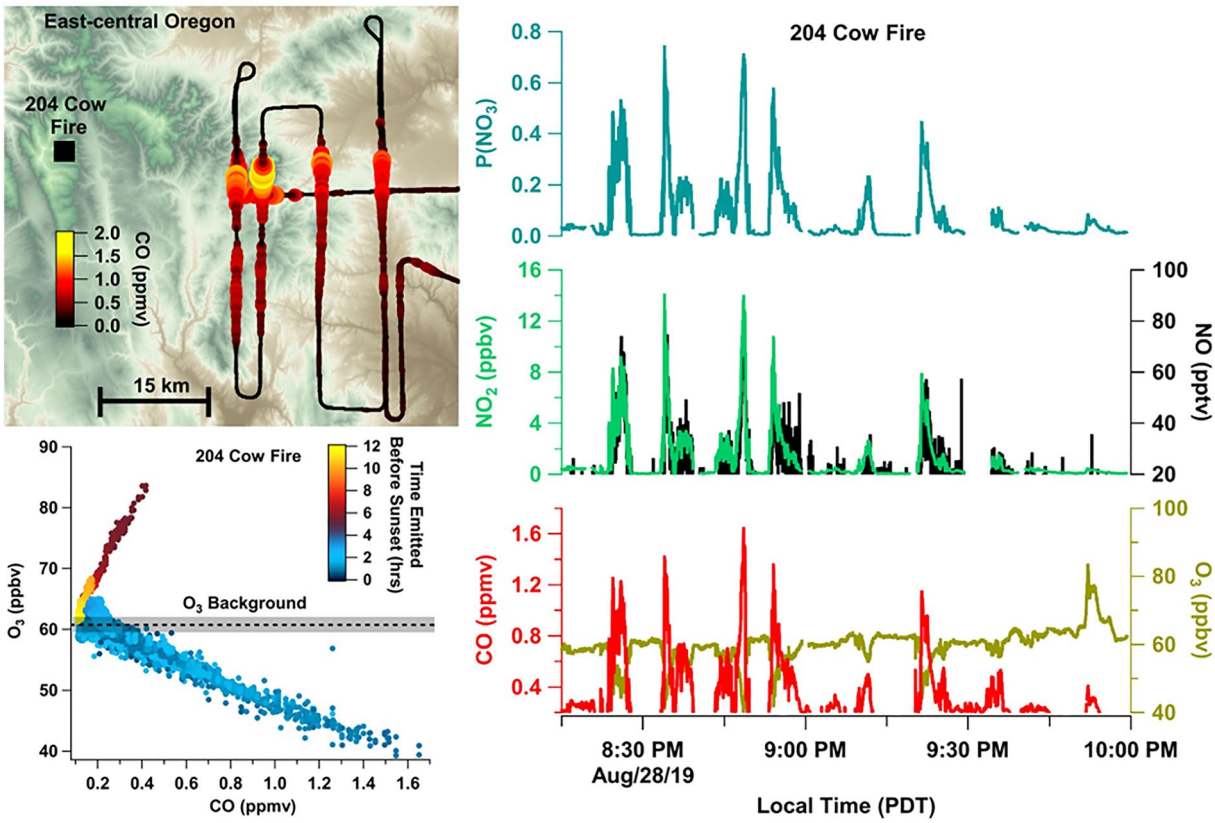

Figure 3. Nighttime processing of a smoke plume from the 204 Cow Fire on 28 August 2019 observed by the NOAA Chem Twin Otter during FIREX-AQ. (top) The flight track color coded by CO. (bottom) CO correlation with O_3. (right) Time series of the NO_3 production rate, NO_2, and O_3.

2.4.2. Aerodyne Mobile Laboratory

The AML operated out of McCall, ID (the location of a ground site as described below), during FIREX-AQ from 9 to 28 August 2019 and during WE-CAN from 11 to 28 August 2018. The AML was well-equipped for detailed gas- and aerosol-phase characterization as listed in Table 8 and included, among other instruments, highly speciated VOC measurements with a Vocus PTR-MS instrument and aerosol composition with an aerosol mass spectrometer (AMS) operated with or without soot-particle mode. Aerodyne Research, Inc. trace gas monitors (using tunable infrared laser differential absorption spectroscopy, TILDAS) measured select trace gases including the fire tracer hydrogen cyanide (HCN) and ethane (C_2H_6). The AML also hosted a number of guest instruments run by external collaborators, also listed in the table below. The goal of the AML was to link the aircraft measurements to the ground by comparing EFs, understanding smoldering versus flaming emissions in close range of the fires, measure the air quality and the nighttime exposure in smoke-filled valleys, and look at plume aging. The AML drives are shown in Figure 2 and the intercepted fires are included in Table 2. The specific drive tracks of the AML for the western wildfires are shown in Figure S6 in Supporting Information S1.

The AML had the opportunity to measure smoke filled valleys, measured very close to the 204 Cow Fire, and intercepted smoke from a prescribed fire close to McCall, ID (Figures 6–10).

In 2019, the Nethker fire, which burned throughout the deployment, provided numerous close and longer-range mobile sampling opportunities, an investigation of VOC EFs with the Vocus PTR-MS and an investigation of smoke photochemistry with an onboard reaction chamber (potential aerosol mass). Excursions to the 204 Cow and Castle/Ikes fires measured smoke accumulation and ventilation in smoke-filled valleys. A small, prescribed burn near McCall, ID provided an opportunity to measure plume aging by intercepting the plume at three different distances from the fire with a clear change in aerosol oxidation state observed. The ground site also observed this prescribed burn.

Table 4
Payload of the NOAA Chem Twin Otter for FIREX-AQ

Parameters measured	Technique	Frequency (Hz)	Investigator	Institution	References
Gas phase measurements					
O_3, NO, NO_2	Chemiluminescence	1	Andrew Weinheimer	NCAR ACOM	Ridley et al. (1992)
CO, CO_2, CH_4, H_2O	Cavity ring-down spectroscopy	1	Michael Robinson	NOAA CSL	Crosson (2008), Karion et al. (2013)
Selected acids (HNO_3, HONO, organics), acid gases (N_2O_5, $ClNO_2$), oxygenated organics, organic nitrates, and halogens	Iodide TOF-CIMS	1	Joel Thornton	University of Washington	Lee et al. (2014)
Speciated VOCs	GC × GC TOF-MS	Variable; discrete samples	Kelley Barsanti	UC Riverside	Pankow et al. (2012)
Aerosol measurements					
Submicron aerosol composition	HR-TOF-AMS	1	Ann Middlebrook	NOAA CSL	DeCarlo et al. (2006)
Water-soluble organic carbon concentration and BrC absorption	BrC-PILS	0.25	Rebecca Washenfelder	NOAA CSL	Zeng et al. (2021)
Aerosol absorption	Continuous light absorption photometer	1	Ale Franchin	NOAA CSL	Ogren et al. (2017)
Submicron particle size distribution	UHSAS optical particle counter	1	Ale Franchin	NOAA CSL	Kupc et al. (2018)
Soluble ions, absorption	Ion chromatography, size-exclusion chromatography with UV/visible spectroscopy	Variable; discrete samples	Cora Young	York University	Di Lorenzo et al. (2017)
Elemental analysis	XRF, others	1 sample/4 min	Alex Laskin	Purdue University	Laskin et al. (2003)
Radiation and Meteorological measurements					
NO_2 photolysis frequency	Filter radiometers	1	Michael Robinson	NOAA CSL	Junkermann et al. (1989)
Meteorological and navigation parameters	ARIM200	1	Michael Robinson	NOAA CSL	(Aventech Research Inc.)

The emission ratios of more than 150 species measured by the Vocus PTR, consisting of a range of VOCs and OVOCs, were calculated for all of the different fires sampled in 2019 (and during earlier work in 2018) and compared with literature values. For the Nethker fire, positive matrix factorization (PMF) was used to identify and apportion low- and high-temperature burning mass-spectral signatures. In addition, the reactivity with daytime and nighttime oxidants of several BB species measured with the Vocus PTR was investigated. Details and discussion of all of these Vocus PTR observations can be found in Majluf et al. (2022).

AML sampling of the 204 Cow fire demonstrated how mobile ground measurements can captured smoke pooling and ventilation in mountain valleys, a phenomenon the aircraft could not sample in 2019 and is even sometimes missed by ground networks. In this example, measurements are done throughout the night, close to the fire, and access mountain valleys and plateaus experiencing differing smoke impacts at different times. The 204 Cow fire occurred in the mountainous Malheur National Forest in eastern Oregon. The AML deployment started in the afternoon (local time) of 26 August 2019 and continued through the night until around 11 a.m. (local time) the next morning. Sampling was possible on a limited number of roads to the east of the fire (Figure 6). Fire fighters were actively working on containing the fire at the time of deployment.

Ground measurements help investigate the impact of boundary layer dynamics on ground-level smoke, something of particular importance for air quality and exposures in mountain valley communities. Figure 7 shows hydrogen

Table 5
Payload of the NASA ER-2 Aircraft for FIREX-AQ in 2019

Parameters measured	Technique	Nominal resolution	PI-name	Institution	References
Aerosol and cloud properties, (research: aerosol plume height)	AirMSPI-1 (Multiangle Spectro-Polarimetric Imager)	10 m and 10 km swath	David Diner	NASA JPL	Diner et al. (2013), van Harten et al. (2018)
Vegetation types, effective fire temperature, H_2O (research, AOD)	AVIRIS-C (Vis-SWIR spectrometer)	18 m and 20km swath	Rob Green	NASA JPL	Green et al. (1998)
Backscatter profile, depolarization ration, aerosol extinction profiles, aerosol layer type	CPL (channel backscatter lidar with polarization)	30 m vertical, 20 m horizontal	Matt McGill	NASA GSFC	McGill et al. (2002)
Cloud and aerosol properties	eMAS (Vis-IR scanning spectrometer)	50 m and 37 km swath	Rob Levy	NASA GSFC	King et al. (1996)
NO_2, HCHO, SO_2, CHOCHO, O_3	GCAS (UV-Vis-NIR spectrometer)	500 m and 16 km swath	Scott Janz	NASA GSFC	Kowalewski & Janz (2014)
Atmospheric thermodynamic profiles; CO, O_3 profiles	NAST-I (IR scanning interferometer)	2,600 m and 40 km swath	Allen Larar	NASA LaRC	Zhou et al. (2002, 2005)
Atmospheric thermodynamic profiles; Research (CO_2, O_3, CO, N_2O, CH_4, SO_2 profiles)	S-HIS (IR scanning interferometer)	2,000 m and 40 km swath	Joe Taylor	U. Wisconsin-SSEC	McCourt et al. (2004), Taylor et al. (2005)

cyanide (HCN) measurements as a function of time along with AML elevation. Acetonitrile (formally $C_3H_4N^+$, as quantified by the Vocus PTR-ToF) and BC (quantified by the SP-AMS) are also shown. These measurements were conducted along repeated transects and stationary locations on the set of roads shown in Figure 6. Fire tracers were generally at low concentrations during the first two third of the deployment. During the last one third of the deployment, HCN and other fire tracers increased rapidly. Then about 2 hr after sunrise, all fire tracers decreased to almost background levels. We attribute this to the dynamics of the atmosphere. At night, the boundary layer height decreases; with a strong inversion layer, all fire tracers are "trapped" in a shallow layer above ground. About 2 hr after sunrise, all fire tracer concentrations decreased rapidly. This was the case even when the AML drove through the eastern part of the fire-impacted area (roads closed during the night). We attribute this to rapid airmass lofting with convection during the day.

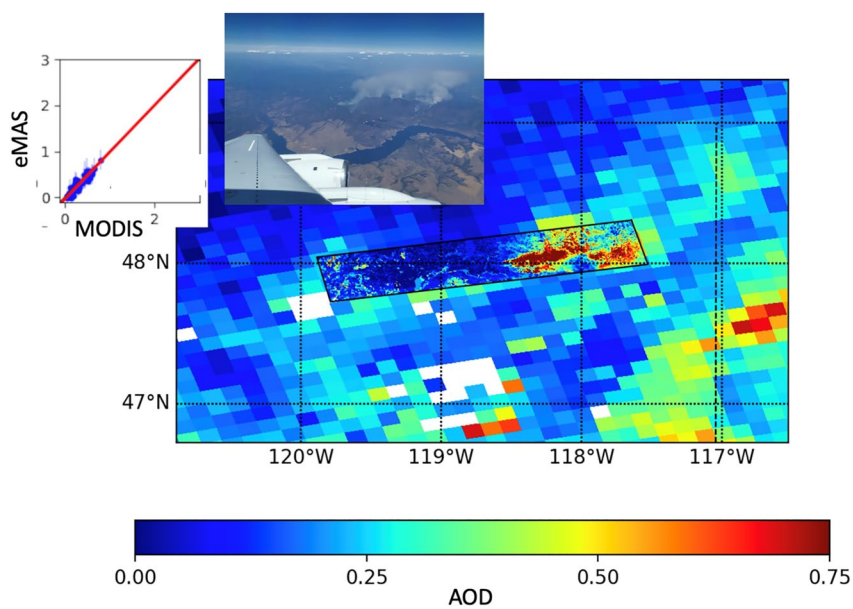

Figure 4. Overlay of the eMAS AOD data on top of the MODIS AOD retrieval for the flight of the NASA ER-2 over the Williams Flats fire on 06 August 2019.

Table 6
Payload of the MET-TO for FIREX-AQ

Parameters measured	Technique	Frequency (Hz)	PI-name	Institution	References
Line-of-sight wind speed and aerosol backscatter intensity (ABI)	Micropulse Doppler lidar	0.15–1	Alan Brewer	NOAA CSL	Schroeder et al. (2020)
Fire radiative power	Scanning Radiometers Imager FLIR Duo R		Ru-Shan Gao	NOAA CSL	

These measurements also show the effects of topography and smoke pooling. At the 204 Cow fire, strong downhill outflow of fire tracers was observed through relatively narrow valley structures, as indicated by the blue arrows in Figure 6. The AML drove through the area where the outflow joined the main valley, and high fire tracer concentrations were measured. The AML could not access the road that followed the main valley floor, but above the valley floor, fire tracer concentrations were low to moderate. This suggests that the main outflow happened only along the lowest altitudes of the valley. Conversely, in northern Arizona, the AML observed very little smoke outflow on the lee side of the plateau where the Castle and Ikes fires burned, and into the deep valley structures of the upper Colorado River. A major difference between the 204 Cow and Castle/Ikes fires is in the topographical scales: shallow valleys funneling smoke, versus a much larger downwind elevation drop in Arizona.

On 27 August 2019, a prescribed burn was conducted east of New Meadows, Idaho. With wind flow out of the WSW, the prescribed fire plume was sampled at various points by the AML. The plume was sampled initially on Idaho State Highway 55 approximately three miles west of McCall and then later sampled at two additional locations on the west and east sides of Payette Lake. Figure 8 depicts HCN associated with this BB plume. The

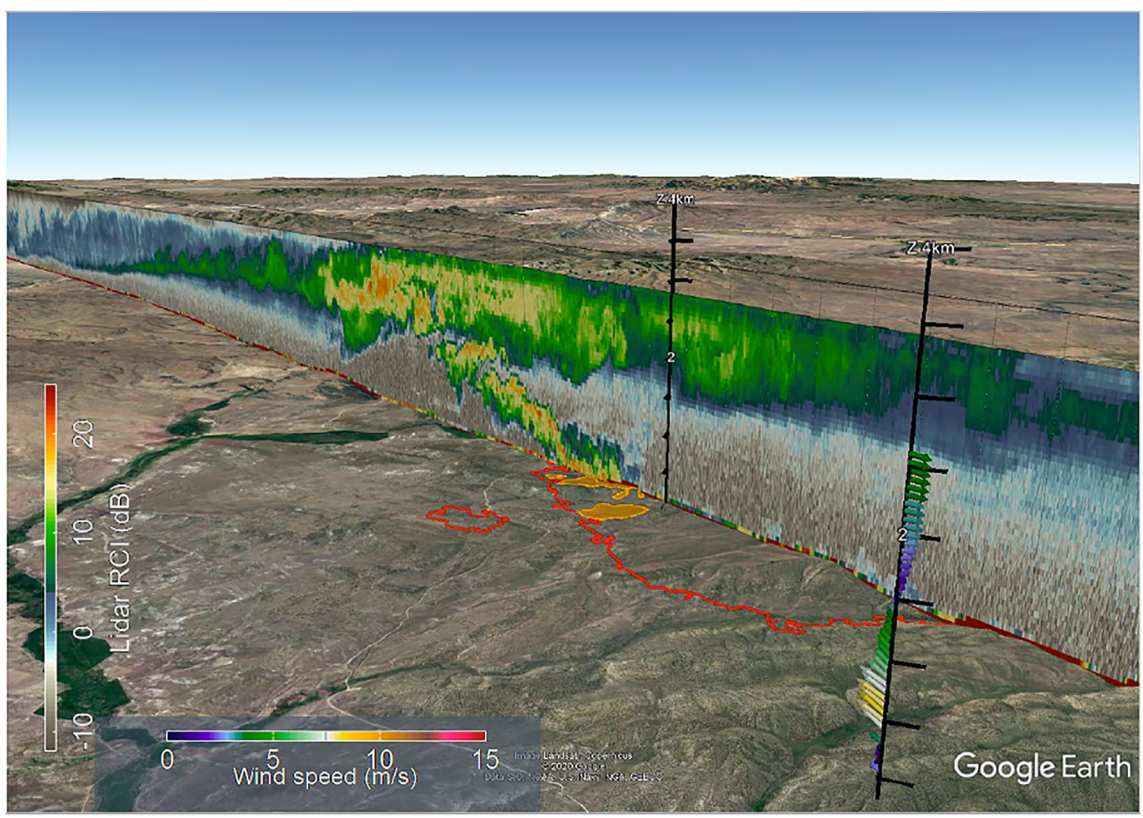

Figure 5. Range corrected aerosol backscatter intensity curtain and horizontal wind profile in the foreground from the Goose Fire measured on 5 August 2019 by the NOAA Met-TO with the Doppler Lidar. The active fire location is shown in orange on the surface map and the vertical ticks on the *Y* axes are every 500 m. The view in this image is from the ENE and the curtain data runs roughly SW to NE (going from left to right).

Table 7
Payload of the NASA MACH-2 for FIREX-AQ

Parameter measured	Technique	Frequency (s)	Investigator	Institution	References
Aerosol measurements					
Particle number density	TSI 3775	1	Bruce Anderson	NASA LaRC	TSI_3775
Aerosol size distribution	TSI SMPS w/3772 CPC	60	Bruce Anderson	NASA LaRC	TSI_SMPS
	Teledyne T640	10			Teledyne_T640
	TSI APS	1			TSI_3321
	TSI Optical Particle Spectrometer	1			TSI_3330
3-λ scattering	Air Photon	5	Bruce Anderson		Air_Photon_IN101
3-λ extinction	3-wavelength CAPS	5	Bruce Anderson		Aerodyne_CAPS
Hyperspectral aerosol absorption photometer	Custom	Variable	Bruce Anderson		Jordan et al. (2022)
Spectral aerosol extinction, absorption, BrC absorption	Hyperspectral Extinctiometer (SpEX)	240	Carolyn Jordan	NIA/LaRC	Jordan et al. (2015, 2021)
3-λ absorption photometer	TAP, PSAP	5	Bruce Anderson		Brechtel_TAP
Aerosol ionic composition	PTFE filters + IC	Intermittent	Bruce Anderson		–
Aerosol organics	PTFE filters + Spectroscopy	Intermittent	Bruce Anderson		–
EC/OC, metals	quartz filters; sunset labs, ICP	Intermittent	Bruce Anderson		OC/EC_Analyzer
$PM_{2.5}$	MetOneE-BAM	3,600	Bruce Anderson		MetOne_E-BAM
$PM_{2.5}$, PM_{10}	Teledyne T640	60	Bruce Anderson		Teledyne_T640
Cloud/aerosol profiles	Vaisala CL5100 Ceiliometer	60	Rich Moore		Vaisala_CL51
Gas phase measurements					
CO, CO_2, H_2O	LGR iCOSSpectrometer	1	Bruce Anderson	NASA LaRC	LGR_CO/CO2
CO_2, H_2O	Licor 840 NDIR	1			LI-840
NOx, NO_2	LGR NO_2 Spectrometer	1			LGR_NO2
O_3	Thermo scientific	1			Thermo_Scientific
HONO, HNO_3	Mist Chamber/IC	300	Jack Dibb	UNH	Scheuer et al. (2010)
N and O isotopes in NO_x, NO_2, HONO, nitrate and ammonium	Impinger for NO_x, denuders for NO_2 and HONO, and filters for nitrate and ammonium	variable (hours)	Meredith Hastings	Brown University	Chai et al. (2021)
Meteorological measurements					
Winds, T, RH, and navigation parameters	AirMar 200WX	1	Bruce Anderson		AirMar_200WX

orientation of this road network perpendicular to the transport of the plume allows for investigation of plume aging with transport.

The SP-AMS instrument showed increases in organic and BC loading associated with this plume. As a BB plume ages, we expect oxidation to occur. Figure 9 depicts the H:C and O:C ratios of fit organic species measured with the SP-AMS. As transects move further downwind relative to the source, the O:C state of the organic aerosol on average increases. Each dot in Figure 10 represents one 20-s sampling point.

Table 8
Payload of the Aerodyne Mobile Laboratory (AML) for FIREX-AQ in 2019

Species measured	Technique	Freq. (Hz)	Investigator	Institution	References
CO, N_2O, H_2O; C_2H_6, CH_4; HCN, C_2H_2, HCHO, HCOOH, NO, NO_2, NH_3	multiple Tunable Infrared Laser Direct Absorption Spectroscopy (TILDAS)	1	Tara Yacovitch, Christoph Dyroff; Scott Herndon; J. Rob Roscioli	Aerodyne research Inc. (ARI)	McManus et al. (2015), Yacovitch et al. (2014)
CO_2, H_2O	Non-dispersive infrared	1	Tara Yacovitch	ARI	LiCOR
O_3	UV absorption	1	Tara Yacovitch	ARI	2B Tech
oxygenated and nitrogen-containing VOCs	Vocus-PTR-MS	1	Francesca Majluf	ARI	Krechmer et al. (2018)
particulate matter size and composition	High-resolution aerosol mass spectrometer (AMS, SP-AMS)	1	Ed Fortner	ARI	Jayne et al. (2000), Onasch et al. (2012)
BC size distribution	Single Particle Soot Photometer (SP2)	1–10	Tim Onasch	ARI	Sedlacek et al. (2018)
particle count	Condensation Particle Counter (CPC)	1	Ed Fortner	ARI	
GPS and meteorology	GPS compass, RMYoung and Airmar anemometers	1–10	Tara Yacovitch	ARI	
NO_2 photolysis frequency	Filter radiometer	1	Samuel Hall	NCAR ACOM	Metcon Inc.
OC, EC, Levoglucosan, dehydroabietic acid	Filter samples with GCxGC-ToF-MS and Sunset OC/EC analyzer	30–60 min	Allen Goldstein	UC Berkeley	Jen et al. (2019), Liang et al. (2022)
Aerosol absorption and extinction at 488 and 561 nm	Multiwavelength Integrated Photoacoustic spectrometer and Nepehelometer (MIPN)	2	Rajan Chakrabarty	Washington Uni. in St. Louis	Sumlin et al. (2021)
Single-particle optical properties and composition	Electron Energy-Loss Spectroscopy (EELS)	10/fire	Rohan Mishra, Rajan Chakrabarty	Washington Uni. in St. Louis	Zhu et al. (2014)

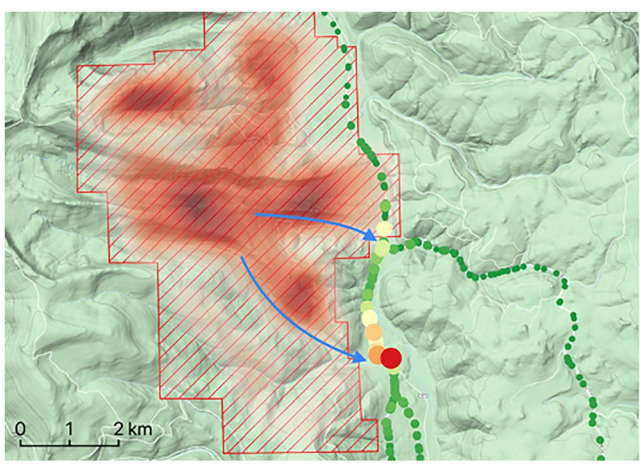

Figure 6. AML deployment at the 204 Cow fire on 26 August 2019. The HCN data are color (and size) coded in bins of 10 ppb from 0–10 ppb (green) to 60–70 ppb (red). The red area indicates the boundary of the fire during the month of August (VIIRS data (University of Maryland, 2020)). The red shaded heatmap shows fire observations as detected from satellite for the same time period. The blue arrows indicate outflow paths of fire tracers downhill through narrow valleys during the second half of the night. Topographical maps from Google.com.

2.4.3. AERONET and DRAGON

In the northwestern U.S. and southwestern Canada, 14 regional AErosol RObotic NETwork (AERONET) sites were located in the FIREX-AQ region and sun/moon/sky photometers performed measurements for aerosol assessment. These permanent AERONET sites were augmented with three Distributed Regional Aerosol Gridded Observation Networks (DRAGONs) located in Missoula, Taylor Ranch, and McCall (locations shown in Figure 3) and two mobile deployed units (Holben et al., 2018). Each DRAGON provided enhanced coverage with temporarily deployed sunphotometers. The goals were to capture aerosol variability, specifically smoke aerosol at varying distances from source regions in complex mountainous terrain and to develop a geo-referenced database that will facilitate comparison and validation investigations with in-situ and remote sensing platforms from FIREX-AQ. The regional DRAGON and AERONET sites operated 22 July–6 September with a nighttime focus 7–21 August for FIREX-AQ.

The payload of the DRAGONs is listed in Table 9 with a Sun-tracking CIMEL CE318T to measure AOD and volume size distribution, where the retrieval algorithms had to be adjusted for mobile instrument data (Giles et al., 2019; Sinyuk et al., 2020). Further the PLASMA (for Photomètre Léger Aéroporté pour la Surveillance des Masses d'Air) sun photometer provided rapid observations of the Sun to provide AOD every 10 s (Karol et al., 2013). Less frequent measurements using Microtops II and Calitoo hand-held sun

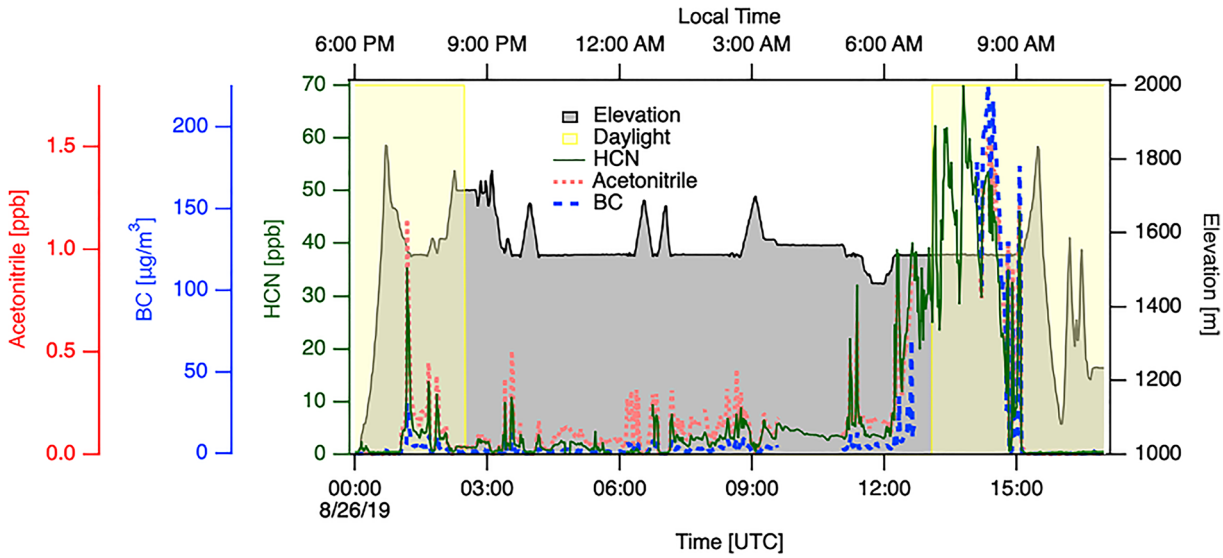

Figure 7. Time series of HCN, BC (from SP-AMS), and $C_3H_4N^+$ (quantified as acetonitrile) during the cow fire deployment. Note the strong increase in fire tracers in the early morning hours (Analysis and figures by Christoph Dyroff).

photometer data were available when the CIMEL CE318T photometer was performing sky scanning measurements (Smirnov et al., 2009). Two CIMEL Lidars (CE370 and CE376 models) were available in each mobile unit to provide aerosol and cloud vertical distribution.

The fires investigated by the DRAGONs are listed in Table 2 and measurements were coordinated with other platforms for example, the DC-8 and ER-2 during Williams Flats fire observations. The DRAGON drives are shown in Figure S7 in Supporting Information S1.

As examples of the aerosol variability observed by AERONET and the DRAGONs, the decrease of AOD with distance from the Williams Flats fire and vertical variation downwind of the 204 Cow Fire are shown in Figures 10 and 11. The goal of examining aerosol variability can be viewed in Figure 10 as AOD changes with the distance to the fire source for the Williams Flats Fire from 5 to 8 August 2019, where several plume crossings were attempted up to 250 km downwind of the fire. The AOD magnitude is highly variable in the vicinity of the fire due to the significant changes in aerosol loading as the vehicles moved in and out of the smoke plume. Peaks in AOD near 120 and 185 km are due to the DRAGON Mobile Unit 2 passing through the downwind smoke plume. The Angstrom Exponent (AE) (440–870 nm) varied between 1.4 and 2.4 indicating aerosol particle sizes vary significantly in the fine mode smoke. The variation in AE stabilized around 1.8 at 100 km from the fire suggesting aging and aggregation of the smoke particles farther away from the fire source.

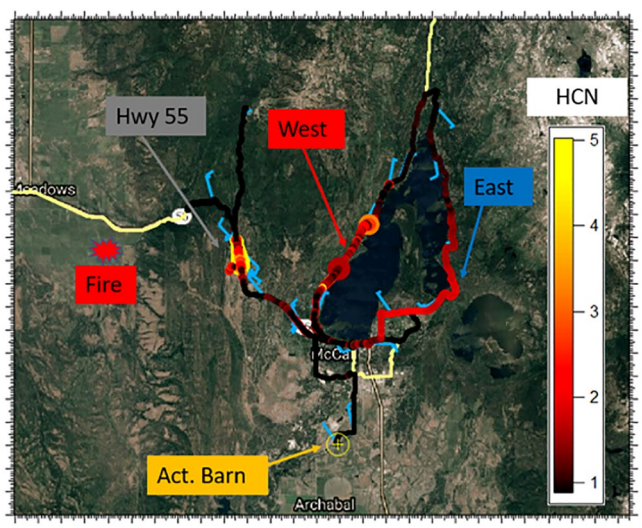

Figure 8. The drive track of the AML on 27 August 2019 color and size coded by HCN.

Figure 11 shows the Cimel CE370 micro-pulse lidar range corrected signal (RCS) measured during the 204 Cow Fire in Oregon on 26 August 2019 by DRAGON Mobile Unit 2. Vertical variation of the aerosols shows the smoke plume rising to about 3 km on the first transect while other transects farther to the east indicate smoke may have subsided near the ground into the nearby valleys (top panels). Coincident measurements from the PLASMA instrument AOD (bottom left) are interpolated to lidar wavelength at 532 nm and AE from 440 to 870 nm. Aqua MODIS true color imagery (bottom right) indicate the extent of the smoke plume at 20:15 UTC.

2.4.4. CARB

The CARB deployed a Mobile Measurement Platform (MMP) equipped with advanced technologies to measure gas- and particle-phase pollutants emitted from wildfires. Over the past decade, CARB's MMPs have been used to

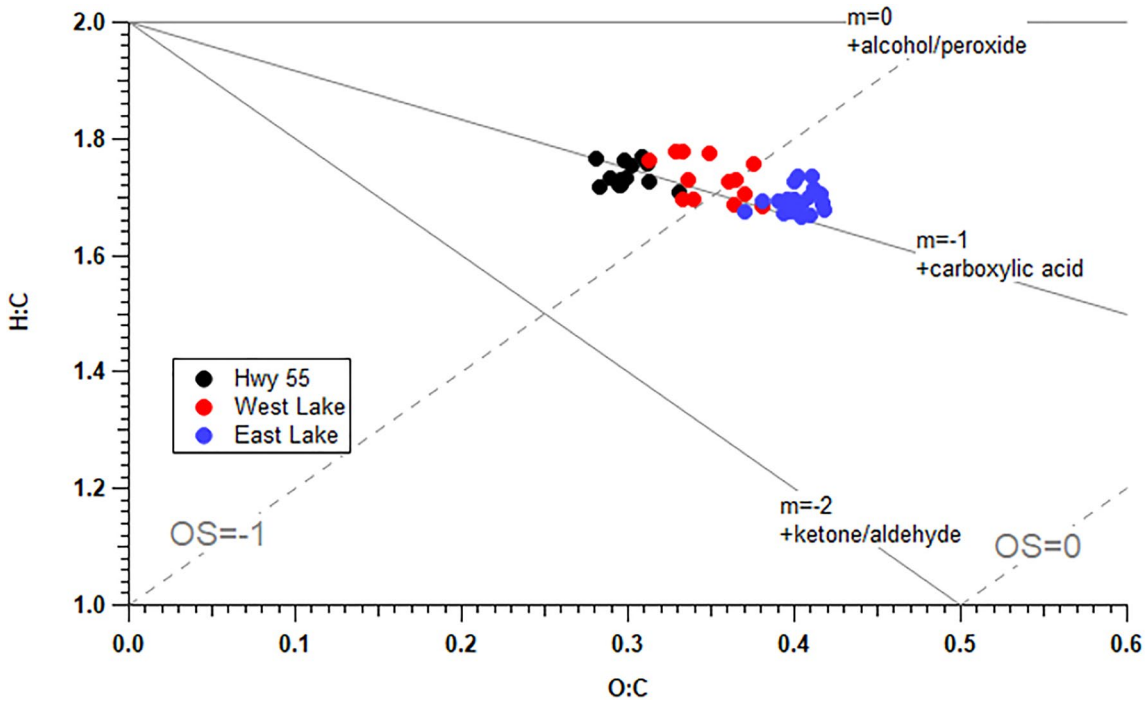

Figure 9. Organic aerosol O:C and H:C ratios are depicted and colored by location of plume intercept by the AML (Analysis and figures by Ed Fortner).

measure a variety of source emissions, study air pollution impacts on communities, and identify fugitive methane leaks throughout California. The measured EFs are used to inform the fire emission model, the First Order Fire Effects Model, used by CARB. The research advances the modeling of wildfire impacts on air quality to safeguard human health.

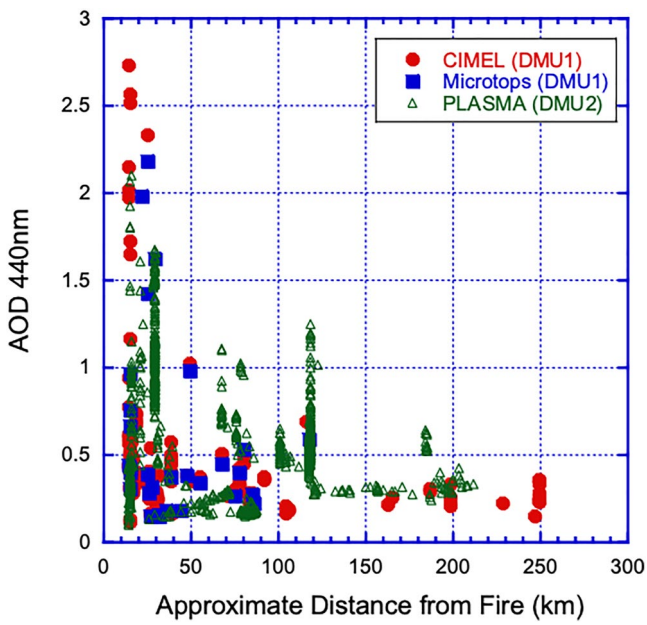

Figure 10. Mobile DRAGON showed a decrease of the AOD with increasing distance from the Williams Flats Fire from 5 to 8 August 2019. The peak at 120 km represents Mobile DRAGON Units 1 and 2 crossing the Williams Flats Fire plume near Spokane, Washington. The lower peak at 185 km represents the plume crossing of Mobile DRAGON 2 at Cour d'Alene.

The payload of the MMP during FIREX-AQ is listed in Table 10, including the guest instruments from UC Berkeley and UC Riverside. CARB deployed the MMP during FIREX-AQ on 15 and 30 August 2019 to the Springs Fire and after FIREX-AQ on 1 and 4 November 2019 to the Kincade Fire in California. During each deployment, CARB staff drove the MMP in the vicinity of the wildfire to detect the wildfire smoke. Once the smoke was identified (i.e., (CO) > 500 ppb), the MMP acted as a stationary site to monitor the fire plumes. The MMP drives are shown in Figure S8 in Supporting Information S1.

The lack of fire activity in California during FIREX-AQ limited the interaction of the MMP with the rest of the FIREX-AQ platforms, but an example of the MMP measurements of the Springs Fire is shown in Figure 12, which shows an example of the evolution of the Springs Fire on 30 August 2019. During the deployment, the MMP was parked ~3 km north of the Springs Fire. The measurement can be categorized into three periods. Period 1 is characterized by fast-changing pollutant concentrations. The smoke evolved quickly as the planetary boundary layer developed during 07:00–09:00, causing the pollutant concentration to decline. The modified combustion efficiency (MCE) also decreased from ~0.95 to ~0.85. Period 2 lasted from 09:00 to 10:30. The measurement was under northwesterly wind conditions. Clean background air entrainment diluted the sampled fire plume, resulting in low pollutant concentrations. The southerly winds dominated during Period 3 (similar to Period 1). The pollutant concentrations showed multiple spikes. The MCE values were around 0.9.

Table 9
Payload of the DRAGON Mobile Units for FIREX-AQ

Parameter measured	Technique	Frequency (Hz)	Investigator	Institution	References
Spectral Irradiance retrieval of AOD and VSD	CIMEL CE318T	1	Brent Holben	NASA GSFC	cimel.fr
Simultaneous AOD and VSD	PLASMA	0.1	Philippe Goloub	Laboratoire d'Optique Atmospherique/CIMEL	Karol et al. (2013)
Aerosol optical thickness	Calitoo	1			cimel.fr
aerosols and clouds vertical distribution	CIMEL Lidar (CE370 and CE376)	0.1			calitoo.fr
Aerosol optical thickness	Microtops II	1	David Giles	NASA	solarlight.com

The EFs of the measured pollutants were quantified as the wildfires evolved. An example is shown for CH_4 during the Springs Fire and the Kincade Fire measurements (Figure 12b) with the following observations: (a) The EF of CH_4 (EF_{CH4}) decreased with increasing MCE for both the Springs Fire and the Kincade Fire emissions, which is consistent with previous studies (Guerette et al., 2018); (b) The EF values are comparable with those reported in the literature (Akagi et al., 2011); and (c) The different slopes of EF_{CH4} versus MCE for the two fires reflected the influence of vegetation type on the EF.

2.5. Ground Sites

2.5.1. McCall, ID

When not driving, the AML measured and operated out of McCall, ID, where additional instruments were deployed to a ground site called the Activity Barn Ground Site. The location is also shown on the map in Figure 2 and Figure S9 in Supporting Information S1. The additional instrument list is shown in Table 11, and the two fires that brought smoke to the site were the Nethker Fire and the prescribed fire listed in Table 2. The Comprehensive Thermal desorption Aerosol Gas chromatograph (C-TAG) with high-resolution time-of-flight mass spectrometer

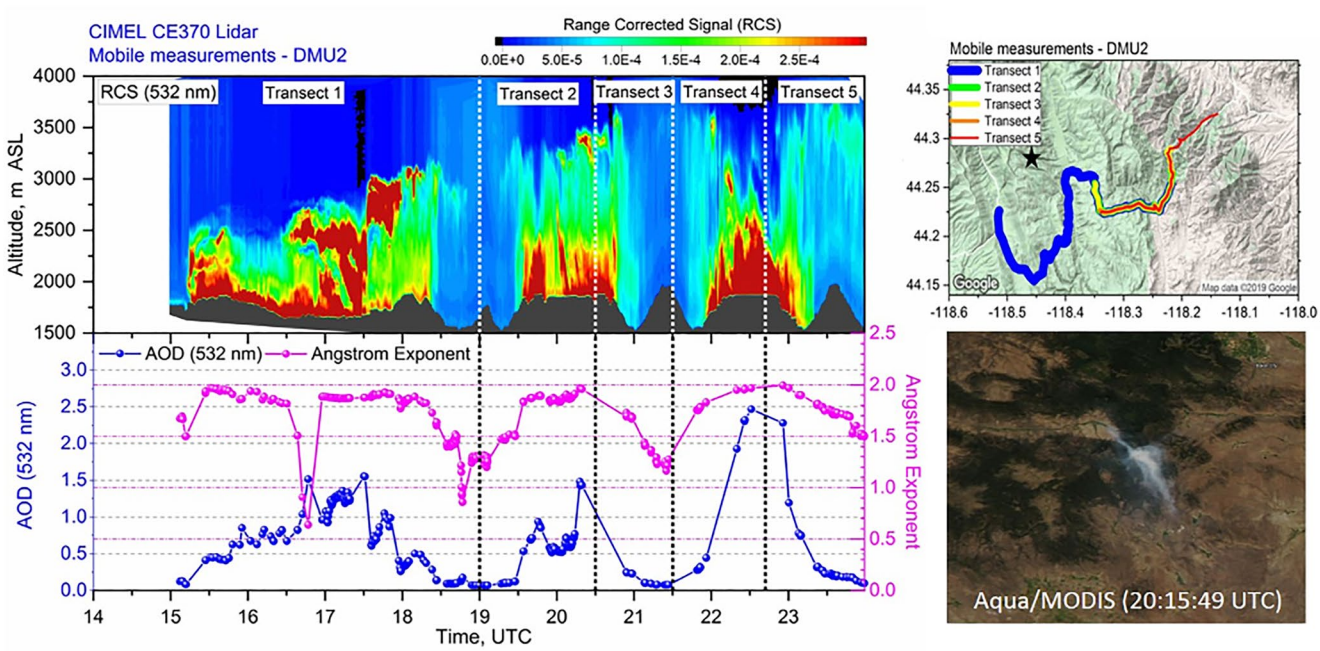

Figure 11. Cimel CE370 lidar range corrected signal (top left) measured during the 204 Cow Fire in Oregon on 26 August 2019 by DRAGON Mobile Unit 2. Coincident measurements from the PLASMA instrument AOD (bottom left) are interpolated to lidar wavelength at 532 nm and Angstrom Exponent from 440 to 870 nm. Aqua MODIS true color imagery (bottom right).

Table 10
Payload of the CARB Mobile Laboratory (MMP) for FIREX-AQ in 2019

Species measured	Technique	Frequency (Hz)	Investigator	Institution	References
NO, NO_2, NO_x	2B Model 405 NO_x Monitor	1	Shang Liu	CARB	Birks et al. (2018)
O_3	2B Model 205 O_3 Monitor	1			Andersen et al. (2010)
CH_4, CO_2, CO, H_2O	Picarro G2401	0.2			Crosson (2008)
BC/7-λ aerosol absorption	Aethalometer AE33	1			Drinovec et al. (2015)
T, RH, WS, WD	Airmar Weather Station 200WX	1			Airmar
OC, EC, Speciated components in $PM_{2.5}$	Filter samples with GCxGC-ToF-MS and Sunset OC/EC analyzer	30–60 min	Allen Goldstein	UC Berkeley	Jen et al. (2019), Liang et al. (2022)
Speciated VOCs	Sorbent tube samples with GC × GC TOF-MS	30–60 min	Kelley Barsanti	UC Riverside	Pankow et al. (2012)

(HR-TOF-MS) was deployed to this site together with a gas chromatograph electron impact high-resolution time of flight mass spectrometer (GC-EI-ToF). Weekly passive sorbent tubes analyzed by thermal desorption-gas chromatography-mass spectrometry (TD-GC-MS) were also collected at the site.

In 2019, the smoke impact on the site was unusually small, and overall, only modest fire influence was detected at McCall during FIREX-AQ. With the exception of the day where the prescribed burn near McCall ID was observed (Figure 13), the ground site experienced smoke impact mostly from residential burning. Time series are shown for BC from the SP-AMS, furfural from the GC-EI-TOF, ACSM-measured organic aerosol mass loading, and an ACSM estimate of BB organic aerosol (BBOA) concentration based on the intensity of the signal measured at m/z 60, a tracer signal for the presence of levoglucosan in the aerosol (Zhang et al., 2015). These instruments all show a plume arriving around 5:45 a.m. UTC (11:45 p.m. local time), likely due to smoke from the prescribed burn settling in the valley. During this event, the GC-EI-TOF saw elevations of VOCs in the gas phase that are considered tracers of BB like furfural. Throughout the campaign, furfural did not demonstrate a strong diurnal pattern (from background of the local Nethker fire and residential buring). The strong spike in concentration on the evening of the prescribed burn indicates that furfural may be a good tracer of fresh, non-residential BB emissions.

2.5.2. Lewis-Clark State College, ID

Researchers from the Lewis-Clark State College (LCSC) Air Chemistry Research Group deployed instrumentation for ground sampling during FIREX-AQ in June–September 2019 with the main goal of determining human exposure to a variety of air toxics from wildfire smoke. Daily to weekly averaged passive (diffusive) sorbent tube air sampling with subsequent thermal desorption/gas chromatography/mass spectrometry (TD/GC/MS) analysis of VOCs (up to 27 hydrocarbons and halogenates) was accomplished at stationary locations including the campaign ground sites at Missoula, MT, McCall, ID, Boise, ID, Lewiston, ID, Moscow, ID, and Spokane, WA (Figure 2 and Figure S9 in Supporting Information S1) (Miller et al., 2022). Mobile sorbent tube grab sampling was also utilized at active fire events, including Williams Flats (eastern WA) and Nethker (central ID) fires, often coinciding with the AML mobile labs and the AERONET sites. This resulted in the analysis of 97 VOC species, including hydrocarbons, halogenates, oxygenates, and sulfur species. In addition to VOC measurements, ambient sulfur dioxide levels were monitored at the Lewiston, ID stationary site, using a Teledyne T102 sulfur fluorescence analyzer.

The measured VOC concentrations were applied to EPA risk assessment techniques to determine human exposure to a variety of air toxics before and during the 2019 wildfire season in the Northwest and nearby populated areas during FIREX-AQ. Although the stationary sites did not have significant wildfire smoke exposures in 2019, they served as background to the wildfire sites mobile sampled. For example, the health risk due to benzene was calculated in the Nethker fire and Williams Flats fire, using the proximal cities of McCall, ID and Spokane, WA as background. The exposure concentration was equated to the mean observed concentration multiplied by an exposure weighting (the product of the exposure time, frequency, and duration divided by the averaging time). The cancer risk was then calculated from the exposure concentration multiplied by the inhalation unit risk (compound dependent). In the Nethker fire samples, elevated benzene (a known carcinogen and air toxic) concentrations were seen over 100 times elevated compared to those at

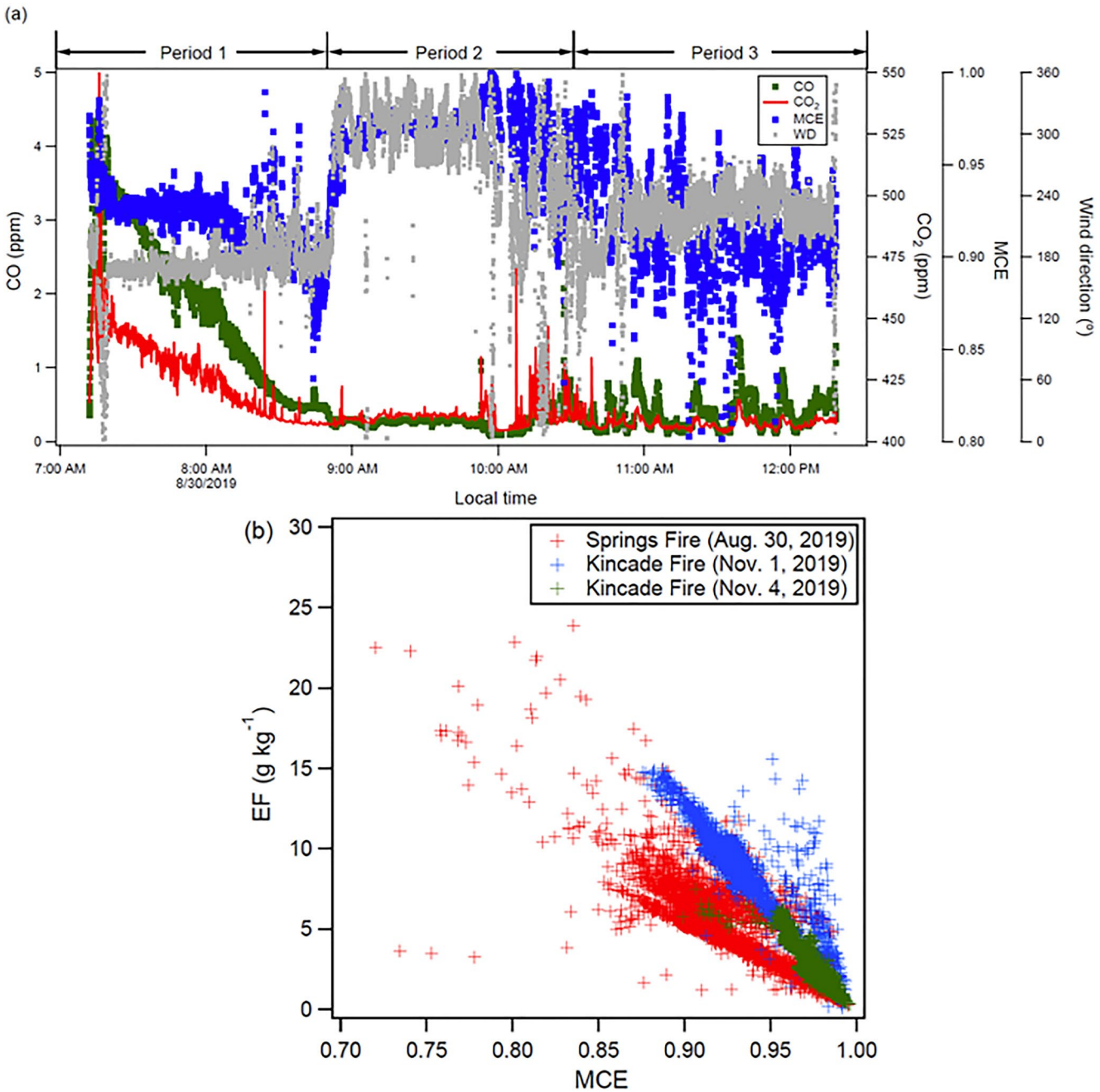

Figure 12. (a) The time series of CO, CO_2, MCE, and wind direction during the Springs Fire measurement on 30 August 2019. (b) The emission factor of CH_4 as a function of MCE.

McCall, ID which lies 30 miles south. Considering a 30-day wildfire smoke exposure scenario such as this each year, for 26 years of one's lifetime (average residence in a locale), the risk of cancer goes up by a factor of 19 compared to background (Dickinson et al., 2022). This results in potentially serious human health implications for sub-chronic to chronic exposure to wildfire smoke, especially with more active and longer duration wildfire seasons in the Northwest. The use of sorbent tube air sampling was successful in determining the effects of many wildfire smoke VOCs on air quality of surrounding regions and the associated health risks to nearby communities.

Table 11
Instrument List for the McCall Ground Site for FIREX-AQ in 2019

Parameters measured	Technique	Freq.	Investigator	Institution	References
Speciated VOCs	GC-EI-TOF	Every 20 min	Megan Claflin	Aerodyne Research, Inc.	Claflin et al. (2021)
Aerosol size and composition	Aerosol Chemical Speciation Monitor (ACSM)	1 min	Phil Croteau		Ng et al. (2011)
NO_x, CO, PM	ARIsense	10s	Eben Cross		Cross et al. (2017)
OC, EC, levoglucosan, dehydroabietic acid	Filter samples with GCxGC-ToF-MS (cTAG) and Sunset OC/EC analyzer	30–60 min	Allen Goldstein	UC Berkeley	Jen et al. (2019), Liang et al. (2022)
Met data (T, RH, P)	Airmar Weather Station 200WX	1 s	Tara Yacovitch	Aerodyne Research, Inc.	
Cloud and aerosol profiles	Micro pulse Lidar[a]	1 min	E.J. Welton	NASA GSFC	Campbell et al. (2002), Welton et al. (2000)

[a]Data are available at: https://mplnet.gsfc.nasa.gov/data?s=McCall&v=V3.

2.5.3. Other Ground Sites

Other sites operating during FIREX-AQ and shown in Figure 3 include long-term observations at Missoula, MT and Mt. Bachelor, as well as a temporary site in Boise, ID. Due to the relatively mild fire conditions in 2019, there was no direct coordination between the FIREX-AQ aircraft observations and these sites. These ground sites documented thousands of hours of fresh to aged smoke impacts on urban areas with a focus on O_3, downwind gas-particle partitioning, evolving aerosol optical properties, etc. and therefore provide valuable context regarding the episodic impact of fires over a longer period than the campaign. Additional material on these sites can be found in the SI (Sections 4.1–4.3).

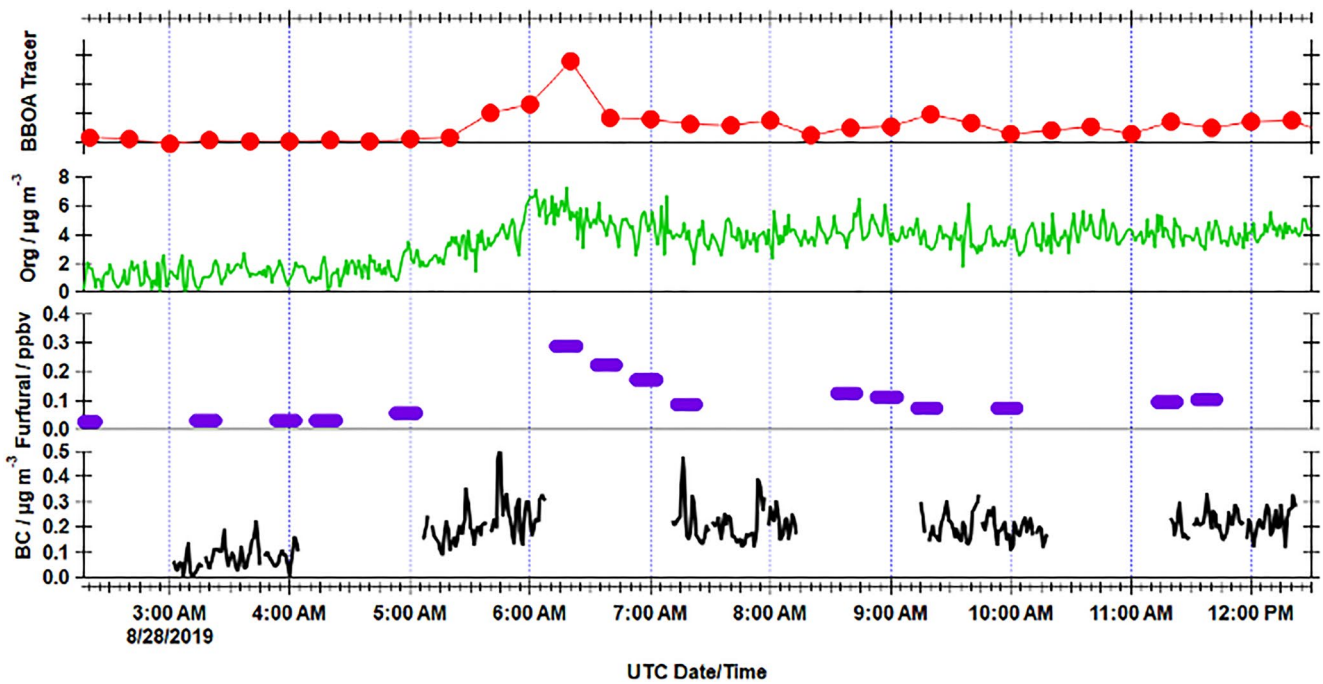

Figure 13. 2019 prescribed burn impact at the McCall, ID ground site. Time series of Organic aerosol (ACSM), BBOA Tracer (ACSM), Furfural (GC-EI-ToF), and Black Carbon aerosol (SP-AMS AML) all measured at the McCall Activity Barn ground site (Analysis and figures by Megan Claflin).

2.6. Forecasting and Nowcasting Support

2.6.1. Meteorology

For the western portion of the campaign, a team from the Naval Research Laboratory provided daily briefings on large scale circulation and regional forecasts in areas where fires were burning. Briefings contained meteorological forecast of the potential for new and sustained fires over the next days and the potential for pyro-Cb (pyro-cumulonimbus) development. Several members of this team were in Boise and then one member provided large-scale support during the Salina portion of the campaign. Briefings were customized for all the mobile platforms listed above except the CARB MMP, and these mobile briefings continued after the DC-8 was based in Salina. In Salina, the team from Florida State University provided the daily meteorological briefings. Included were experimental forecasts of prescribed fire activity based on forecast weather conditions.

2.6.2. Fire Weather and Fire Behavior

The Fuel2Fire team combined data from multiple sources to prepare daily reports to provide information to guide the FIREX-AQ campaign on the timing and selection of fires to target. For the western fires, the Fuel2Fire team assessed the previous day's fire activity, overnight fire activity, and the forecasted fire weather to determine which fires and regions showed the most potential to burn. Data analyzed to determine fire potential and behavior included: National Interagency Coordination Center Incident Management Situation Report, USFS Wildland Fire Assessment System (WFAS), Fire Weather and Fire Behavior maps, and overnight and 24-hr remotely-derived fire activity (see Section 3.4 for more detail). The Fuel2Fire team provided the fires and regions that were most likely to burn to Stan Kubota (Stan's Consulting Service), to the meteorological and smoke forecasting teams, and to the entire FIREX-AQ team. The forecasting teams needed the target fires to model well in advance of the flights. Kubota provided insights from the Incident Commanders (IC) that were leading fire actions on the ground and aircraft attacks. A representation from the National Interagency Fire Center (NIFC) attended the daily briefings and provided information to support the campaign. This information was essential to coordinate sampling by the FIREX-AQ aircraft and mobile units and included continually updated IC reports on fire behavior and planned suppression efforts.

In the southeast, the fires were largely smaller and often burned on private lands. Prescription fires are intentional ignitions, where the fires are planned to meet management or cultural objectives, when fire weather is minimal. Several prescription fires were planned and/or coordinated by the Fuel2Fire team, and others were identified through relationships with regional extensions, state agencies, and conservation organizations that were established in advance of the campaign. Cropland and pile fires burn rapidly, so near-real-time 5- to 15-min Geostationary Operational Environmental Satellites (GOES 16 and 17) were critical to identifying small fires and guiding the DC-8 aircraft. Additionally, the Fuel2Fire team provided background on the typical cropland fire timing by hosting a Fuel2Fire van that identified potential fire activity.

2.6.3. Smoke Forecasting

Forecasts of smoke, aerosol, and trace gas concentrations were provided by several groups using 16 different models as described in Table 12. These forecasts ranged from operational to highly experimental. The differences among models include: fire emissions, plume injection parameterization, assimilation of satellite AOD retrievals, complexity of chemistry, dynamic core and meteorology, time of initialization, and domain extent and resolution. Representatives of most modeling teams deployed to Boise and Salina and contributed to flight planning activities; teams in the field included GEOSFP, RAQMS and WISC WRF-Chem, NAAPS, WACCM and NCAR WRF-Chem, UIOWA WRF-Chem, NAQFC Experimental, HRRR-Smoke, GEFS-Aerosols, FLEXPART, and UCLA WRF-Chem. CU-Boulder team was also in the field and contributed to flight planning. The model PIs are listed in the SI. High resolution (2.5 km) experimental forecasts for western North America (ARQI FireWork experimental) specially implemented for FIREX-AQ were provided by campaign partner Environment and Climate Change Canada. Other forecasting systems listed in Table 12 that run operationally were obtained through collaborations.

Model output from the majority of these systems was downloaded in near-real time from the providers and was plotted using the NASA GMAO Framework for Live User-Invoked Data (FLUID) system (https://fluid.nccs.nasa.gov/about/), which enabled the science team to have all forecasts plotted in the same domain and color-scale. Spatial maps at pressure levels and total column, as well as vertical cross-sections at fixed locations were included

Table 12
Sixteen Different Forecast Models Predicting Smoke Used During FIREX-AQ in 2019

Model	Forecast domain	Institution	Grid resolution	Initial time (UTC)	Chemical mechanism	Fire emission key parameter (inventory)	Plume injection	Assim. satellite data
GEOSFP	Global	NASA GMAO	5/16 × 1/4 deg	00	Simplified	FRP (QFED)	No	Yes
CAMS	Global	ECMWF	0.4 deg	00	Full	FRP (GFASv1.2)	Yes	Yes
RAQMS	Global	University of Wisconsin	1.0 deg	12	Full	hotspots (RAQMS)	No	Yes
NAAPS	Global	NRL	30 km	00	Simplified	hotspots (FLAMBE)	No	Yes
WACCM	Global	NCAR	1.0 deg	00	Full	hotspots (FINN)	No	No
GEFS-Aerosols	Global	NOAA CSL	25 km	00	Simplified	blended (GBBEPx)	Yes	No
ARQI FireWork experimental	NW US and SW Canada	ECCC	2.5 km	12	Full	hotspots (CFFEPSv4.0)	Yes	No
HRRR-Smoke	CONUS	NOAA GSL	3 km	00	Smoke tracer	FRP	Yes	No
AIRPACT	NW US	Washington State University	4 km	08	Full	hotspots (SMARTFIRE/ Bluesky)	Yes	No
UCLA WRF-Chem	W US	UCLA	4 km	00	Simplified	FRP (QFED, with inversion)	Yes	Yes
UIWOA WRF-Chem	W US	University of Iowa	8 km	12	Full	FRP (QFED)	Yes	No
WISC WRF-Chem	CONUS	University of Wisconsin	8 km	12	Full	hotspots (PREP-CHEM)	Yes	Yes
FireWork	North America	ECCC	10 km	12	Full	hotspots (CFFEPSv2.1)	Yes	No
NAQFC	CONUS	NOAA NCEP	12 km	12	Full	hotspots (HMS/Bluesky)	Yes	No
NAQFC Experimental	CONUS	NOAA ARL	12 km	12	Full	hotspots (HMS/Bluesky)	Yes	Yes
NCAR WRF-Chem	CONUS	NCAR ACOM	12 km	00	Full	hotspots (FINN)	Yes	No
FLEXPART	CONUS	NCAR and Ludwig-Maximilians Uni.-Munich	25 km	00	Smoke tracers	Hotspots (GFAS)	Yes	No

Note. See additional details in Ye et al. (2021).

in these plots which enabled a better comparison of the guidance provided by the different models. Individual forecasting teams contributed more specialized products from their forecasting systems which included vertical cross-section along user defined locations, tracers tracking emissions from different sectors and from different BB emission inventories, and plume age estimates.

2.6.4. Nowcasting

During all flights by any of the FIREX-AQ aircraft, representatives of the meteorology, fire weather, and chemical forecasting teams provided updates on the behavior of all fires in the region of operations. These were based on near-real-time satellite imagery (primarily GOES 16 and 17) and reports from IC overseeing firefighting actions. During the Salina phase the nowcasting team was essential to direct the DC-8 to regions where small fires were burning, as these were nearly always very short-lived and could not be targeted more than 10–15 min in advance. Cropland, pile, and silviculture fire nowcasting relied heavily on thermal anomalies in the shortwave infrared window (3.9 μm band) from GOES-16 (e.g., active fire detections). Key information was saved during each flight to support data interpretation after the campaign.

3. Execution of the FIREX-AQ 2019 Intensive Campaign

3.1. Fire Season 2019

NIFC publishes the annual fire activity on their website (www.nifc.gov/fireInfo/fireInfo_statistics.html) and the data can be used to relate the 2019 fire season of the FIREX-AQ field experiments to previous years including

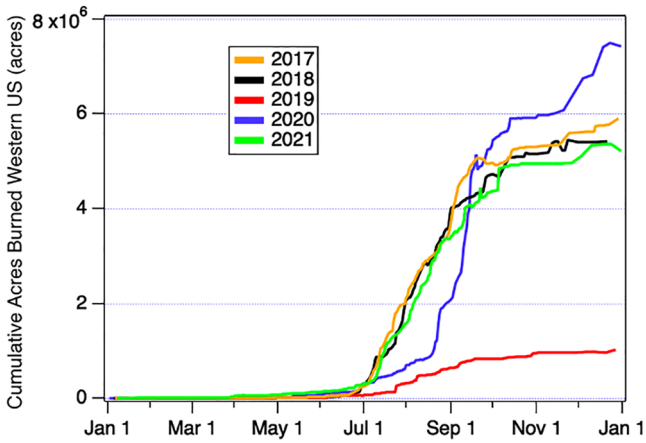

Figure 14. Cumulative area burned in the western US (California, Great Basin, Northern Rockies, and Northwest) for 2017–2021. (Data source: NIFC: https://www.predictiveservices.nifc.gov/intelligence/archive/archive2021.html).

2018 for the WE-CAN experiment. The wildfire seasonality for wildfires in the Northwest is shown in Figure 14 and typically peaks between August and September as was the case for 2017–2021. The western U.S., targeted from Boise, ID, had about a quarter of the 10-year average area burned (0.97 million acres). In 2019 there were only eight wildfires over 40,000 acres in the mainland U.S. and the DC-8 aircraft investigated two of those fires: The Sheep Fire (112,106 acres, a ∼1 day grass fire) and the Williams Flats fire (44,446 acres, which burned over 1 week). The U.S. trend in 2019 does not change long-term patterns and likely resulted from anomalies such as heavy spring and mid-season precipitation that left forests and grasslands wetter than normal (Frank, 2020).

In contrast, the 2018 fire season that WE-CAN experienced was more normal and had 5.4 million acres burned in the western U.S. and 45 significant fires above 40,000 acres. The low 2019 fire season provided the FIREX-AQ aircraft opportunities to investigate individual isolated fire plumes well, while the C-130 during WE-CAN had the additional opportunity to study complex mixtures of multiple fire plumes.

3.2. Weather Forecast and Meteorological Conditions in Summer 2019

Meteorological conditions in 2019 were a significant driver for the low fire year. While individual fires can be influenced by a variety of small-scale features, larger-scale (synoptic) weather patterns are the primary driver of regional fire activity, fire danger, and fire potential. During the months prior to FIREX-AQ, the western U.S. was affected by a persistent and anomalously deep trough of low pressure (negative Arctic Oscillation pattern), resulting in relatively cool and moist weather. Measurable rainfall occurred unusually late in California, when the dry season is typically setting in. Fuel moisture therefore remained elevated as the fire season began, likely explaining the lack of widespread, large wildfires during FIREX-AQ. This synoptic weather pattern also resulted in a relatively wet and stormy spring and early summer in the central U.S.

The Boise deployment can be separated into three distinct phases based on synoptic meteorology (Figures 15a–15c): (a) persistent anticyclone, (b) ridge breakdown, and (c) northern trough. The first phase (22 July–05 August) featured a relatively strong, and persistent anticyclone (high pressure), centered over the Four Corners region (Figure 15a). This anticyclone is the primary feature controlling the transport of monsoonal moisture from the tropical Eastern Pacific, Gulf of California, and/or Gulf of Mexico to the western U.S. (e.g., Higgins et al., 1997). At the start of FIREX-AQ, moisture transport persisted in the mid-troposphere (4–7 km) over portions of Arizona, Nevada, and Utah, resulting in widespread cloud cover and thunderstorm development during the local afternoon and evening hours. Surges of moisture intermittently reached portions of the interior Pacific Northwest, facilitating thunderstorm development above a very dry, near-surface mixed layer. Precipitation generally evaporated before reaching the ground, allowing lightning strikes to ignite several fires. Airborne sampling was generally focused temporally between moisture surges to the north and west of the primary moisture pathway, including the Shady, Tucker, North Hills, and Williams Flats fires.

The ridge axis associated with the anticyclone amplified and extended over the Pacific Northwest during the second phase of the Boise deployment (06–08 August; Figure 15b). A low-pressure trough concurrently approached from the west. This "ridge breakdown" weather pattern is often associated with periods of extreme fire and smoke plume behavior (e.g., Westphal & Toon, 1991), including the development of wildfire-driven, smoke-infused thunderstorms, known as pyrocumulonimbus or pyroCb (Peterson, Fromm, et al., 2017; Peterson, Hyer, et al., 2017; Peterson et al., 2018, 2021). Approaching weather disturbances also coincide with persistence of intense burning well into the nighttime hours (Peterson et al., 2015; Saide et al., 2015). The Williams Flats fire in Washington State was significantly affected by this unique meteorology. Fire spread and smoke release gradually increased as the approaching low-pressure trough gradually enhanced surface wind speeds in the preceding hot and dry air mass. Smoke plume altitude also increased each day, coinciding with enhanced moisture transport and decreased stability in the mid-troposphere. Both the DC-8 and ER-2 obtained measurements on all 3 days of this short sampling phase, providing a comprehensive data set over a period of extreme

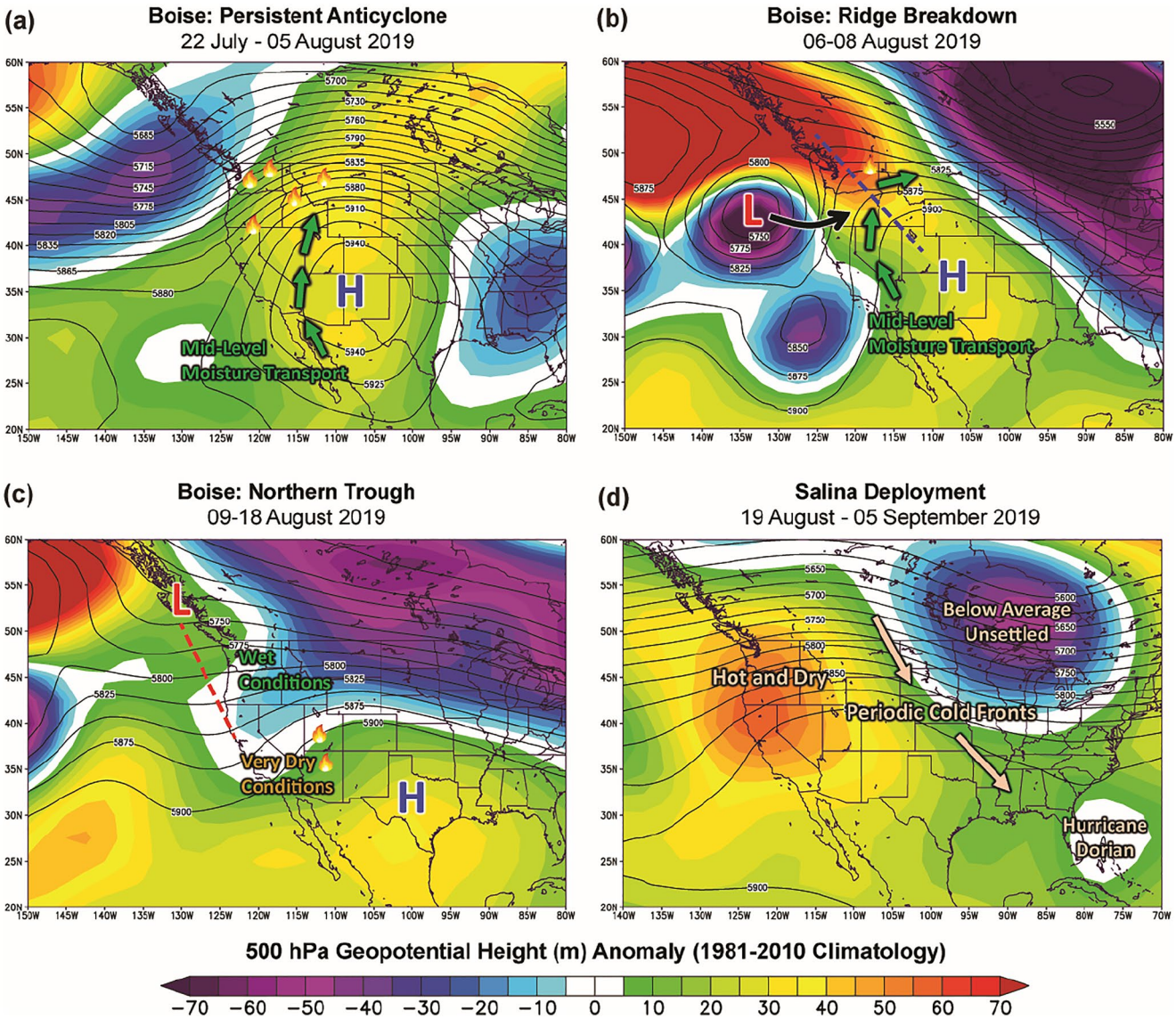

Figure 15. The large-scale weather patterns influencing fire patterns during FIREX-AQ in 2019.

fire behavior. This culminated on 08 August, when the DC-8 obtained the first detailed measurements from inside the high-altitude outflow region of a pyroCb (Peterson et al., 2022) (https://earthobservatory.nasa.gov/images/145446/flying-through-a-fire-cloud).

The third phase of the Boise deployment (9–18 August; Figure 15c) occurred after the change in synoptic meteorology described above. The low-pressure trough moved ashore, producing relatively cool, moist, and cloudy conditions over the northern portion of the study region. Fire activity decreased and the Williams Flats fire was effectively extinguished by rainfall. To the south, the anticyclone shifted into Texas, deflecting monsoonal moisture to the east of the primary study region. This resulted in significant drying and clearing over much of the southwestern U.S. Fire activity rapidly increased, especially in Arizona and Utah. FIREX-AQ sampling therefore shifted to this region, with an emphasis on the Springs, Castle, Trumbull, Sheridan, Ikes, and Boulin fires.

Synoptic meteorology for the final portion of FIREX-AQ (19 August–05 September) is summarized in Figure 15d. This period featured an amplified synoptic pattern over North America, with anomalous ridging (high pressure) over the western U.S. and a deep trough (low pressure) in the east. The high-pressure ridge over the western US promoted a return to warm and dry conditions. Fires that survived the preceding period of cool and damp weather in the Northwest were reinvigorated. New fire ignitions also occurred, providing a variety of sampling

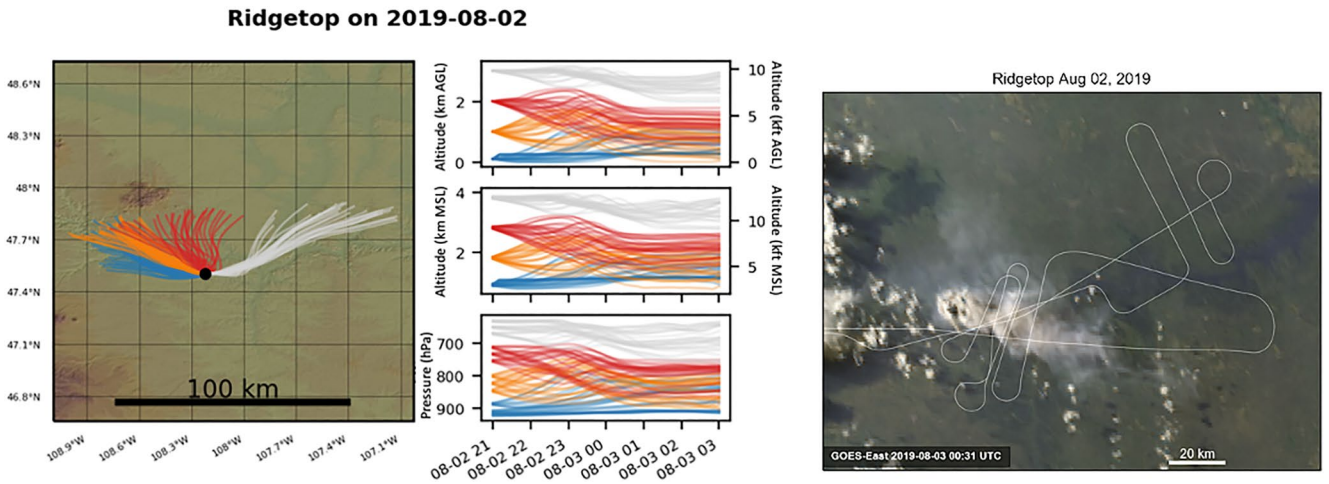

Figure 16. Left: Smoke trajectory ensemble forecast for the Ridgetop fire in Montana for multiple potential smoke injection altitudes in which low-level trajectories depict extensive vertical plume spreading to the north and northwest (blue, orange, and red lines) while high-level trajectories show horizontal plume confinement to the east (gray lines). (Above Ground Level (AGL), Mean Sea Level (MSL)). Right: Satellite image of smoke distribution at the time of aircraft sampling (gray line), showing diffuse low-level smoke transported to the north and high-elevation smoke outflow from pyroconvection transported to the east.

opportunities for the FIREX-AQ assets that remained in that region after DC-8 moved to Salina. Relatively cool and moist conditions prevailed over much of the Midwest. Intermittent frontal boundaries traversed the central U.S. and portions of the Southeast, occasionally reaching the Gulf Coast. These fronts served as a forcing mechanism for convective activity (thunderstorms) and rainfall. Sampling of fires with the DC-8 out of Salina was generally limited to periods between frontal passages in the greater MRV area, Texas, Oklahoma, Nebraska, and Kansas.

3.3. Forecast Models Predicting Smoke

Smoke trajectory forecasts were used frequently for flight planning. Fire locations, size, containment, and suppression plans were often known with good accuracy from fire incident reports (e.g., InciWeb, https://inciweb.nwcg.gov). After several fires were identified by the Fuel2Fire team (Section 2.6.2) for potential sampling on future days, HYSPLIT forward trajectory ensembles were run with high-resolution meteorological forecasts (NAM CONUS Nest 3 km) for all of these fires by the Florida State University team. Trajectories were initialized at multiple altitudes from the surface to 4 km altitude to encompass a range of possible smoke injection heights. The resulting trajectory maps provided guidance on interpreting satellite images of active smoke plumes with a quick visualization of plume development or stagnation, plume transport direction at multiple potential altitudes, height of the smoke above terrain downwind, and wind shifts over the course of the day, all of which were used for determining the suitability of a smoke plume to be sampled by the aircraft. Figure 16 shows a sample smoke trajectory ensemble forecast for the Ridgetop fire, which had a lot of diversity on the trajectory direction for the different altitudes. The Ridgetop Fire was sampled on 2 August 2019 by the DC-8 and trajectories are compared to satellite imagery of the sampled plume.

Chemical and smoke forecasts served multiple purposes for flight planning. Global models and regional models covering the whole of North America were important to provide guidance on the influence of long-range transport during the campaign. There were two major smoke events that were tracked during the campaign. The first was smoke from Canadian fires located in northern Alberta that stayed out of reach from Boise but ended up producing surface $PM_{2.5}$ enhancements in the eastern US between 24 and 26 July. Observed surface PM levels were raised to Moderate AQI (12–35 $\mu g/m^3$) over extended regions of the central and eastern US, with most forecasts showing similar PM enhancements. HRRR-Smoke showed similar patterns of enhancements, and thus this confirms the source is smoke (as this model only tracks smoke). The second was smoke from Siberia during the first half of August that affected the sampling region occasionally but remained mostly lofted. This smoke layer was sampled by the DC-8 during the 3 August 2019 flight.

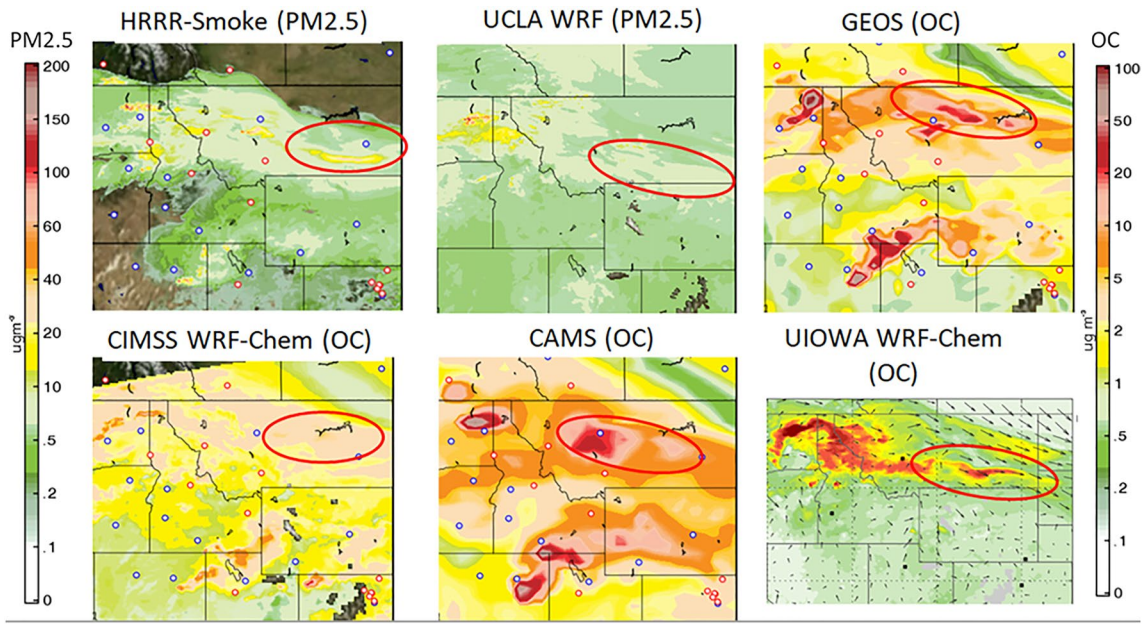

Figure 17. Forecasts of aerosol concentrations (OC and $PM_{2.5}$) at 700 hPa valid at 6 p.m. on 7 August 2019 showing enhancements due to 1-day old Williams Flats fire smoke (red ovals) from multiple forecasting systems. Open circles represent locations of interest (blue: cities, red: AERONET sites). Source: FIREX-AQ Chemical forecasts on 6 August 2019.

These forecasts were rarely used for flight planning for fresh smoke plumes, because multiple limitations were encountered. Model resolution from global models was generally too coarse to provide this type of guidance. Higher resolution models had other limitations. One of them was the latency on which emissions are updated, which created issues of fires not showing up when they had recently started or when clouds obscured the fire during a satellite overpass. At other times fires remained in the forecasts even when they had been mostly contained in reality. Assumptions related to smoke emissions and injection heights also created large diversity between models. Guidance on 1-day old smoke was generally more useful and helped interpret the satellite images as the effect of some of these limitations was reduced. An example of this guidance is shown in Figure 17 for the DC-8 flight on 7 August 2019 that sampled 1-day old smoke from the Williams Flats fire over Montana.

3.4. Active Fire Information for Flight Planning

As part of the flight planning and preparation, the Fuel2Fire team provided active fire information during the mission for decisions on which fires to target. The objective of this active-fire support was to identify active-fire regions and specific fires that were expected to burn. During the western campaign, these data were provided daily to model and meteorological forecasting teams for flight planning preparations (Section 2.6.2). The data and information presented included: basic fire information such as fire name, location, and size; fire weather and likelihood of continued fire growth, satellite data (fire detection, FRP, and smoke); ecosystem types and a fuels narrative; status of fuel lidar data collection; fire behavior; percent contained and estimated date of containment; actioned status (personnel, crews, engines, helicopters); daily 209 and NIFC reports; and Temporary Flight Restrictions.

Also available for flight planning were: (a) fire weather information, which provides the potential likelihood of continued fire growth, (b) National Weather Service 7-day fire potential, WFAS observed and forecasted Fire Danger ratings, severe fire weather, and fire behavior potential maps, (c) Satellite data of visible and active-fire detection data (MODIS and Visible Infrared Imaging Radiometer Suite (VIIRS)), (d) National Infrared Operations (NIROPS) data showing the active overnight firelines, (e) smoke extent using visible imagery and the NOAA Hazard Mapping System smoke product, (f) coincident satellite overpass potential (Aqua, Terra, Met-Op-B, Sentinel-5, CALIPSO), and (g) ecosystem types. Daily briefings are available on the FIREX-AQ data archive (https://www-air.larc.nasa.gov/missions/firex-aq/).

For the eastern campaign, fire support was reliant on information from the fire science exchanges (https://southernfireexchange.org/), states, parks, and conservation networks (see Section 3.6 for more detail). GOES data were crucial for locating small cropland and pile burning fires, due to the instruments capacity to provide 5-min data. Even though GOES is a moderate-to-low resolution instrument, it has a demonstrated ability to detect smaller fires due the instruments high-temporal resolution (Soja et al., 2009). The Fuel2Fire team planned several prescribed fires in advance of the campaign that were targeted by the DC-8 and the Fuel2Fire ground crew during the campaign.

3.5. Sampling of Western Wildfires

The sampling strategy of western wildfires is discussed using the DC-8 as an example and further explained by describing the coordinated sampling of the Williams Flats fire by multiple FIREX-AQ platforms.

3.5.1. DC-8

Flight planning for the Western wildfires considered fire weather, forecast models, and firefighting/monitoring operations input. Additional factors considered in flight planning included: satellite overpass locations and timing, fire fuel type, fire size and intensity, firefighting and flight restrictions, smoke age and fresh smoke accessibility, resampling of smoke measured the previous day, coordination with other platforms, and potential smoke impact on urban areas.

Flights were designed to measure the emissions as fresh as possible, determine the chemical transformation in the smoke during transport, and understand the variability in emissions and chemistry over time. An example of a flight for western wildfires is shown in Figure 18 for the Williams Flats fire on 7 August 2019. The flight track color-coded by carbon monoxide (CO) is shown on the top in the figure. This flight used the typical sampling strategy for the fresh smoke, but also included aged smoke, which was sampled after take-off in Boise, ID.

On most DC-8 flights, the fresh fire plume was initially approached with a longitudinal (i.e., over the length of the plume determined by local winds) overflight to map the vertical structure of the plume in aerosol backscatter using the DIAL-HSRL, and to provide a level flight leg for the MASTER instrument to record the active fire and the burn scar. Visible and IR images of the Williams Flats fire from MASTER are shown in the insert in Figure 18. Ideally the plume was first overflown from the aged smoke towards the fire location as was done on the Williams Flats fire in Figure 18. With this approach, the DC-8 was able to immediately start sampling smoke as young/close as possible at the fire itself with minimal time lost to aircraft positioning requirements. During some flights, the transit from Boise came from a direction such that two remote sensing overflights had to be flown to measure the plume structure, first away from fire along the smoke plume followed by a return flight to the fire and freshest smoke.

The HSRL-DIAL backscatter data (also shown in Figure 18) were available in real-time on the aircraft and were used to determine the ideal in situ sampling altitude of the plume, which was generally the center of the plume. In situ plume sampling patterns started with an upwind leg in clear air followed by a series of plume crossings at increasing distance downwind of the fire. Near the fire, the legs were spaced more closely than further downwind as seen in Figure 8. On some flights, select legs were repeated at different altitudes to investigate the difference in chemistry in the center of the plume, where light is strongly attenuated, compared to the top edge of the plume with higher photolysis values. The in-situ backscatter data were also used to adjust the aircraft altitude during plume sampling further away from the fire to account for changes in plume height as can be seen in Figure 18.

This pattern was repeated two or three times on some fires to investigate changes in emissions and chemistry. Fire emissions can change rapidly due to changes in local meteorology or the fire moving to areas with different slopes that impact fire spread rates or have different fuels or fuel loadings. The MCE, also shown in Figure 18, for the two repeat patterns of the Williams Flats changed from 0.904 to 0.908 on 07 August 2019, while the MCE from the Williams Flats flight on 03 August 2019 changed more substantially from 0.919 to 0.908.

The aged smoke that was targeted on the first part of the flight on 7 August 2019 was predicted by most forecast models and was observed in GOES 16 and 17 images, shown in Figure 19. Using the HSRL the vertical distribution of the smoke was determined with a longitudinal overflight at 25,000 ft (pressure altitude) of the one-day old smoke plume starting from fresher towards more aged smoke. The same flight track in reverse direction was flown at 12,000 ft inside the smoke plume. Aged smoke was only clearly observed from the Williams Flats fire

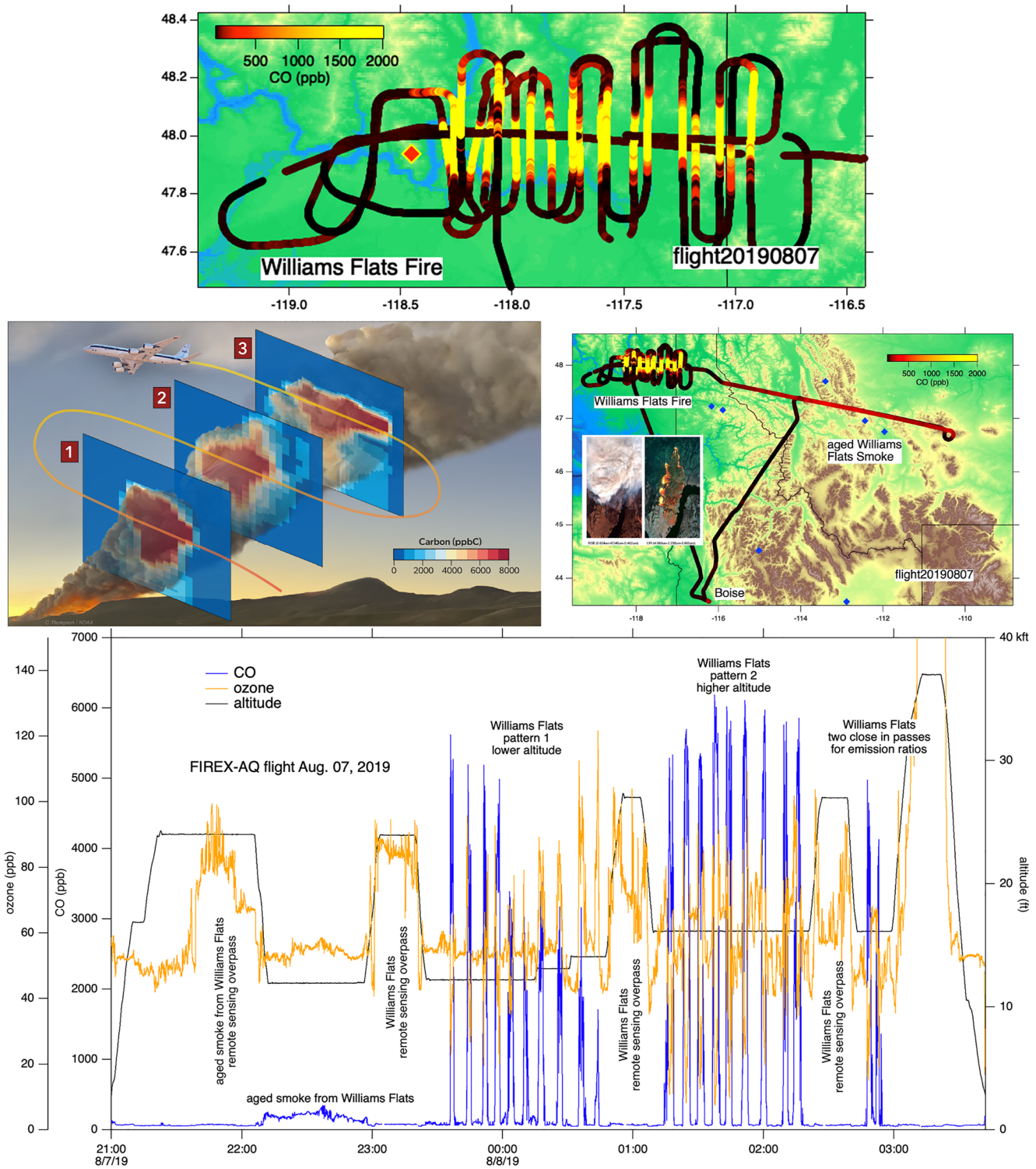

Figure 18. (a) Flight track of the NASA DC-8 FIREX-AQ flight on 07 August 2019 to the Williams Flats fire in Washington color coded with CO. (b) The carbon flux for several plume crossings computed from the carbon to aerosol backscatter measured by the HSRL LIDAR as calculated by Stockwell et al. (2022). (c) Regional overview of the flight plan including sampling aged smoke. The insert shows data from the MASTER instrument of the fire in the visible and IR. (d) The time series of CO and ozone together with the flight altitude.

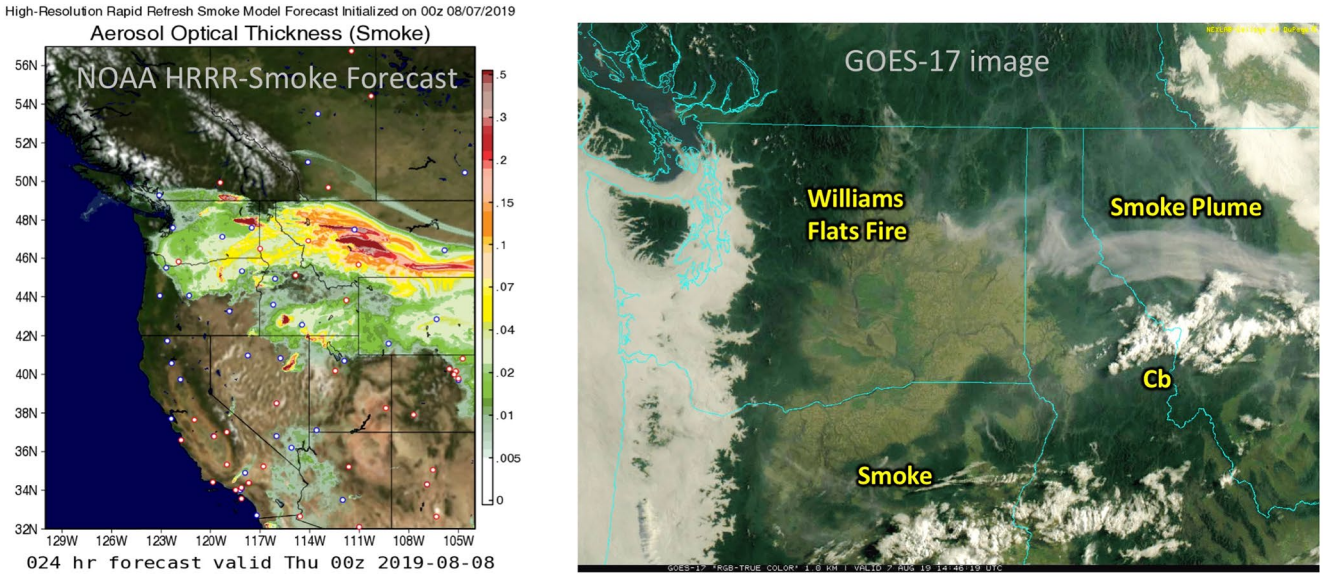

Figure 19. A typical forecast product available for the fresh and aged smoke from the Williams Flats fire on 07 August 2019 along with the nowcast satellite.

on two flights and only one other flight sampled aged smoke, where the emission location and time was well understood (FIREX-AQ flight on 3 July 2019).

The results of the smoke sampling strategy are demonstrated by the time series of CO and ozone in Figure 18. The first part of the flight sampled the aged smoke and a clear enhancement of CO (and ozone) is observed that is significantly smaller than in the fresh smoke. The first sample pattern in the fresh smoke showed significant CO decreases with plume age due to dilution, but also potentially due to decreases in emissions during the extended plume sampling with the aircraft (Wiggins et al., 2020), while the second pattern had a more constant mixing ratios during transport. The ozone time series indicates very active photochemistry. In the closest transects to the fire ozone is titrated. Ozone enhancements occur downwind first at the edges of the plume, where more light is available. In the furthest downwind transects ozone is enhanced in the whole plume.

3.5.2. Coordinated Sampling of Western Wildfires

One of the primary objectives of FIREX-AQ was to combine near and far-field observations to understand emissions, chemical evolution and transport to evaluate downwind impacts of wildfires. To look at fires holistically and achieve this objective, input from multiple research disciplines, platforms, models, and satellite observations had to be coordinated. The FIREX-AQ campaign brought an unprecedented opportunity to coordinate differently focused research platforms.

The NASA DC-8 sampled wildfire plumes from near the point of emission to downwind impacts on a regional scale. These efforts provided data to understand the influence of fire emissions on atmospheric composition with continuity from initial emissions to evolved impacts several hours downwind. With its ability to explore an extremely wide range of smoke ages, the NASA DC-8 coordinated with the NASA ER-2 and the two NOAA Twin Otter aircraft with complementary payloads and goals. For example, the Chem Twin Otter sampled fire plumes at night to investigate the nighttime chemical evolution of fire plumes. The mobile laboratories were used to examine smoke in locations and at times inaccessible to any of the aircraft, such as smoke from smoldering parts of the fire that did not get lofted high enough to be measurable by aircraft, which can cause smoke filled valleys at night and early morning (Selimovic et al., 2019), leading to some of the highest exposures for local residents.

The NASA ER-2 flew 11 science flights out of Palmdale, CA with ~70 science flight hours between 01 and 21 August 2019: flight tracks are shown in Figure 2. The ER-2 team, working with the DC-8 leads and the FIREX-AQ forecasting team, coordinated NASA ER-2 and NASA DC-8 aircraft over the Williams Flats fire, reachable by both aircraft, on 6, 7, and 8 August 2019. NASA ER-2 instruments captured the smoke development of the Williams Flats fire over the 3 days, and provided a variety of remote sensing observations of meteorological conditions and smoke heights prior to pyro-cumulonimbus clouds (pyroCbs) development captured by the NASA

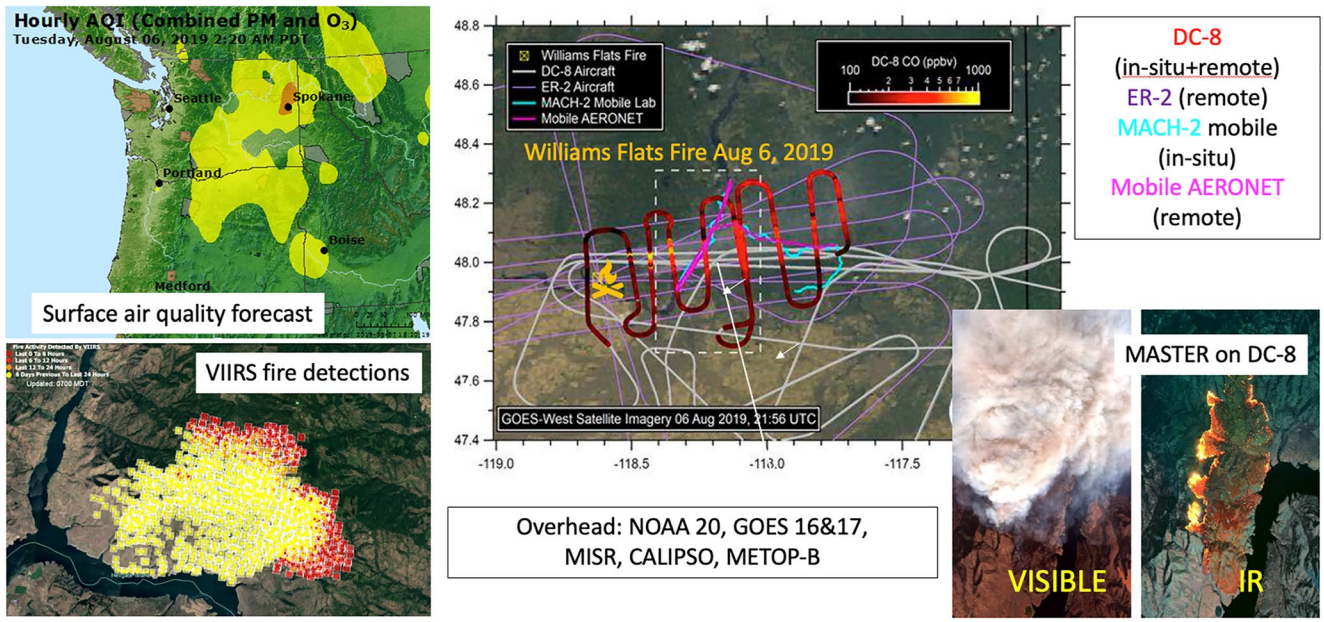

Figure 20. Coordination of multiple platforms at the Williams Flats fire on 6 August 2019 during FIREX-AQ.

DC-8 on 8 August 2019. NASA ER-2 and NASA DC-8 aircraft were coordinated under satellites on 6 August 2019, addressing the main NASA ER-2 goal to bridge in-situ and satellite observations. As fire activity moved to the Southwest, the NASA ER-2 shifted flight patterns to Arizona and Utah, coordinating again with NASA DC-8 aircraft over the Sheridan fire on 15 August 2019. The ER-2 team was also closely working with NOAA aircraft leads, and coordinated with the NOAA Chem Twin Otter aircraft over Little Bear and Ikes fires on August 20 and 21, 2019. NASA ER-2 flights were coordinated with satellites in a variety of smoke conditions to evaluate how well satellite retrievals can handle small-scale sub-pixel variabilities. The satellite coordination included NASA ER-2 flight legs on and parallel to satellite tracks to evaluate viewing angle uncertainties in satellite retrievals.

Figure 20 shows results from the most detailed coordination by several platforms during FIREX-AQ: DC-8, ER-2, LARGE mobile lab, mobile AERONET, and several satellite overpasses (NOAA20, GOES 16 and 17, VIIRS, MISR, CALIPSO, and METOP-B) on the Williams Flats fire on 06 August 2019. The top left shows that smoke was expected from the hourly AQI forecasting on that day and the routine air quality monitoring sites detected smoke around Spokane, WA. The fire was clearly detected by satellites as is demonstrated by the VIIRS fire detections shown in the left bottom of Figure 20. The flight and drive tracks of the DC-8, ER-2, MACH-2, mobile AERONET are shown in the center plot. The NASA DC-8 flew the typical pattern with a downward looking remote sensing overflight followed by several plume crossings. Images from the Williams Flats fire by the MASTER instrument on the DC-8 in the visible and IR are also shown in Figure 20. At the same time, the NASA ER-2 flew high above along the length of the plume six times and the DRAGONs and MACH-2 drove under the plume and aircraft for upward looking remote sensing and in-situ measurements. In addition to all the measurements during the fire, the fuels on the ground were sampled after the fire season by the Fuel2Fire team.

The comparison between the MACH-2 and the DC-8 during the 6 August 2019 sampling of the Williams Flats fire is shown in Figure 21. While the NASA DC-8 and ER-2 were completing longitudinal runs along the length of the smoke plume and cross-sectional transects across the width of the smoke plume, the MACH-2 and mobile AERONET platform drove from the southwest corner to the northeast corner of the dashed box as denoted by the blue and magenta traces in Figure 20. Similar aerosol optical measurements on the DC-8 and the MACH-2 allow for direct comparisons between remotely-sensed, vertically-resolved smoke backscatter and in situ extinction coefficients. For example, airborne HSRL curtains of calibrated aerosol backscatter coefficient that show the smoke plume being injected up to an altitude of roughly 2–3 km Above Ground Level (AGL) and then being subsequently mixed down to the surface (Figure 21a). The surface elevation in Figure 21a is given by the white trace. Meanwhile, the uncalibrated, attenuated backscatter curtain from MACH-2 zenith-point ceilometer in Figure 21c shows similar structure in the boundary layer height also extending up to about 2 km AGL with

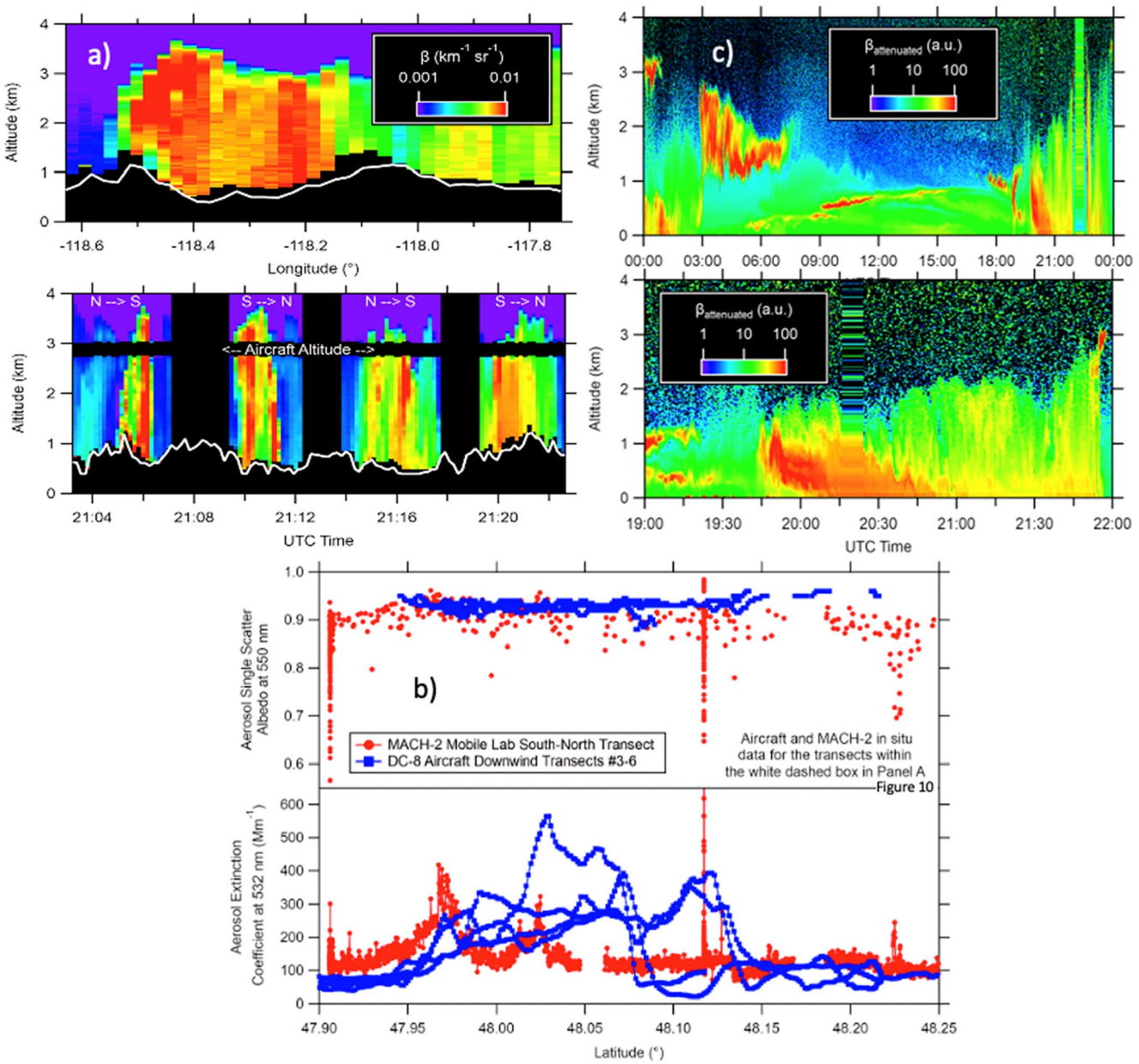

Figure 21. Comparison of the NASA MACH-2 with the DC-8 during the Williams Flats fire measurements on 6 August 2019. (a) DC-8 HSRL longitudinal (top) and cross-section (bottom) flight curtains. (b) MACH-2 ceilometer curtains for the day (top) and collocation times (bottom). (c) Comparison of in situ aerosol SSA and extinction measurements with DC-8 and MACH-2 within the white dashed box in Figure 20.

periods of elevated plumes and periods where the smoke mixed down to the surface. It should be noted here that the data in Figure 21 from the DC-8 is covering a large distance over a short time and the data from MACH-2 is covering a short distance over a long time. A direct comparison of select aerosol intensive and extensive aerosol optical properties is shown in Figure 21b for the complementary DC-8 and MACH-2 measurements. While the relatively slow-moving MACH-2 and fast-moving DC-8 are not spatially coordinated in time, the elevated background measurements are consistent with each other, as well as the aerosol single scattering albedo of approximately 0.9–0.95.

These early analyses of the combined airborne and ground-based mobile laboratory aerosol measurements demonstrate the power of lidar-based remote sensing for placing the measurement results in proper context. While the detailed information obtained from the HSRL is invaluable, it is worth noting that the layer height

information and un-calibrated attenuated aerosol backscatter structure from the ceilometer clearly show when the plume mixed down to the MACH-2 sampling level and when it did not.

3.6. Flight Planning and Sampling Strategies for Smaller Eastern Fires

Liu et al. (2016) analyzed 15 crop fires in the MRV sampled from the NASA DC-8 during SEAC^{4}RS in 2013 and emissions from those fires showed some statistically significant differences from previously published emissions estimates, indicating that crop residue fires are a diverse and globally understudied source. This motivated the second main objective for FIREX-AQ, which was to sample a large number of small mostly prescribed fires to build statistics on EFs and fuels, plume rise, satellite detectability, and integrated impacts for these types of sources.

Small fire activity occurred within the reach of the DC-8 every day during the Salina, KS deployment 19 August–3 September 2019. Flight planning for the small fire sampling drew on multiple sources of information including data on burning permits issued by state and local organizations, fire spotting by members of the Fuel2Fire team collecting fuels in the region, and weather forecasting specialized for prescribed fire conditions. With the important exceptions of several large prescribed burns that were coordinated in advance between Fuel2Fire and the responsible agencies, all of these planning tools could only indicate general regions where small fires were expected to occur. Near-real-time fire detections from GOES-16 provided essential guidance enabling the DC-8 to effectively sample as many fires as possible on each flight. The nowcasting team on the ground would inform the aircraft of current fire detections, which often happened in regional clusters, and the aircraft would re-direct to that location quickly, before the short-lived small agricultural fires had run their course.

The flight tracks of the NASA DC-8 for the southeastern small fires are shown in Figure 22 and the fires that were investigated are listed in Table 13 with more detail. The DC-8 conducted seven flights out of Salina, KS and investigated 87 different small fires in 12 states. The fires investigated included prescribed fires in prairies and forests, agricultural burning of corn, soybeans, and rice fields, slash and pile burning. The area around Kansas, Nebraska and Northern Texas has mostly rangeland and cropland, the MRV mostly cropland, and Louisiana, Georgia, Northern Florida mostly silviculture, cropland and wildland fires. In coordination with the respective land management agency, several larger prescribed fires were investigated in the southeast. The Blackwater River prescribed fire in the Florida Panhandle was in an oak and mature-longleaf pine forest with shrub-grass and litter understory. Several grass prairie prescribed fires were sampled during the growing season in Nebraska and Kansas in the Tallgrass Prairie National Reserve.

A photo of a typical fire is shown in Figure 22 taken just before the aircraft penetrated the plume at about 1,000 ft altitude above ground right over the fire. Most fire plumes were crossed at least two times in two different directions. For some fires the plume was crossed at different altitudes as well. The time series of CO in Figure 22 for a section of the flight on 31 August 2019 shows that very high mixing ratios of trace gases and aerosol (up to 20 ppm of CO) were observed in the plumes, which were only a few seconds wide. The high frequency measurements on the aircraft as shown in Table 3 were essential for the precise determination of emission ratios and factors in such short plume encounters.

The MCE from the small fires, shown in Figure 23, varied greatly between the various southeastern burns due to the different fire stages and also fuel type, but in general corn fields burn at a higher MCE than land clearing, grassland fires or pile burning. The timeseries also shows the high variability in MCE and resulting CO, CO_2, and NO emissions. Shown are 13 s of data that included two separate plume crossings from two adjacent corn fields, which had very different CO/CO_2 and CO/NO ratios.

4. Data From FIREX-AQ 2019

4.1. Plume Identification and Smoke Age Calculation

A detailed description of each smoke transect is available on the FIREX-AQ data archive. CO and BC enhancements above the background were used to identify and flag all of the sampled smoke plume transects. The start and end times of the plume, the fire, fuel, ignition, and transect type were determined together with the fire name or source. For each of these transects, the MCE was also calculated and provided.

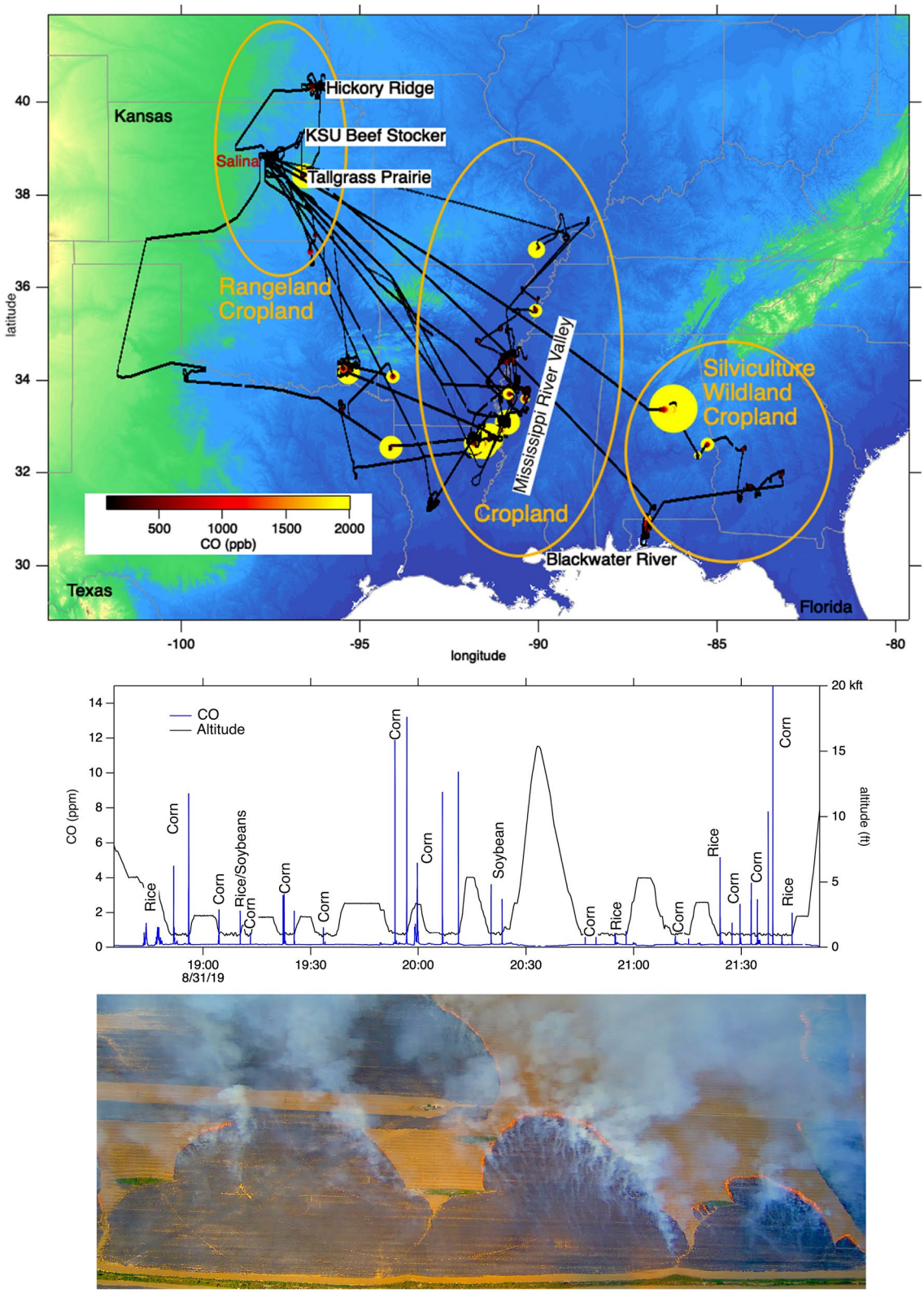

Figure 22. (Top) Flight tracks of the NASA DC-8 color and size coded by CO for the FIREX-AQ eastern fire portion flown out of Salina, KS. (middle) The time series of CO for a section of the flight from 31 August 2019 that investigated 15 small agricultural fires from mostly corn fields. (bottom) A photo of a typical fire.

Table 13
Small Fires Investigated During FIREX-AQ by the NASA DC-8 From Salina, KS

State	Latitude	Longitude	Major fuel	Detailed fuel type
08/21/2019				
TX	34.0575	−99.8753	Forest	Mesquite savanna
TX	34.1602	−99.7702	Savanna	Post-blackjack oak forest/Mesquite savanna
TX	32.5380	−94.1157	Slash	Silviculture: conifer slash (minimal piles), post harvest
TX	32.6473	−94.3526	Pile	Land clearing of grass, shrub, young trees mix
LA	32.7412	−91.3834	Cropland	Corn
LA	32.6653	−91.2677	Cropland	Corn
LA	32.5442	−91.4962	Urban/Barren	House
LA	32.6006	−91.5481	Cropland	Corn
LA	32.6247	−91.7975	Cropland	Corn
MS	32.8147	−90.9172	Cropland	Corn
MS	32.7792	−90.9529	Cropland	Corn
MS	33.0429	−90.8815	Cropland	Corn
MS	33.1205	−90.8801	Cropland	Corn
08/23/2019				
MS	33.6811	−90.3483	Cropland	Corn
MS	33.5939	−90.3648	Cropland	Corn
MS	33.1014	−90.8664	Cropland	Corn
MS	33.1293	−90.8964	Pile	Silviculture: Pile (mixed deciduous/coniferous), post harvest
MS	32.9036	−91.0292	Cropland	Corn
LA	32.7511	−91.3865	Cropland	Soybean
LA	32.8191	−91.4972	Shrubland	Uncertain - found mixed shrub and rice near
LA	32.6100	−91.5408	Cropland	Corn
LA	32.6219	−91.7284	Cropland	Corn
LA	32.5856	−91.8398	Cropland	Corn
AR	34.4652	−90.8945	Cropland	Corn
MS	33.8409	−90.6277	Cropland	Rice
MS	33.7486	−90.3361	Cropland	Corn
08/26/2019				
OK	34.1538	−95.3132	Slash	Silviculture: slash, piles, mixed (deciduous/coniferous), post harvest
AR	34.0675	−94.0568	Slash	Silviculture: slash, piles, mixed (deciduous/coniferous), post harvest
TX	33.34108	−95.48532	Cropland	Corn
LA	32.4413	−91.7402	Cropland	Corn
LA	32.4490	−91.8393	Cropland	Corn
LA	32.5623	−91.8286	Cropland	Corn
LA	32.6317	−91.7834	Cropland	Corn
LA	32.7603	−91.3526	Cropland	Corn
OK	34.2237	−95.451	Forest	Prescribed severe and understory, mature not harvested and young coniferous pine timber w/deciduous - some accidental
OK	34.1538	−95.3132	Slash	Silviculture: slash, piles, and understory; coniferous/deciduous mix
08/29/2019				
NE	40.3142	−96.3607	Grassland	Green growing season grass (not dry)
KS	38.4107	−96.5549	Grassland	Tallgrass Prairie, Green growing season grass (not dry)

Table 13
Continued

State	Latitude	Longitude	Major fuel	Detailed fuel type
KS	38.8749	−97.4115	Pile	Vegetation, trash, and/or BBQ
KS	38.8453	−97.4501	Cropland	Rice
KS	38.8685	−97.3258	Cropland	Fallow winter wheat
OK	36.7578	−96.373	Grassland	Pasture
OK	36.8521	−96.319	Grassland	Pasture, shrub, timber litter
KS	37.0902	−96.2498	Grassland	Pasture
08/30/2019				
FL	30.9779	−86.9288	Understory	Blackwater River Prescription: primarily shrubs, grasses and litter from loblolly-longleaf-slash pine, willow-laurel-turkey-water oak, and magnolia forest
GA	32.0596	−83.1305	Shrubland	Land clearing, shrub, grass, coniferous
GA	31.9658	−83.189	Pile	Longleaf pine w/tree stump
GA	31.8816	−83.5098	Slash	Near mixed coniferous, deciduous silviculture
GA	31.5406	−83.8855	Slash	Land clearing, mix deciduous coniferous
GA	31.712	−84.086	Cropland	Corn
GA	31.7416	−84.0305	Cropland	Corn
GA	31.4995	−84.3223	Pile	Piles next to pecan fields and slash mixed forest, post cleared
GA	31.7416	−84.0305	Cropland	Corn
GA	32.5132	−84.2492	Cropland	Corn
AL	32.6060	−85.2553	Slash	Land clearing of mixed deciduous/coniferous forest, slash with piles, post harvest
AL	32.3715	−85.5115	Slash	Silviculture: slash, piles, mixed (deciduous/coniferous), post harvest
AL	33.3762	−86.2203	Slash	Silviculture: conifer slash (minimal piles), post harvest
8/31/2019				
MS	33.1391	−90.9207	Cropland	Rice
MS	33.0937	−90.8297	Cropland	Corn
MS	33.3493	−90.3351	Cropland	Corn
MS	33.3016	−90.5021	Cropland	Soybean and grass
MS	33.6099	−91.0219	Cropland	Corn
AR	33.9333	−91.4202	Cropland	Corn and soybean
AR	33.8983	−91.4059	Cropland	Soybean
AR	34.5803	−90.7037	Cropland	Corn
AR	35.0924	−90.8554	Cropland	Soybean
MS	33.8936	−90.6083	Cropland	Corn
MS	34.0614	−90.5754	Cropland	Rice
MS	33.1535	−91.025	Cropland	Rice
MS	33.1501	−90.8568	Cropland	Corn
MS	33.0777	−90.8157	Cropland	Corn
LA	31.3626	−92.9486	Slash	Silviculture: conifer slash (minimal piles), post harvest
9/3/2109				
MO	36.8085	−90.0508	Cropland	Corn
MO	36.9949	−90.0102	Shrubland	Shrubs, grass
IL	37.4367	−88.6022	Cropland	Rice
AR	35.9493	−90.4444	Cropland	Corn

Table 13
Continued

State	Latitude	Longitude	Major fuel	Detailed fuel type
AR	35.7377	−90.0215	Cropland	Rice
AR	35.5140	−90.0742	Cropland	Rice
AR	35.5194	−90.6233	Cropland	Rice
AR	35.526	−90.7043	Pile	Land clearing, mix deciduous coniferous
AR	35.0903	−91.0314	Pile	Shrubs, grass, crop residue
AR	34.8254	−91.686	Cropland	Corn
AR	34.4610	−90.7637	Cropland	Corn
AR	34.4006	−90.6913	Cropland	Rice
MS	33.8584	−90.7738	Cropland	Rice
MS	33.7019	−90.777	Cropland	Corn
MS	33.6976	−90.803	Cropland	Corn
MS	33.69036	−90.8265	Cropland	Corn w/rice
MS	33.5931	−90.7076	Cropland	Corn

The physical age of smoke, meaning the time elapsed since the smoke was produced in a fire, is a critical parameter for understanding the chemical aging of fire emissions. For each transect as described above, two methods of estimating smoke physical age at the time of sampling by aircraft were used during FIREX-AQ. The first method used the mean horizontal wind speed, as measured on the aircraft in the vicinity of the fire on each flight day. Using this wind speed, the smoke age was inferred from the distance between the fire and the center point of a smoke plume transect. The second method used the HYSPLIT model (Stein et al., 2015) to compute air parcel back trajectories from the aircraft to the upwind source fire. Smoke ages were determined with trajectories from multiple high-resolution meteorological datasets (HRRR 3 km, NAM CONUS Nest 3 km, and GFS 0.25°), which were then averaged, plus time for buoyant plume rise (at 7 m s^{-1} mean vertical velocity (Clark et al., 1996; Lareau & Clements, 2017)). Uncertainties in the smoke ages are assessed from the range of ages between meteorological datasets, mismatch between measured and modeled winds, and trajectory spatial error in missing the known fire source.

While the first method for estimating smoke age benefits from accurate wind measurements, it assumes that winds are homogeneous in space and time during the plume transport, which can systematically bias the age estimates. In FIREX-AQ these systematic biases are most commonly due to wind changes during the day-to-night transition. The second method accounts for spatial and temporal variations in winds, but is susceptible to errors in the meteorological model. Through careful comparison of the simulated trajectories to smoke transport observed from geostationary satellites, however, periods with large meteorological errors can be identified and removed from calculations to improve the smoke age estimates. The two methods of estimating smoke age (trajectory-based and mean wind-based) typically differ by 27% (median absolute difference) for smoke plume ages up to several hours. The ensemble statistics of trajectories with different meteorological fields can also identify periods when the smoke age uncertainties are likely greater. Figure 24 shows the flight track color coded with physical plume age on top of a GOES17 smoke image of the Williams Flats fire.

4.2. Fuels and Fuel Consumption

The Fuel2Fire team provided detailed fire and fuels information post-mission such as FRP, burned area, fuels, total daily and 1-s carbon emissions, diurnal fire cycles for each western fire, and other related data products for both the western wildland fires and the southeastern prescribed, silviculture, and cropland fires. The fuel type for forest and shrublands was determined using the FCCS database, and cropland fires were classified using the Cropland Data Layer and videos from the DC-8 overflights. A subset of the fire and fuel information is shown in Tables 2 and 13 for fires investigated by each platform in this manuscript. The goal was to connect the fuels and fire burning on the ground to the smoke composition measured by the DC-8 to improve modeling of impacts on chemistry, air quality, and health.

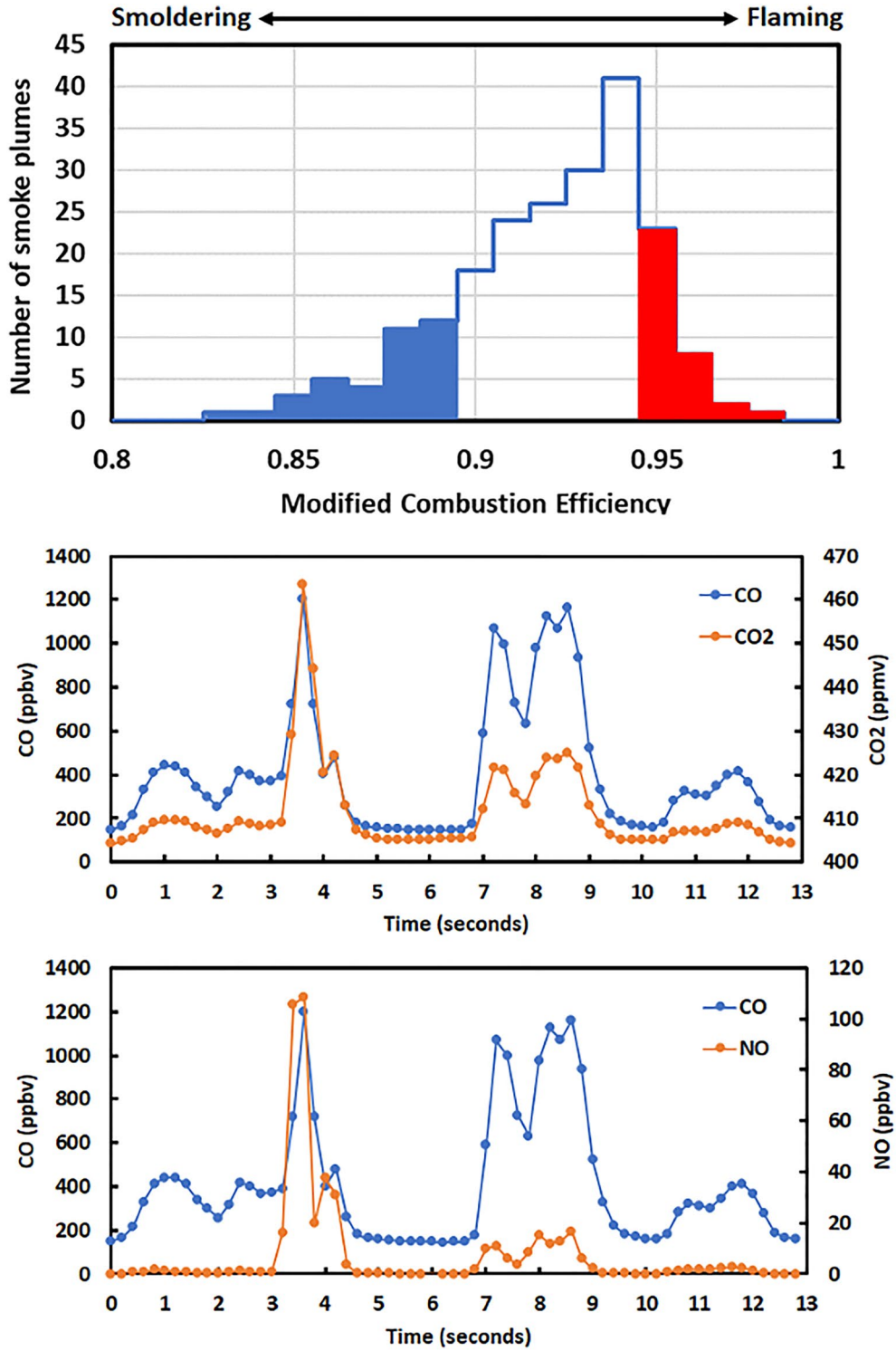

Figure 23. The modified combustion efficiency (MCE) of all the southeastern small fires. Highest MCE values shown in red are dominated by crop fires, while lowest MCE values shown in blue are dominated by land clearing, green grassland fires, and pile burning. An example timeseries of CO, CO_2, and NO of two smoke plumes from adjacent fields demonstrates the varying chemical signatures with changes in MCE.

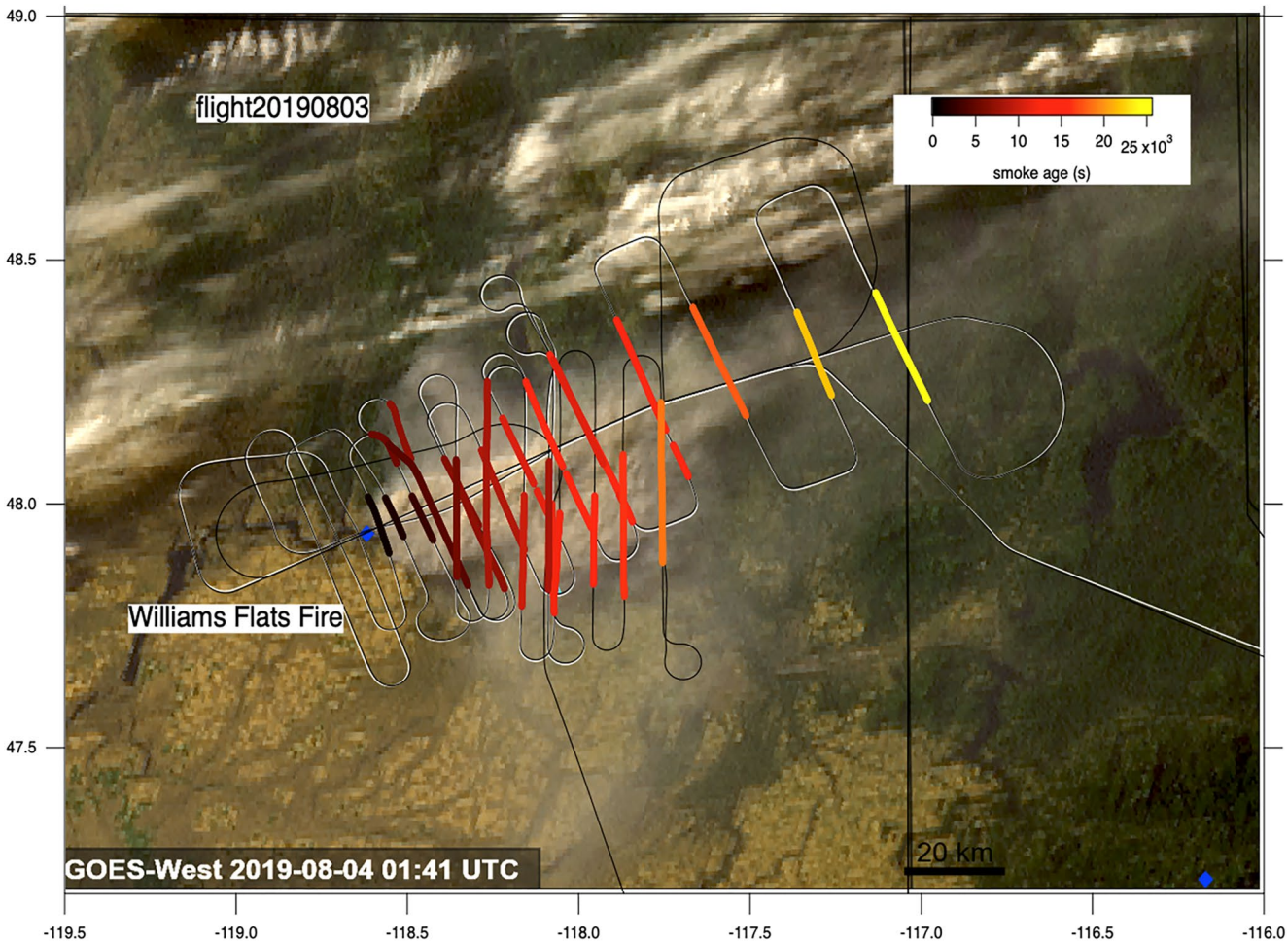

Figure 24. The flight track of the NASA DC-8 on 3 August 2019 color coded with the physical plume age calculated with the trajectory method.

For the western campaign, Fuel2Fire provided daily post-fire data for every fire flown on the fuels and burned area, fire behavior, and daily 1-s carbon emissions. Fuel types can change as fires burn across a landscape (Figure 25), and the amount of fuel burned is dependent on what is available or dry enough to burn, under the control of cumulative fire weather (temperature, wind speed, precipitation and RH). Using the Williams Flats fire as an example, burned area is greater on 3 August 2019 (fire weather High), but the amount of fuel consumed is greater on 6 August 2019 (fire weather Very High). The diurnal cycle and relative energy released by a fire is also under the control of fire weather conditions. Typically fire fuel consumption rates peak in the late afternoon when temperatures are highest and RH is the lowest (Figure 25).

Post-fire analysis for the eastern campaign included fire location identification using Google Earth and the DC-8 flight videos, as well as ecosystem-specific data. The diversity of fires sampled during this 7-day period includes: 5 crop types, slash and pile burning, silviculture, grassland, understory, pasture, and several prescribed fires (e.g., Tallgrass prairies) (Table 13). The Blackwater River State Forest prescribed understory fire was sampled in detail before and after the fire to gather detailed fuels data to connect to satellite data and chemistry.

4.3. Satellite Data

While satellite data are publicly available, a subset of satellite products are archived to facilitate analysis of the FIREX-AQ observations. This includes active fire detections from both polar orbiting and geostationary satellites provided through the Wildfire Automated Biomass Burning Algorithm (WF-ABBA) processing system. Polar orbiting data available from the VIIRS sensor onboard the Suomi National Polar-orbiting Partnership and NOAA-20 Joint Polar Satellite System (JPSS-1) satellites. Geostationary data are available from the Advanced Baseline

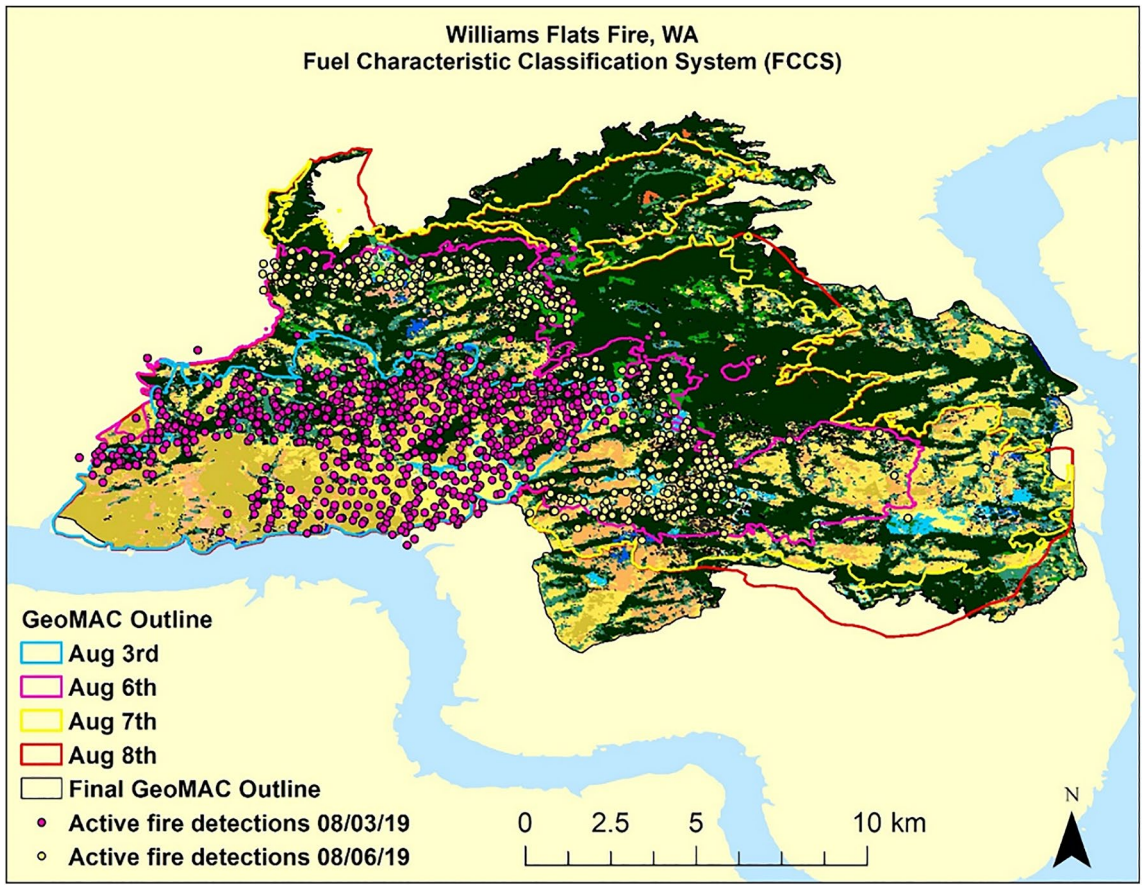

Figure 25. Ecosystem types for the Williams Flats fire. Thirty eight different fuel types are mapped at 30-m resolution for the Williams Flats fire using the FCCS database. All the GeoMAC perimeter maps are shown with active fires overlaid on 3 and 6 August, highlighting the unique fuels combusted on different days as the fire burns across the landscape. On 3 August, the primary fuels burned were in grasslands (beige colors), and in contrast, the primary fuels burned on the 6th are forests (green colors).

Imager (ABI) sensors onboard GOES-16 (East) and GOES-17 (West). Time-resolved FRP from these assets relevant to FIREX-AQ in-situ and remotely sensed fires is also included in the data archive.

Satellite visible imagery is also of great value given that the flight paths alone do not convey the dynamic nature of fire plume evolution. True color imagery from GOES-16 and GOES-17 are available on the FIREX-AQ archive as still images and movies for all the sampled western wildfires and a few selected eastern fires. Each image is overlaid with the aircraft locations and flight paths until that point in time.

5. Emerging Results From FIREX-AQ

5.1. Emissions

A major science goal of FIREX-AQ was to improve estimates of BB gas and aerosol emissions and their representation in models. To enable a detailed assessment of emissions based on the FIREX-AQ in situ observations, a key element was daily total carbon emissions estimates provided by the Fuel2Fire team for the specific fires sampled by the DC-8 aircraft. These emissions estimates were grounded in observed and estimated fuel consumption and temporally distributed with a diurnal variation proportional to the FRP observed by the GOES satellites. Along with the plume age calculations, these emissions could then be related to specific cross-plume sampling transects downwind of the fires.

As a first step, Wiggins et al. (2020) were able to show that between consecutive transects the relative trend in FRP was correlated to the relative trend in conserved smoke tracers (CO_2, CO, and BC aerosol). Thus, when continuously available, FRP measurements can be used to account for changes in the amount of emissions and

these changes have to be considered together with dilution and chemistry in the transported fire plumes. This work only looked at the relative rate of change, but did not directly estimate the magnitude of emissions.

To more fully evaluate Fuel2Fire estimated emissions versus emission fluxes based on airborne observations, HSRL lidar data were necessary to extrapolate in situ observations across the full cross section of the plume at each downwind distance in combination with transport speeds based on wind observations. Two independent emissions assessments based on DC-8 observations were conducted by Wiggins et al. (2021) and Stockwell et al. (2022). While each assessment took a slightly different approach, both found reasonable agreement across all western wildfires between Fuel2Fire emissions estimates and their own based on airborne observations with regression slopes of 1.15 ($r^2 = 0.83$) and 1.33 ($r^2 = 0.92$), respectively.

Stockwell et al. (2022) focused on total carbon emissions from in-situ observations and HSRL lidar data, which provide the most direct comparison with the Fuel2Fire inventory, and also compared in situ estimated emissions broadly to existing model inventories of total carbon. The FIREX-AQ in situ and Fuel2Fire emissions estimates compared the best to the top-down FRP-based inventories (GFAS, QFED, and FEER), while bottom-up inventories (FINN, GFED, and 3BEM) tended to underestimate emissions. Two other experimental inventories (GBBEP and HRRR) exhibited strong overestimates.

Using the continuous, time-resolved GOES FRP product from the Fuel2Fire team, Stockwell et al. (2022) also provide a comprehensive set of smoke emission coefficients for 88 trace gas and aerosol components of smoke from western wildfires. While smoke coefficients have been reported in the literature for bulk aerosol, the FIREX-AQ data provide the first such information for many of the trace gas species and specific aerosol components.

Wiggins et al. (2021) focused on aerosol emissions, assessing uncertainty in bottom-up emissions through comparison to the GFED4.1s and in top-down emissions to the FEERv1.0 inventory. For GFED, the average aerosol EF calculated from the FIREX-AQ in situ observations agreed well with GFED. For FEER, the smoke emission coefficient was estimated by regressing estimated emissions versus GOES FRP for the in situ estimated emissions, Fuel2Fire emissions, and a lidar-based estimate using lidar AOD. The estimates from these high-resolution inventories were all lower than the FEER value, but still within the large statistical uncertainties. Two potential causes for this difference were the use of MODIS FRP instead of temporally resolved GOES FRP and the used constant mass extinction efficiency (MEE) instead of one that is increasing with smoke age as observed on the DC-8. This result raised the question of whether top-down methods are more vulnerable to uncertainties in MEE than previously thought.

FIREX-AQ data are contributing a very comprehensive set of EFs for use in models. FIREX-AQ consistently sampled a large number of fires with a larger suite of instruments than previous experiments. Emission factors for the western wildfires (Gkatzelis et al., in prep) largely corroborate results from FireLab and recent compilations from SEAC^{4}RS (Liu et al., 2017), WE-CAN (Permar et al., 2021), and the literature update of Andreae (2019) for temperate forest EFs. For the smaller eastern fires Travis et al., (in prep), is providing valuable information on the diversity of fuels (e.g., corn, rice, soybeans, grass, land-clearing) and how these fuels differ in expected MCE and resulting EFs. Method advancements allowed the AMS to report EFs for submicron potassium and organic sulfur with high time resolution and estimate their EFs, both for wildfires and agricultural fires (Guo et al., 2021).

Ground measurements from the AML enabled an assessment of VOC emissions from near-field sampling of seven western wildfires (Majluf et al., 2022). Emissions ratios for 240 mass spectral signals were calculated and evaluated using PMF to identify two factors relating to high and low temperature pyrolysis. These factors corroborated the temperature dependent factors obtained by Sekimoto et al. (2018) from the FireLab. These factors indicate processes that cannot be discriminated using MCE.

5.2. Plume Chemistry

Fire emissions undergo rapid changes in the near field and continue to evolve as smoke ages and is transported downwind. These changes are particularly important for understanding impacts on air quality, climate, ozone production, and the evolution of aerosol abundance, composition, and optical properties. FIREX-AQ provided an opportunity to look at these impacts through both observational constraints and model evaluation of observed changes.

5.2.1. Role of HONO

The importance of HONO from fires has been well established and several FIREX-AQ publications address the dominant role of HONO in the rapid chemical changes occurring in the first few hours after emission. FIREX-AQ observations suggest that subsequent chemical production of HONO is also important (Chai et al., 2021). Using stable isotopes of oxygen and nitrogen in HONO from the NASA MACH-2, Chai et al. (2021) provided evidence for significant secondary production in near-ground smoke samples in both daytime and nighttime smoke. Additional analysis of the NASA MACH-2 observations of HONO by Kaspari et al. (2021) showed that HONO was not depleted in far-field smoke compared to near-field smoke sampled at ground level. While ground-surface chemistry is expected to play a significant role in these observations, conditions aloft are also expected to contribute to HONO production when dense smoke with sufficient particle surface area is present. Secondary production of HONO in fresh smoke plumes is corroborated by large eddy simulations of near-field smoke evolution by Wang et al. (2021). Using FIREX-AQ observations for comparison, the model captures the strong variability in HONO across the plume due to the variation in photolysis rates between the well-lit plume edges and the darker conditions in the center and lower parts of dense plumes. To capture the observed downwind gradient in total HONO, the model requires a secondary heterogeneous source constrained by aerosol uptake of NO_2. This secondary chemistry is able to best reproduce the downwind decay in total HONO as compared to simply increasing expected emissions. Even when increasing HONO emissions by a factor of five to match observed HONO concentrations in the smoke sampling transects closest to the fire, the decay is still more rapid than that observed across subsequent downwind transects (Wang et al., 2021).

5.2.2. Ozone Production

Several FIREX-AQ studies advanced understanding of ozone production in fire plumes. As shown by Akagi et al. (2013) a large range of ozone formation rates and total ozone formed were observed in various fire plumes during several field experiments. Prior to FIREX-AQ, the reasons for the large variation in ozone formation rates were not well understood, but clearly depended on fuel specific emissions, VOC/NO_x ratios, meteorology, and plume thickness influencing the light availability (Akagi et al., 2012; de Gouw et al., 2006; Jaffe & Wigder, 2012; Yokelson et al., 2009).

Using the detailed observations from FIREX-AQ, Xu et al. (2021) provided the first observationally constrained analysis of near-field daytime ozone production in fire plumes by recognizing that individual crosswind smoke sampling transects provide a continuum between fresher (plume center, slower photochemistry) and more aged (plume edge, faster photochemistry) air. The similarity in physical age across each perpendicular transect allows the spectrum of chemical age to be interpreted without the need to consider changes in fire state and emissions that complicate a comparison between consecutive downwind transects. Twenty-five "Single Transect Analyses" were identified with adequate physical conditions and chemical gradients to estimate ozone production. These analyses used observationally estimated OH exposure, VOC reactivity, and peroxy radical fate (based on ratios of organic peroxides to hydroxynitrates) to calculate O_x chemical closure ($O_x = O_3 + NO_2 + HNO_3$ + peroxyacylnitrates + particulate nitrate). The resulting agreement between observationally estimated O_x production and observed changes in O_x enabled a deeper evaluation of near-field photochemistry resulting in a parameterization of $O_3 + NO_2$ production for use in models. The parameterization accounts for both the initial NO_2 emissions (dependent on MCE) and the subsequent photochemical production of O_3 (dependent on OH exposure) (Xu et al., 2021). This parameterization is intended to enable Chemical Transport Models to incorporate near-field ozone production that primarily occurs at subgrid scales.

An important aspect of fire plume chemistry is the potential for extreme variability in actinic flux throughout the plume. To look deeper into the range of chemical conditions in fire plumes, Decker et al. (2021) examined evidence for "dark chemistry" both during the day and night for plumes sampled by the Twin Otter and DC-8. They found evidence for NO_3 chemistry at all times of day due to the reactivity of NO_3 radicals in fire plumes that is orders of magnitude larger than urban or forested environments. In terms of BB VOC oxidation, NO_3 was found to be important mainly for phenolic compounds and was competitive with OH and O_3 even during the day. Thus, NO_3 chemistry was found to be an important element to understanding SOA and BrC formation in fire plumes.

Recognizing that fire emissions often peak in the late afternoon and extend into the evening, Robinson et al. (2021) investigated the time-of-day dependence of plume chemistry. Using a 0-D box model approach, key differences in the rate and NO_x-VOC sensitivity of O_3 production were identified. In typical afternoon conditions, O_3 production

and NO_x depletion occurred extremely rapidly following emission (~20 min) with HONO and formaldehyde photolysis being the dominant radical sources. The near-field transition from VOC-sensitive to NO_x-sensitive conditions for ozone production was similar for afternoon versus evening plumes, although on average the NO_x depletion occurred more rapidly for afternoon plumes. The O_3 to CO ratio subsequent to the most rapid phase of the O_3 production varied strongly with time of day and was larger on average for afternoon than evening plumes.

5.2.3. Aerosol Chemistry and Physics

The complexity of the near-field environment for aerosol chemistry was investigated from a number of perspectives, including emissions, trends in BrC absorption, and organic aerosol volatility. Considering that secondary production of BrC in smoke plumes is competing with multiple loss processes (evaporation, chemical processing, and photobleaching) it is perhaps not surprising that both the DC-8 and Chem Otter observed wildly variable trends in normalized BrC concentrations, with increasing, relatively constant, and decreasing trends in dilution-corrected BrC observed during the first few hours of downwind transport and evolution (Washenfelder et al., 2022; Zeng et al., 2022).

The need to better understand the components of BrC and their chemistry is highlighted in a case study from the Sheridan fire which provided the opportunity to sample a descending smoke plume with an associated downwind temperature increase of 15° (287–302K). Across this temperature gradient, evaporation was shown to decrease 4-nitrocatechol by two-thirds while total BrC absorption was unchanged (Zeng et al., 2022). Despite the clear decrease in normalized OA mass as temperature increased during this plume transect, the normalized absorption by BrC measured with a photoacoustic spectrometer was essentially constant. Zeng et al. (2022) note that 4-nitrocatechol is a major contributor to BrC, which means there must have been substantial production of additional chromophores to maintain nearly constant absorption. Washenfelder et al. (2022) found that 4-nitrocatechol accounted for a much smaller fraction of BrC absorption in selected smoke plumes sampled from the Chem Twin Otter during FIREX-AQ than was found from an analysis of WE-CAN plumes discussed by Palm et al. (2020). Washenfelder et al. (2022) suggested that BrC arises from a much larger number of chromophores with a complex time evolution that includes both primary and secondary sources, a change from the previous view of BrC as having a well-defined lifetime from limited prior aircraft work (Forrister et al., 2015).

In spite of the near-field complexity in aerosol chemistry, clear evidence for decreasing absorption in smoke sampled over longer aging further downwind was lacking. Figure S11 in Supporting Information S1 shows the initial aerosol Angstrom exponent (AAE) in FireLab smoke that was about 5 s old (Selimovic et al., 2018), where AAE is expected to scale with BrC fractional absorption contributions. Figure S11 in Supporting Information S1 also shows the trend in AAE values for four precisely aged and isolated smoke plumes that impacted Missoula in 2017–2019. The youngest smoke was from the Rice Ridge Fire in 2017 and other plumes were wildfire season prescribed fires, one in 2018 and two in 2019. Note that in contrast to brief airborne plume transects, the Missoula measurements benefit from hours of signal averaging at a reasonably narrow range of physical age. The data indicate a decrease in AAE with a half-life of about 10 hr. Airborne data are more scattered and sometimes in thicker smoke but are not inconsistent with the UM ground-based trend (Forrister et al., 2015; Selimovic et al., 2020).

Diversity in near-field observations during FIREX-AQ imply that both the initial AAE and subsequent evolution in the first few hours substantially broaden the range of AAE values that can be expected in downwind observations. With only three opportunities during FIREX-AQ to sample smoke 1 day after emission, it is difficult to determine whether the complexity in downwind behavior is entirely due to differences in near-field conditions.

The complexity in BrC absorption is further examined by Jordan et al. (2022) based on in situ hyperspectral absorption (300–700 nm) measurements taken from the LARGE mobile lab. Results show that the spectral curvature in absorption as a function of wavelength is better represented by a second order polynomial than the linear AE fit commonly used for observations at a few discrete wavelengths. Even when second order polynomials are applied, remaining deviations from the fit can differ substantially from fire to fire. These deviations also occur across the full wavelength range, not just the shorter visible and near-UV wavelengths. While the exact nature of these spectral details remains to be understood, they do provide a potential path for understanding the observed diversity in BrC absorption behavior.

A more comprehensive assessment of OA volatility was made possible by measurements using a thermal denuder coupled to an AMS and Extractive Electrospray Ionization Time-of-Flight Spectrometer (EESI-MS) (Pagonis et al., 2021). These measurements allow for the relative roles of temperature and dilution to be tested along with

changes in aerosol composition in the ambient atmosphere for comparison with expectations from laboratory and ground studies.

The efficiency of smoke aerosol mass at producing light extinction and scattering (mass extinction efficiency and mass scattering efficiency) was studied by Saide et al. (2022). It was found that mid-visible smoke MEE can change from 2.5 to 3.2 m^2/g for fresh smoke (<2 hr old) to 6–7 m^2/g for one-day-old smoke emitted on the day the Williams Flats fire was showing its most extreme behavior. While increases in aerosol size partially explained this trend, changes in the real part of the aerosol refractive index (real(n)) were necessary to provide full closure assuming Mie theory. Real(n) estimates from multiple days were found to be positively correlated with organic aerosol oxidation state and negatively correlated with smoke volatility. Future studies should focus on better understanding and parameterizing these relationships to fully represent smoke aging.

Adding further to understanding of the complexity of aerosol composition in fire plumes, Adachi et al. (2022) identified fine ash-bearing particles, which represent a small, but significant, component of aerosol mass and number. This identification was made possible through analysis of filter samples with both transmission electron microscopy and ion chromatography. While ash is often recognized as a contributor to coarse particle emissions, these fine ash particles composed mainly of Ca and Mg carbonates are carried much further downwind, with implications for BB aerosol indirect effects for example, as ice nuclei. Overall, fine ash was found to account for ~8% and 5% of aerosol number and mass in smoke plumes. The fine ash component was observed in both the western wildfires and eastern agricultural burning plumes.

5.3. Improving Models and the Importance Satellite Observations

One of the stated goals for FIREX-AQ was to evaluate and improve the ability of models to predict fire impacts on local to regional scales. A first step toward this goal was the comparison of 12 forecast models performed by Ye et al. (2021). The comparison focused on the multi-day sampling of the Williams Flats fire to evaluate model differences in fire emissions, plume injection height, diurnal cycle of emissions, initialization time, chemical mechanisms, satellite AOD assimilation, treatment of aerosol processes, and boundary conditions. Given the diversity in the models, the resulting recommendations were generally applicable rather than specific to any particular model. In terms of emissions, a major limitation relates to the use of fixed diurnal emission cycles. The adoption of satellite FRP-based emissions and diurnal variation were highlighted as an important path for improvement. Assimilation of satellite AOD was also shown to benefit model forecasts, leading to better predictions of smoke AOD. Smoke AOD was not a good indicator of model performance for surface $PM_{2.5}$ concentration, raising the importance of representing plume rise and the subsequent vertical distribution of smoke. The use of persistence for emissions is a problem across all models, especially for days with drastic fire growth. A potential way to reduce the impact of the persistence assumption would be to more frequently integrate satellite-based updates to emissions, but such solutions are not trivial to implement.

In a specific case study, better WRF-Chem (v3.5.1) performance was demonstrated by Kumar et al. (2022) after adopting FRP-based fire emissions and plume rise estimation (adopted from HRRR-Smoke (Ahmadov et al., 2017)) as well as diurnal emissions profiles based on mean FRP profiles for three longitude bands across North America. Incorporation of FRP-based emissions was shown to have the greatest impact, raising emissions by a few orders of magnitude above the severely underestimated values provided by 3BEM (Brazilian Burning Emission Model), which is the burned area, bottom-up approach normally used in WRF-Chem (Freitas et al., 2011). Also important was the improved diurnal cycle of emissions, which was better suited for western wildfires rather than the Amazonian fire cycle used in the base model. The impact of FRP-based plume rise was more subtle without clear evidence for improved performance.

Thapa et al. (2022) took a closer look at the commonly used plume rise parameterization in WRF-Chem and HRRR-Smoke from Freitas et al. (2007). Using Active Fire Area and FRP measured by the MASTER instrument during overflights by the DC-8, Fire Radiative Energy (FRE) was calculated and compared to the model estimates. Modeled FRE exhibited a much wider range across different fuels than was seen in the observations. Observed values fell within the range of model values for savannah and grassland, despite many of the western wildfires including forest for which model estimates were significantly high. This contributed to an overprediction of smoke injection height into the free troposphere. HSRL data revealed that smoke lofted into the free troposphere for 37% of fire plumes, while the model predicted this condition for 80%–95% of the plumes between

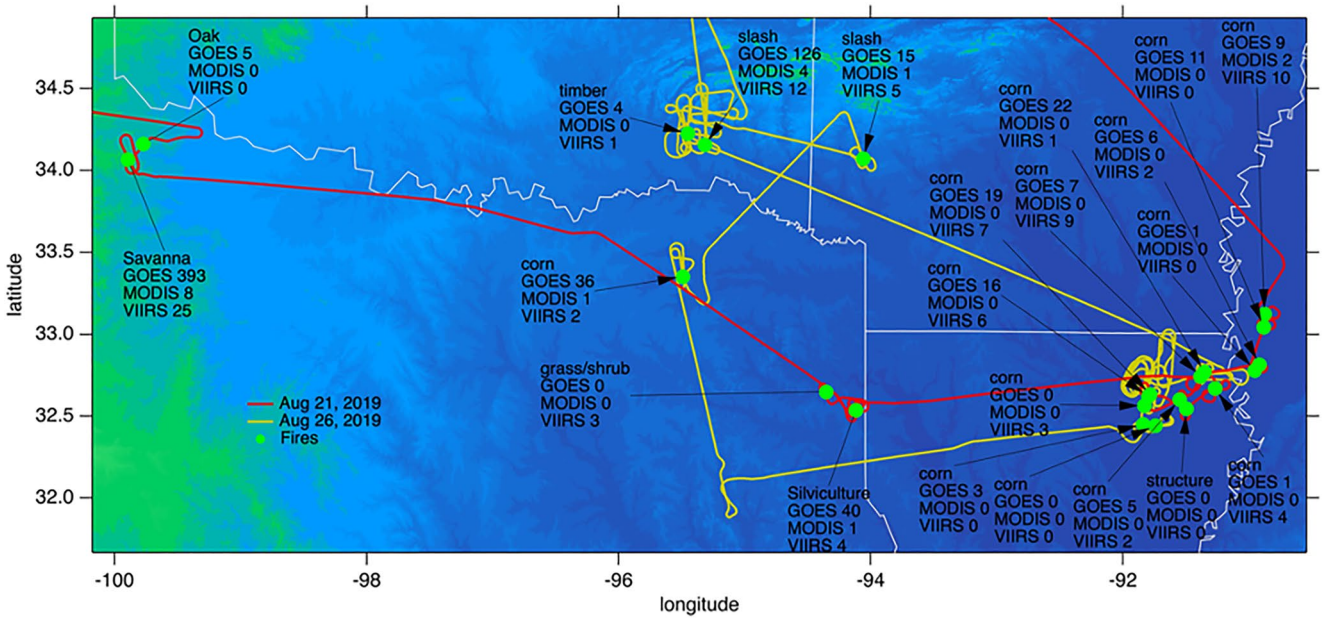

Figure 26. Two flight tracks from the eastern fires sampled on 21 and 26 August 2019, highlight the improved capability of satellites to detect small fires. The fuel type and the number of satellite detects from GOES, MODIS, and VIIRS is indicated for each sampled fire.

the two models. Adjusting model calculations based on observed FRE resulted in fewer injections to the free troposphere but did not entirely eliminate the bias.

Ye et al. (2022) further addressed model plume rise by examining the vertical distribution of smoke in WRF-Chem. Taking four observed cases of smoke reaching into the free troposphere identified by Thapa et al. (2022), the vertical distribution of fire emissions was constrained with an inversion system used to assimilate HSRL observations. These constrained runs were compared to base runs using the Freitas et al. (2007) parameterization. While the base runs apportioned the smoke roughly equally between the boundary layer and free troposphere, the constrained runs showed that more than 80% of the smoke was reaching the free troposphere in each of the four cases. Despite an evaluation of several model parameters related to fire and atmospheric conditions, no clear relationships were found to enable an empirical prediction of the fraction of smoke reaching the free troposphere. Thus, there remains a need to improve both the frequency with which models inject smoke into the free troposphere and the fraction of smoke injected when this occurs. This is of particular importance to smoke transport and impacts downwind.

Tang et al. (2022) showed that the MUSICAv0 (Multi-Scale Infrastructure for Chemistry and Aerosols Version 0) model during the FIREX-AQ was improved using plume rise parameterizations and diurnal cycle of fire emissions, where the impact of plume rise is the larger effect.

For representation of small fire activity in models, detection continues to be a major challenge. GOES-16 and 17 FRP has greatly improved prospects for small fire detection. The DC-8 flight paths on August 21 and 26, 2019 are shown in Figure 26. Over these two days, 2 wildland fires, 4 silviculture burns, 2 pile burns, 13 corn field burns, 1 prescribed fire, and 1 structural fire were sampled. Most of the cropland fires were burning more than one corn residue field (~mean 3 fields), and most of these were detectable from space, with only one exception. GOES was able to detect 83% of the fires sampled; VIIRS detected 74%; and MODIS identified 30% of the fires. Also, note the large number of fire detections by GOES for the slash (126) and silviculture (40) fires. This demonstrates that detected fire duration from GOES is a potential discriminator between crop residue and land clearing fires that would not be distinguishable from polar orbiting satellites.

In addition to the value of satellite FRP and AOD observations, remote sensing of trace gas concentrations from fires (e.g., CO, HCHO, NO_2, HONO) are also improving. Stockwell et al. (2022) compared satellite derived CO emissions from TROPOMI with estimates derived from airborne in situ measurements of smoke emitted within

90 min of the satellite overpass. For the five fires satisfying this criteria, satellite and airborne estimates were in excellent agreement.

Griffin et al. (2021) focused on satellite-derived NO_x emissions using the high-spatial-resolution TROPOMI NO_2 data set. They demonstrated that emissions can be accurately estimated from single TROPOMI overpasses, but an explicit aerosol correction had to be applied to improve the agreement with aircraft observations (by about 10%–25%). Based on chemistry transport model simulations and aircraft observations, the net emissions of NO_x are 1.3–1.5 times greater than the satellite-derived NO_2 emissions and a correction factor needs to be used to infer net NO_x from satellite NO_2.

Liao et al. (2021) analyzed western and eastern fires for secondary HCHO production. Secondary HCHO was calculated by subtracting initially emitted HCHO from the measured HCHO. The primary HCHO contribution time profile was calculated from HCHO observed close to the fire and estimated loss from OH oxidation. In 9 of 12 fires, this production more than offset the photochemical loss of the initially emitted HCHO. A comparison of the plumes revealed that OH abundance (determined from decay of VOC pairs of different reactivity) rather than the dilution-normalized reactivity of the VOC mixture was the source of variability in the strength of HCHO production. From this result, it was suggested that satellite observations of HCHO and CO might be used to estimate oxidant levels in smoke plumes. This would also depend on the need to accurately represent photolysis rates in the plume, where the complex radiative environment challenges satellite retrievals as well.

6. Summary

The FIREX-AQ experiment was a large coordinated multi-agency, multi-platform research effort to investigate US fires in 2019. Various platforms for in situ and remote sensing measurements, several models, and expansive satellite research were coordinated with fuels and fuel consumption data to investigate the atmospheric science of fires in the most complete way to date. An overview of the FIREX-AQ effort is presented here that includes the study motivation, design, science goals, and outcomes. Detailed descriptions of all the measurements and analyses conducted to date are provided.

Even though 2019 was a below average fire year, FIREX-AQ was able to collect a large and unique new data set of western wildfires and smaller eastern fires and a summary of emerging and novel results on emissions, plume chemistry, model improvements, and important satellite observations are presented here and represent major advances in our understanding; for example, linking fire emissions to satellite FRP data and parametrizing ozone formation in fire plumes. Many more publications are expected from FIREX-AQ results in the future.

While FIREX-AQ was a milestone in fire research, many questions remain unanswered; for example, the emissions and reasons for the observed trends of BrC in aging fire plumes remains unclear. With extreme fire seasons expected to continue into the future, fire research needs are at an all-time high and need to be continued after FIREX-AQ.

Appendix A

https://espo.nasa.gov/firex-aq/content/FIREX-AQ_Participants.

Data Availability Statement

FIREX-AQ was primarily funded by the public through support of NOAA and NASA research and the full quality-assured data set acquired from all aspects of the mission and value-added products described below are publicly available. The data can be found on the FIREX-AQ website (https://www-air.larc.nasa.gov/missions/firex-aq/) and the data archive (https://doi.org/10.5067/SUBORBITAL/FIREXAQ2019/DATA001) (FIREX-AQ science team, 2019). A custom merging tool is available that can generate the full data set or just a subset.

Acknowledgments
The authors acknowledge generous support from the NOAA AC4 program from FIREX Firelab and FIREX-AQ. The authors thank the AERONET (NASA GSFC and LOA PHOTONS) and Cimel Electronique teams for providing instrumentation, calibration, measurements and data processing for the mobile DRAGON measurements as well as NASA AERONET staff for coordination with the US Forest Service, Fire Chemistry Lab and the University of Idaho Taylor Ranch Wilderness School staff for set up maintenance and decommission of the stationary DRAGON networks. The authors acknowledge the use of imagery from the NASA Worldview application (https://worldview.earthdata.nasa.gov), part of the NASA Earth Observing System Data and Information System (EOSDIS). Part of this work was performed at the Jet Propulsion Laboratory, California Institute of Technology, under a contract with the National Aeronautics and Space Administration (80NM0018D0004).

References

Abatzoglou, J. T., Battisti, D. S., Williams, A. P., Hansen, W. D., Harvey, B. J., & Kolden, C. A. (2021). Projected increases in western US forest fire despite growing fuel constraints. *Communications Earth & Environment*, *2*(1), 227. https://doi.org/10.1038/s43247-021-00299-0

Abatzoglou, J. T., Rupp, D. E., O'Neill, L. W., & Sadegh, M. (2021). Compound extremes drive the Western Oregon wildfires of September 2020. *Geophysical Research Letters*, *48*(8). https://doi.org/10.1029/2021gl092520

Adachi, K., Dibb, J. E., Scheuer, E., Katich, J. M., Schwarz, J. P., Perring, A. E., et al. (2022). Fine ash-bearing particles as a major aerosol component in biomass burning smoke. *Journal of Geophysical Research: Atmospheres*, *127*(2), e2021JD035657. https://doi.org/10.1029/2021JD035657

Adachi, K., Oshima, N., Gong, Z., de Sa, S., Bateman, A. P., Martin, S. T., et al. (2020). Mixing states of Amazon basin aerosol particles transported over long distances using transmission electron microscopy. *Atmospheric Chemistry and Physics*, *20*(20), 11923–11939. https://doi.org/10.5194/acp-20-11923-2020

Addington, R. N., Hudson, S. J., Hiers, J. K., Hurteau, M. D., Hutcherson, T. F., Matusick, G., & Parker, J. M. (2015). Relationships among wildfire, prescribed fire, and drought in a fire-prone landscape in the south-eastern United States. *International Journal of Wildland Fire*, *24*(6), 778–783. https://doi.org/10.1071/wf14187

Adetona, O., Reinhardt, T. E., Domitrovich, J., Broyles, G., Adetona, A. M., Kleinman, M. T., et al. (2016). Review of the health effects of wildland fire smoke on wildland firefighters and the public. *Inhalation Toxicology*, *28*(3), 95–139. https://doi.org/10.3109/08958378.2016.1145771

Adler, G., Wagner, N. L., Lamb, K. D., Manfred, K. M., Schwarz, J. P., Franchin, A., et al. (2019). Evidence in biomass burning smoke for a light-absorbing aerosol with properties intermediate between brown and black carbon. *Aerosol Science and Technology*, *53*(9), 976–989. https://doi.org/10.1080/02786826.2019.1617832

Agarwal, J. K., & Sem, G. J. (1980). Continous-flow, single-particle-counting condensation nucleus counter. *Journal of Aerosol Science*, *11*(4), 343–357. https://doi.org/10.1016/0021-8502(80)90042-7

Ahern, A. T., Robinson, E. S., Tkacik, D. S., Saleh, R., Hatch, L. E., Barsanti, K. C., et al. (2019). Production of secondary organic aerosol during aging of biomass burning smoke from fresh fuels and its relationship to VOC precursors. *Journal of Geophysical Research: Atmospheres*, *124*(6), 3583–3606. https://doi.org/10.1029/2018jd029068

Ahmadov, R., Grell, G., James, E., Csiszar, I., Tsidulko, M., Pierce, B., et al. (2017). Using VIIRS Fire Radiative Power data to simulate biomass burning emissions, plume rise and smoke transport in a real-time air quality modeling system. In *IEEE international geoscience & remote sensing symposium*.

Akagi, S. K., Craven, J. S., Taylor, J. W., McMeeking, G. R., Yokelson, R. J., Burling, I. R., et al. (2012). Evolution of trace gases and particles emitted by a chaparral fire in California. *Atmospheric Chemistry and Physics*, *12*(3), 1397–1421. https://doi.org/10.5194/acp-12-1397-2012

Akagi, S. K., Yokelson, R. J., Burling, I. R., Meinardi, S., Simpson, I., Blake, D. R., et al. (2013). Measurements of reactive trace gases and variable O-3 formation rates in some South Carolina biomass burning plumes. *Atmospheric Chemistry and Physics*, *13*(3), 1141–1165. https://doi.org/10.5194/acp-13-1141-2013

Akagi, S. K., Yokelson, R. J., Wiedinmyer, C., Alvarado, M. J., Reid, J. S., Karl, T., et al. (2011). Emission factors for open and domestic biomass burning for use in atmospheric models. *Atmospheric Chemistry and Physics*, *11*(9), 4039–4072. https://doi.org/10.5194/acp-11-4039-2011

Andersen, P. C., Williford, C. J., & Birks, J. W. (2010). Miniature personal ozone monitor based on UV Absorbance. *Analytical Chemistry*, *82*(19), 7924–7928. https://doi.org/10.1021/ac1013578

Andreae, M. O. (2019). Emission of trace gases and aerosols from biomass burning - An updated assessment. *Atmospheric Chemistry and Physics*, *19*(13), 8523–8546. https://doi.org/10.5194/acp-19-8523-2019

Andreae, M. O., Anderson, B. E., Blake, D. R., Bradshaw, J. D., Collins, J. E., Gregory, G. L., et al. (1994). Influence of plumes from biomass burning on atmospheric chemistry over the equatorial and tropical Atlantic during CITE 3. *Journal of Geophysical Research*, *99*(D6), 12793–12808. https://doi.org/10.1029/94jd00263

Ansmann, A., Baars, H., Chudnovsky, A., Mattis, I., Veselovskii, I., Haarig, M., et al. (2018). Extreme levels of Canadian wildfire smoke in the stratosphere over central Europe on 21-22 August 2017. *Atmospheric Chemistry and Physics*, *18*(16), 11831–11845. https://doi.org/10.5194/acp-18-11831-2018

Apel, E. C., Emmons, L. K., Karl, T., Flocke, F., Hills, A. J., Madronich, S., et al. (2010). Chemical evolution of volatile organic compounds in the outflow of the Mexico City Metropolitan area. *Atmospheric Chemistry and Physics*, *10*(5), 2353–2375. https://doi.org/10.5194/acp-10-2353-2010

Apel, E. C., Hornbrook, R. S., Hills, A. J., Blake, N. J., Barth, M. C., Weinheimer, A., et al. (2015). Upper tropospheric ozone production from lightning NOx-impacted convection: Smoke ingestion case study from the DC3 campaign. *Journal of Geophysical Research: Atmospheres*, *120*(6), 2505–2523. https://doi.org/10.1002/2014jd022121

Baker, K. R., Woody, M., Valin, L., Szykman, J., Yates, E., Iraci, L., et al. (2018). Photochemical model evaluation of 2013 California wild fire air quality impacts using surface, aircraft, and satellite data. *Science of the Total Environment*, *637*, 1137–1149. https://doi.org/10.1016/j.scitotenv.2018.05.048

Balch, J. K., Bradley, B. A., Abatzoglou, J. T., Nagy, R. C., Fusco, E. J., & Mahood, A. L. (2017). Human-started wildfires expand the fire niche across the United States. *Proceedings of the National Academy of Sciences of the United States of America*, *114*(11), 2946–2951. https://doi.org/10.1073/pnas.1617394114

Baumgardner, D., Jonsson, H., Dawson, W., O'Connor, D., & Newton, R. (2001). The cloud, aerosol and precipitation spectrometer: A new instrument for cloud investigations. *Atmospheric Research*, *59*, 251–264. https://doi.org/10.1016/s0169-8095(01)00119-3

Baumgardner, D., Newton, R., Krämer, M., Meyer, J., Beyer, A., Wendisch, M., & Vochezer, P. (2014). The cloud particle spectrometer with polarization detection (CPSPD): A next generation open-path cloud probe for distinguishing liquid cloud droplets from ice crystals. *Atmospheric Research*, *142*, 2–14. https://doi.org/10.1016/j.atmosres.2013.12.010

Bertschi, I., Yokelson, R. J., Ward, D. E., Babbitt, R. E., Susott, R. A., Goode, J. G., & Hao, W. M. (2003). Trace gas and particle emissions from fires in large diameter and belowground biomass fuels. *Journal of Geophysical Research*, *108*(D13), 8472. https://doi.org/10.1029/2002JD002100

Birks, J. W., Andersen, P. C., Williford, C. J., Turnipseed, A. A., Strunk, S. E., Ennis, C. A., & Mattson, E. (2018). Folded tubular photometer for atmospheric measurements of NO2 and NO. *Atmospheric Measurement Techniques*, *11*(5), 2821–2835. https://doi.org/10.5194/amt-11-2821-2018

Bodhaine, B. A., Ahlquist, N. C., & Schnell, R. C. (1991). Three-wavelength nephelometer suitable for aircraft measurement of background aerosol scattering coefficient. *Atmospheric Environment, Part A: General Topics*, *25*(10), 2267–2276. https://doi.org/10.1016/0960-1686(91)90102-D

Bond, T. C., Anderson, T. L., & Campbell, D. (1999). Calibration and intercomparison of filter-based measurements of visible light absorption by aerosols. *Aerosol Science and Technology*, *30*(6), 582–600. https://doi.org/10.1080/027868299304435

Bond, T. C., Doherty, S. J., Fahey, D. W., Forster, P. M., Berntsen, T., DeAngelo, B. J., et al. (2013). Bounding the role of black carbon in the climate system: A scientific assessment. *Journal of Geophysical Research: Atmospheres*, *118*(11), 5380–5552. https://doi.org/10.1002/jgrd.50171

Bond, T. C., Streets, D. G., Yarber, K., Nelson, S., Woo, J., & Klimont, Z. (2004). A technology-based global inventory of black and organic carbon emissions from combustion. *Journal of Geophysical Research*, *109*(D14), D14203. https://doi.org/10.1029/2003JD003697

Bourgeois, I., Peischl, J., Neuman, J. A., Brown, S. S., Thompson, C. R., Aikin, K. C., et al. (2021). Large contribution of biomass burning emissions to ozone throughout the global remote troposphere. *Proceedings of the National Academy of Sciences*, *118*(52), e2109628118. https://doi.org/10.1073/pnas.2109628118

Burling, I. R., Yokelson, R. J., Akagi, S. K., Urbanski, S. P., Wold, C. E., Griffith, D. W. T., et al. (2011). Airborne and ground-based measurements of the trace gases and particles emitted by prescribed fires in the United States. *Atmospheric Chemistry and Physics*, *11*(23), 12197–12216. https://doi.org/10.5194/acp-11-12197-2011

Burling, I. R., Yokelson, R. J., Griffith, D. W. T., Johnson, T. J., Veres, P., Roberts, J. M., et al. (2010). Laboratory measurements of trace gas emissions from biomass burning of fuel types from the southeastern and southwestern United States. *Atmospheric Chemistry and Physics*, *10*(22), 11115–11130. https://doi.org/10.5194/acp-10-11115-2010

Campbell, J. R., Hlavka, D. L., Welton, E. J., Flynn, C. J., Turner, D. D., Spinhirne, J. D., et al. (2002). Full-time, eye-safe cloud and aerosol lidar observation at atmospheric radiation measurement program sites: Instruments and data processing. *Journal of Atmospheric and Oceanic Technology*, *19*(4), 431–442. https://doi.org/10.1175/1520-0426(2002)019<0431:Ftesca>2.0.Co;2

Canagaratna, M. R., Jayne, J., Jimenez, J., Allan, J., Alfarra, M., Zhang, Q., et al. (2007). Chemical and microphysical characterization of ambient aerosols with the aerodyne aerosol mass spectrometer. *Mass Spectrometry Reviews*, *26*(2), 185–222. https://doi.org/10.1002/mas.20115

Cazorla, M., Wolfe, G. M., Bailey, S. A., Swanson, A. K., Arkinson, H. L., & Hanisco, T. F. (2015). A new airborne laser-induced fluorescence instrument for in situ detection of formaldehyde throughout the troposphere and lower stratosphere. *Atmospheric Measurement Techniques*, *8*(2), 541–552. https://doi.org/10.5194/amt-8-541-2015

Chai, J. J., Dibb, J. E., Anderson, B. E., Bekker, C., Blum, D. E., Heim, E., et al. (2021). Isotopic evidence for dominant secondary production of HONO in near-ground wildfire plumes. *Atmospheric Chemistry and Physics*, *21*(17), 13077–13098. https://doi.org/10.5194/acp-21-13077-2021

Christian, T. J., Kleiss, B., Yokelson, R. J., Holzinger, R., Crutzen, P. J., Hao, W. M., et al. (2003). Comprehensive laboratory measurements of biomass-burning emissions: 1. Emissions from Indonesian, African, and other fuels. *Journal of Geophysical Research*, *108*(D23), 4719. https://doi.org/10.1029/2003JD003704

Claflin, M. S., Pagonis, D., Finewax, Z., Handschy, A. V., Day, D. A., Brown, W. L., et al. (2021). An in situ gas chromatograph with automatic detector switching between PTR- and EI-TOF-MS: Isomer-resolved measurements of indoor air. *Atmospheric Measurement Techniques*, *14*(1), 133–152. https://doi.org/10.5194/amt-14-133-2021

Clair, S. J. M., Swanson, A. K., Bailey, S. A., & Hanisco, T. F. (2019). CAFE: A new, improved nonresonant laser-induced fluorescence instrument for airborne in situ measurement of formaldehyde. *Atmospheric Measurement Techniques*, *12*(8), 4581–4590. https://doi.org/10.5194/amt-12-4581-2019

Clark, T. L., Jenkins, M. A., Coen, J., & Packham, D. (1996). A coupled atmosphere–fire model: Convective feedback on fire-line dynamics. *Journal of Applied Meteorology and Climatology*, *35*(6), 875–901. https://doi.org/10.1175/1520-0450(1996)035<0875:Acamcf>2.0.Co;2

Clarke, A., McNaughton, C., Kapustin, V., Shinozuka, Y., Howell, S., Dibb, J., et al. (2007). Biomass burning and pollution aerosol over North America: Organic components and their influence on spectral optical properties and humidification response. *Journal of Geophysical Research*, *112*(D12), D12S18. https://doi.org/10.1029/2006JD007777

Coggon, M. M., Lim, C. Y., Koss, A. R., Sekimoto, K., Yuan, B., Gilman, J. B., et al. (2019). OH chemistry of non-methane organic gases (NMOGs) emitted from laboratory and ambient biomass burning smoke: Evaluating the influence of furans and oxygenated aromatics on ozone and secondary NMOG formation. *Atmospheric Chemistry and Physics*, *19*(23), 14875–14899. https://doi.org/10.5194/acp-19-14875-2019

Cross, E. S., Williams, L. R., Lewis, D. K., Magoon, G. R., Onasch, T. B., Kaminsky, M. L., et al. (2017). Use of electrochemical sensors for measurement of air pollution: Correcting interference response and validating measurements. *Atmospheric Measurement Techniques*, *10*(9), 3575–3588. https://doi.org/10.5194/amt-10-3575-2017

Crosson, E. R. (2008). A cavity ring-down analyzer for measuring atmospheric levels of methane, carbon dioxide, and water vapor. *Applied Physics B-Lasers & Optics*, *92*(3), 403–408. https://doi.org/10.1007/s00340-008-3135-y

Crounse, J. D., McKinney, K. A., Kwan, A. J., & Wennberg, P. O. (2006). Measurement of gas-phase hydroperoxides by chemical ionization mass spectrometry. *Analytical Chemistry*, *78*(19), 6726–6732. https://doi.org/10.1021/ac0604235

Crutzen, P. J., & Andreae, M. O. (1990). Biomass burning in the tropics - impact on atmospheric chemistry and biogeochemical cycles. *Science*, *250*(4988), 1669–1678. https://doi.org/10.1126/science.250.4988.1669

Crutzen, P. J., Heidt, L. E., Krasnec, J. P., Pollock, W. H., & Seiler, W. (1979). Biomass burning as a source of atmospheric gases CO, H2, N2O, NO, CH3CL and COS. *Nature*, *282*(5736), 253–256. https://doi.org/10.1038/282253a0

DeCarlo, P. F., Kimmel, J. R., Trimborn, A., Northway, M. J., Jayne, J. T., Aiken, A. C., et al. (2006). Field-deployable, high-resolution, time-of-flight aerosol mass spectrometer. *Analytical Chemistry*, *78*(24), 8281–8289. https://doi.org/10.1021/ac061249n

Decker, Z. C. J., Robinson, M. A., Barsanti, K. C., Bourgeois, I., Coggon, M. M., DiGangi, J. P., et al. (2021). Nighttime and daytime dark oxidation chemistry in wildfire plumes: An observation and model analysis of FIREX-AQ aircraft data. *Atmospheric Chemistry and Physics*, *21*(21), 16293–16317. https://doi.org/10.5194/acp-21-16293-2021

Dickinson, G. N., Miller, D. D., Bajracharya, A., Bruchard, W., Durbin, T. A., McGarry, J. K. P., et al. (2022). Health risk implications of volatile organic compounds in wildfire smoke during the 2019 FIREX-AQ campaign and beyond. *GeoHealth*, *6*, e2021GH000546. https://doi.org/10.1029/2021GH000546

de Gouw, J. A., Warneke, C., Stohl, A., Wollny, A. G., Brock, C. A., Cooper, O. R., et al. (2006). Volatile organic compounds composition of merged and aged forest fire plumes from Alaska and western Canada. *Journal of Geophysical Research*, *111*(D10). D10303. https://doi.org/10.1029/2005JD006175

Di Lorenzo, R. A., Washenfelder, R. A., Attwood, A. R., Guo, H., Xu, L., Ng, N. L., et al. (2017). Molecular -size -separated brown carbon absorption for biomass burning aerosol at multiple field sites. *Environmental Science & Technology*, *51*(6), 3128–3137. https://doi.org/10.1021/acs.est.6b06160

Diner, D. J., Xu, F., Garay, M. J., Martonchik, J. V., Rheingans, B. E., Geier, S., et al. (2013). The airborne multiangle Spectropolarimetric imager (AirMSPI): A new tool for aerosol and cloud remote sensing. *Atmospheric Measurement Techniques*, *6*(8), 2007–2025. https://doi.org/10.5194/amt-6-2007-2013

Doubleday, A., Schulte, J., Sheppard, L., Kadlec, M., Dhammapala, R., Fox, J., & Isaksen, T. B. (2020). Mortality associated with wildfire smoke exposure in Washington state, 2006-2017: A case-crossover study. *Environmental Health*, *19*(1), 4. https://doi.org/10.1186/s12940-020-0559-2

Drinovec, L., Mocnik, G., Zotter, P., Prevot, A. S. H., Ruckstuhl, C., Coz, E., et al. (2015). The "dual-spot" aethalometer: An improved measurement of aerosol black carbon with real-time loading compensation. *Atmospheric Measurement Techniques*, *8*(5), 1965–1979. https://doi.org/10.5194/amt-8-1965-2015

Eilerman, S. J., Peischl, J., Neuman, J. A., Ryerson, T. B., Aikin, K. C., Holloway, M. W., et al. (2016). Characterization of ammonia, methane, and nitrous oxide emissions from concentrated animal feeding operations in northeastern Colorado. *Environmental Science & Technology*, *50*(20), 10885–10893. https://doi.org/10.1021/acs.est.6b02851

Fernandes, P. M., & Botelho, H. S. (2003). A review of prescribed burning effectiveness in fire hazard reduction. *International Journal of Wildland Fire*, *12*(2), 117–128. https://doi.org/10.1071/wf02042

FIREX-AQ science team (2019). Fire influence on regional to global environments and air quality [Dataset]. NASA. https://doi.org/10.5067/SUBORBITAL/FIREXAQ2019/DATA001

Fishman, J., Hoell, J. M., Bendura, R. D., McNeil, R. J., & Kirchhoff, V. (1996). NASA GTE TRACE A experiment (September October 1992): Overview. *Journal of Geophysical Research*, *101*(D19), 23865–23879. https://doi.org/10.1029/96jd00123

Fleming, L. T., Lin, P., Roberts, J. M., Selimovic, V., Yokelson, R., Laskin, J., et al. (2020). Molecular composition and photochemical lifetimes of brown carbon chromophores in biomass burning organic aerosol. *Atmospheric Chemistry and Physics*, *20*(2), 1105–1129. https://doi.org/10.5194/acp-20-1105-2020

Forrister, H., Liu, J., Scheuer, E., Dibb, J., Ziemba, L., Thornhill, K. L., et al. (2015). Evolution of brown carbon in wildfire plumes. *Geophysical Research Letters*, *42*(11), 4623–4630. https://doi.org/10.1002/2015gl063897

Frank, T. (2020). *U.S. wildfires plummeted in 2019. Experts say it won't last*. E&E News. https://doi.org/10.1126/science.abb7869

Freitas, S. R., Longo, K. M., Alonso, M. F., Pirre, M., Marecal, V., Grell, G., et al. (2011). PREP-CHEM-SRC-1.0: A preprocessor of trace gas and aerosol emission fields for regional and global atmospheric chemistry models. *Geoscientific Model Development*, *4*(2), 419–433. https://doi.org/10.5194/gmd-4-419-2011

Freitas, S. R., Longo, K. M., Chatfield, R., Latham, D., Silva Dias, M. A. F., Andreae, M. O., et al. (2007). Including the sub-grid scale plume rise of vegetation fires in low resolution atmospheric transport models. *Atmospheric Chemistry and Physics*, *7*(13), 3385–3398. https://doi.org/10.5194/acp-7-3385-2007

Giles, D. M., Sinyuk, A., Sorokin, M. G., Schafer, J. S., Smirnov, A., Slutsker, I., et al. (2019). Advancements in the Aerosol Robotic Network (AERONET) Version 3 database - Automated near-real-time quality control algorithm with improved cloud screening for Sun photometer aerosol optical depth (AOD) measurements. *Atmospheric Measurement Techniques*, *12*(1), 169–209. https://doi.org/10.5194/amt-12-169-2019

Goode, J. G., Yokelson, R. J., Ward, D. E., Susott, R. A., Babbitt, R. E., Davies, M. A., & Hao, W. M. (2000). Measurements of excess O_3, CO2, CO, CH4, C2H2, HCN, NO, NH3, HCOOH, CH3COOH, HCHO, and CH3OH in 1997 Alaskan biomass burning plumes by airborne Fourier transform infrared spctroscopy (AFTIR). *Journal of Geophysical Research*, *105*(D17), 22147–22166. https://doi.org/10.1029/2000jd900287

Green, R. O., Eastwood, M. L., Sarture, C. M., Chrien, T. G., Aronsson, M., Chippendale, B. J., et al. (1998). Imaging spectroscopy and the airborne visible infrared imaging spectrometer (AVIRIS). *Remote Sensing of Environment*, *65*(3), 227–248. https://doi.org/10.1016/s0034-4257(98)00064-9

Griffin, D., McLinden, C. A., Dammers, E., Adams, C., Stockwell, C. E., Warneke, C., et al. (2021). Biomass burning nitrogen dioxide emissions derived from space with TROPOMI: Methodology and validation. *Atmospheric Measurement Techniques*, *14*(12), 7929–7957. https://doi.org/10.5194/amt-14-7929-2021

Guerette, E. A., Paton-Walsh, C., Desservettaz, M., Smith, T. E. L., Volkova, L., Weston, C. J., & Meyer, C. P. (2018). Emissions of trace gases from Australian temperate forest fires: Emission factors and dependence on modified combustion efficiency. *Atmospheric Chemistry and Physics*, *18*(5), 3717–3735. https://doi.org/10.5194/acp-18-3717-2018

Guo, H., Campuzano-Jost, P., Nault, B. A., Day, D. A., Schroder, J. C., Kim, D., et al. (2021). The importance of size ranges in aerosol instrument intercomparisons: A case study for the atmospheric Tomography mission. *Atmospheric Measurement Techniques*, *14*(5), 3631–3655. https://doi.org/10.5194/amt-14-3631-2021

Hair, J. W., Hostetler, C. A., Cook, A. L., Harper, D. B., Ferrare, R. A., Mack, T. L., et al. (2008). Airborne high spectral resolution lidar for profiling aerosol optical properties. *Applied Optics*, *47*(36), 6734–6752. https://doi.org/10.1364/ao.47.006734

Hall, S. R., Ullmann, K., Prather, M. J., Flynn, C. M., Murray, L. T., Fiore, A. M., et al. (2018). Cloud impacts on photochemistry: Building a climatology of photolysis rates from the atmospheric Tomography mission. *Atmospheric Chemistry and Physics*, *18*(22), 16809–16828. https://doi.org/10.5194/acp-18-16809-2018

Hannun, R. A., Swanson, A. K., Bailey, S. A., Hanisco, T. F., Bui, T. P., Bourgeois, I., et al. (2020). A cavity-enhanced ultraviolet absorption instrument for high-precision, fast-time-response ozone measurements. *Atmospheric Measurement Techniques*, *13*(12), 6877–6887. https://doi.org/10.5194/amt-13-6877-2020

Hatch, L. E., Luo, W., Pankow, J. F., Yokelson, R. J., Stockwell, C. E., & Barsanti, K. C. (2015). Identification and quantification of gaseous organic compounds emitted from biomass burning using two-dimensional gas chromatography-time-of-flight mass spectrometry. *Atmospheric Chemistry and Physics*, *15*(4), 1865–1899. https://doi.org/10.5194/acp-15-1865-2015

Hatch, L. E., Yokelson, R. J., Stockwell, C. E., Veres, P. R., Simpson, I. J., Blake, D. R., et al. (2017). Multi-instrument comparison and compilation of non-methane organic gas emissions from biomass burning and implications for smoke-derived secondary organic aerosol precursors. *Atmospheric Chemistry and Physics*, *17*(2), 1471–1489. https://doi.org/10.5194/acp-17-1471-2017

Hecobian, A., Liu, Z., Hennigan, C. J., Huey, L. G., Jimenez, J. L., Cubison, M. J., et al. (2011). Comparison of chemical characteristics of 495 biomass burning plumes intercepted by the NASA DC-8 aircraft during the ARCTAS/CARB-2008 field campaign. *Atmospheric Chemistry and Physics*, *11*(24), 13325–13337. https://doi.org/10.5194/acp-11-13325-2011

Heim, E. W., Dibb, J., Scheuer, E., Jost, P. C., Nault, B., Jimenez, J., et al. (2020). Asian dust observed during KORUS-AQ facilitates the uptake and incorporation of soluble pollutants during transport to South Korea. *Atmospheric Environment*, *224*, 117305. https://doi.org/10.1016/j.atmosenv.2020.117305

Herron-Thorpe, F. L., Mount, G. H., Emmons, L. K., Lamb, B. K., Jaffe, D. A., Wigder, N. L., et al. (2014). Air quality simulations of wildfires in the Pacific Northwest evaluated with surface and satellite observations during the summers of 2007 and 2008. *Atmospheric Chemistry and Physics*, *14*(22), 12533–12551. https://doi.org/10.5194/acp-14-12533-2014

Higgins, R. W., Yao, Y., & Wang, X. L. (1997). Influence of the North American monsoon system on the US summer precipitation regime. *Journal of Climate*, *10*(10), 2600–2622. https://doi.org/10.1175/1520-0442(1997)010<2600:Iotnam>2.0.Co;2

Hodshire, A. L., Akherati, A., Alvarado, M. J., Brown-Steiner, B., Jathar, S. H., Jimenez, J. L., et al. (2019). Aging effects on biomass burning aerosol mass and composition: A critical review of field and laboratory studies. *Environmental Science & Technology*, *53*(17), 10007–10022. https://doi.org/10.1021/acs.est.9b02588

Hoell, J. M., Davis, D. D., Jacob, D. J., Rodgers, M. O., Newell, R. E., Fuelberg, H. E., et al. (1999). Pacific Exploratory mission in the tropical Pacific: PEM-tropics A, August-September 1996. *Journal of Geophysical Research*, *104*(D5), 5567–5583. https://doi.org/10.1029/1998jd100074

Holben, B. N., Kim, J., Sano, I., Mukai, S., Eck, T. F., Giles, D. M., et al. (2018). An overview of mesoscale aerosol processes, comparisons, and validation studies from DRAGON networks. *Atmospheric Chemistry and Physics*, *18*(2), 655–671. https://doi.org/10.5194/acp-18-655-2018

Hook, S. J., Myers, J. E. J., Thome, K. J., Fitzgerald, M., & Kahle, A. B. (2001). The MODIS/ASTER airborne simulator (MASTER) - A new instrument for Earth science studies. *Remote Sensing of Environment*, *76*(1), 93–102. https://doi.org/10.1016/s0034-4257(00)00195-4

Huntrieser, H., Lichtenstern, M., Scheibe, M., Aufmhoff, H., Schlager, H., Pucik, T., et al. (2016). Injection of lightning-produced NOx, water vapor, wildfire emissions, and stratospheric air to the UT/LS as observed from DC3 measurements. *Journal of Geophysical Research: Atmospheres*, *121*(11), 6638–6668. https://doi.org/10.1002/2015jd024273

Jacob, D. J., Crawford, J. H., Maring, H., Clarke, A. D., Dibb, J. E., Emmons, L. K., et al. (2010). The arctic research of the composition of the troposphere from aircraft and satellites (ARCTAS) mission: Design, execution, and first results. *Atmospheric Chemistry and Physics*, *10*(11), 5191–5212. https://doi.org/10.5194/acp-10-5191-2010

Jaffe, D. A., & Wigder, N. L. (2012). Ozone production from wildfires: A critical review. *Atmospheric Environment*, *51*, 1–10. https://doi.org/10.1016/j.atmosenv.2011.11.063

Jayne, J. T., Leard, D. C., Zhang, X., Davidovits, P., Smith, K. A., Kolb, C. E., & Worsnop, D. R. (2000). Development of an aerosol mass spectrometer for size and composition analysis of submicron particles. *Aerosol Science and Technology*, *33*(1–2), 49–70. https://doi.org/10.1080/027868200410840

Jen, C. N., Hatch, L. E., Selimovic, V., Yokelson, R. J., Weber, R., Fernandez, A. E., et al. (2019). Speciated and total emission factors of particulate organics from burning western US wildland fuels and their dependence on combustion efficiency. *Atmospheric Chemistry and Physics*, *19*(2), 1013–1026. https://doi.org/10.5194/acp-19-1013-2019

Jordan, C. E., Anderson, B. E., Barrick, J. D., Blum, D., Brunke, K., Chai, J., et al. (2022). Beyond the ångström exponent: Probing additional information in spectral curvature and variability of in situ aerosol hyperspectral (0.3–0.7 μm) optical properties. *Journal of Geophysical Research: Atmospheres*, *127*(21), e2022JD037201. https://doi.org/10.1029/2022JD037201

Jordan, C. E., Anderson, B. E., Beyersdorf, A. J., Corr, C. A., Dibb, J. E., Greenslade, M. E., et al. (2015). Spectral aerosol extinction (SpEx): A new instrument for in situ ambient aerosol extinction measurements across the UV/visible wavelength range. *Atmospheric Measurement Techniques*, *8*(11), 4755–4771. https://doi.org/10.5194/amt-8-4755-2015

Jordan, C. E., Stauffer, R. M., Lamb, B. T., Hudgins, C. H., Thornhill, K. L., Schuster, G. L., et al. (2021). New in situ aerosol hyperspectral optical measurements over 300-700 nm - Part 1: Spectral Aerosol Extinction (SpEx) instrument field validation during the KORUS-OC cruise. *Atmospheric Measurement Techniques*, *14*(1), 695–713. https://doi.org/10.5194/amt-14-695-2021

Junkermann, W., Platt, U., & Volzthomas, A. (1989). A photoelectric detector for the measurement of photolyis frequencies of ozone and other atmospheric molecules. *Journal of Atmospheric Chemistry*, *8*(3), 203–227. https://doi.org/10.1007/bf00051494

Karion, A., Sweeney, C., Petron, G., Frost, G., Michael Hardesty, R., Kofler, J., et al. (2013). Methane emissions estimate from airborne measurements over a western United States natural gas field. *Geophysical Research Letters*, *40*(16), 4393–4397. https://doi.org/10.1002/grl.50811

Karol, Y., Tanre, D., Goloub, P., Vervaerde, C., Balois, J. Y., Blarel, L., et al. (2013). Airborne sun photometer PLASMA: Concept, measurements, comparison of aerosol extinction vertical profile with lidar. *Atmospheric Measurement Techniques*, *6*(9), 2383–2389. https://doi.org/10.5194/amt-6-2383-2013

Kaspari, J. H., Chai, J., Anderson, B. E., Jordan, C., Scheuer, E., Hastings, M. G., & Dibb, J. E. (2021). Influence of solar irradiation on nitrous acid production in Western U.S. wildfire smoke. *Earth and Space Science Open Archive*, *21*. https://doi.org/10.1002/essoar.10506007.1

Kaufman, Y. J., Hobbs, P. V., Kirchhoff, V. W. J. H., Artaxo, P., Remer, L. A., Holben, B. N., et al. (1998). Smoke, clouds, and radiation - Brazil (SCAR-B) experiment. *Journal of Geophysical Research*, *103*(D24), 31783–31808. https://doi.org/10.1029/98jd02281

King, M. D., Menzel, W. P., Grant, P. S., Myers, J. S., Arnold, G. T., Platnick, S. E., et al. (1996). Airborne scanning spectrometer for remote sensing of cloud, aerosol, water vapor, and surface properties. *Journal of Atmospheric and Oceanic Technology*, *13*(4), 777–794. https://doi.org/10.1175/1520-0426(1996)013<0777:Assfrs>2.0.Co;2

Kitzberger, T., Brown, P. M., Heyerdahl, E. K., Swetnam, T. W., & Veblen, T. T. (2007). Contingent Pacific–Atlantic Ocean influence on multicentury wildfire synchrony over western North America. *Proceedings of the National Academy of Sciences*, *104*(2), 543–548. https://doi.org/10.1073/pnas.0606078104

Kleinman, L. I., Sedlacek, A. J. III, Adachi, K., Buseck, P. R., Collier, S., Dubey, M. K., et al. (2020). Rapid evolution of aerosol particles and their optical properties downwind of wildfires in the western US. *Atmospheric Chemistry and Physics*, *20*(21), 13319–13341. https://doi.org/10.5194/acp-20-13319-2020

Koss, A. R., Sekimoto, K., Gilman, J. B., Selimovic, V., Coggon, M. M., Zarzana, K. J., et al. (2018). Non-methane organic gas emissions from biomass burning: Identification, quantification, and emission factors from PTR-ToF during the FIREX 2016 laboratory experiment. *Atmospheric Chemistry and Physics*, *18*(5), 3299–3319. https://doi.org/10.5194/acp-18-3299-2018

Kowalewski, M. G., & Janz, S. J. (2014). Remote sensing capabilities of the GEO-CAPE airborne simulator. In J. J. Butler, X. Xiong, & X. Gu (Eds.), *Earth observing systems XIX*. https://doi.org/10.1117/12.2062058

Krechmer, J., Lopez-Hilfiker, F., Koss, A., Hutterli, M., Stoermer, C., Deming, B., et al. (2018). Evaluation of a new reagent-ion source and focusing ion–molecule reactor for use in proton-transfer-reaction mass spectrometry. *Analytical Chemistry*, *90*(20), 12011–12018. https://doi.org/10.1021/acs.analchem.8b02641

Kumar, A., Pierce, R. B., Ahmadov, R., Pereira, G., Freitas, S., Grell, G., et al. (2022). Simulating wildfire emissions and plumerise using geostationary satellite fire radiative power measurements: A case study of the 2019 Williams flats fire. *Atmospheric Chemistry and Physics Discussions*, *2022*, 1–68. https://doi.org/10.5194/acp-2022-33

Kupc, A., Williamson, C., Wagner, N. L., Richardson, M., & Brock, C. A. (2018). Modification, calibration, and performance of the Ultra-High Sensitivity Aerosol Spectrometer for particle size distribution and volatility measurements during the Atmospheric Tomography Mission (ATom) airborne campaign. *Atmospheric Measurement Techniques*, *11*(1), 369–383. https://doi.org/10.5194/amt-11-369-2018

Lack, D. A., Richardson, M. S., Law, D., Langridge, J. M., Cappa, C. D., McLaughlin, R. J., & Murphy, D. M. (2012). Aircraft instrument for comprehensive characterization of aerosol optical properties, Part 2: Black and Brown carbon absorption and absorption enhancement measured with photo acoustic spectroscopy. *Aerosol Science and Technology*, *46*(5), 555–568. https://doi.org/10.1080/02786826.2011.645955

Lance, S., Brock, C. A., Rogers, D., & Gordon, J. A. (2010). Water droplet calibration of the Cloud Droplet Probe (CDP) and in-flight performance in liquid, ice and mixed-phase clouds during ARCPAC. *Atmospheric Measurement Techniques*, *3*(6), 1683–1706. https://doi.org/10.5194/amt-3-1683-2010

Lareau, N. P., & Clements, C. B. (2017). The mean and turbulent properties of a wildfire convective plume. *Journal of Applied Meteorology and Climatology*, *56*(8), 2289–2299. https://doi.org/10.1175/jamc-d-16-0384.1

Laskin, A., Iedema, M. J., & Cowin, J. P. (2003). Time-resolved aerosol collector for CCSEM/EDX single-particle analysis. *Aerosol Science and Technology*, *37*(3), 246–260. https://doi.org/10.1080/02786820300945

Lee, B. H., Lopez-Hilfiker, F. D., Mohr, C., Kurten, T., Worsnop, D. R., & Thornton, J. A. (2014). An iodide-adduct high-resolution time-of-flight chemical-ionization mass spectrometer: Application to atmospheric inorganic and organic compounds. *Environmental Science & Technology*, *48*(11), 6309–6317. https://doi.org/10.1021/es500362a

Lefer, B. L., Talbot, R. W., Harriss, R. H., Bradshaw, J. D., Sandholm, S. T., Olson, J. O., et al. (1994). Enhancement of acidic gases in biomass burning impacted air masses over Canada. *Journal of Geophysical Research*, *99*(D1), 1721–1737. https://doi.org/10.1029/93jd02091

Lerner, B. M., Gilman, J. B., Aikin, K. C., Atlas, E. L., Goldan, P. D., Graus, M., et al. (2017). An improved, automated whole air sampler and gas chromatography mass spectrometry analysis system for volatile organic compounds in the atmosphere. *Atmospheric Measurement Techniques*, *10*(1), 291–313. https://doi.org/10.5194/amt-10-291-2017

Liang, Y., Stamatis, C., Fortner, E. C., Wernis, R. A., Van Rooy, P., Majluf, F., et al. (2022). Emissions of organic compounds from western US wildfires and their near-fire transformations. *Atmospheric Chemistry and Physics*, *22*(15), 9877–9893. https://doi.org/10.5194/acp-22-9877-2022

Liao, J., Wolfe, G. M., Hannun, R. A., St. Clair, J. M., Hanisco, T. F., Gilman, J. B., et al. (2021). Formaldehyde evolution in US wildfire plumes during the fire influence on regional to global environments and air quality experiment (FIREX-AQ). *Atmospheric Chemistry and Physics*, *21*(24), 18319–18331. https://doi.org/10.5194/acp-21-18319-2021

Lin, C.-I., Baker, M., & Charlson, R. J. (1973). Absorption coefficient of atmospheric aerosol: A method for measurement. *Applied Optics*, *12*(6), 1356–1363. https://doi.org/10.1364/AO.12.001356

Lindaas, J., Pollack, I. B., Garofalo, L. A., Pothier, M. A., Farmer, D. K., Kreidenweis, S. M., et al. (2021). Emissions of reactive nitrogen from western U.S. wildfires during summer 2018. *Journal of Geophysical Research: Atmospheres*, *126*(2), e2020JD032657. https://doi.org/10.1029/2020JD032657

Liu, X. X., Huey, L. G., Yokelson, R. J., Selimovic, V., Simpson, I. J., Muller, M., et al. (2017). Airborne measurements of western US wildfire emissions: Comparison with prescribed burning and air quality implications. *Journal of Geophysical Research: Atmospheres*, *122*(11), 6108–6129. https://doi.org/10.1002/2016jd026315

Liu, X. X., Zhang, Y., Huey, L. G., Yokelson, R. J., Wang, Y., Jimenez, J. L., et al. (2016). Agricultural fires in the southeastern US during SEAC(4)RS: Emissions of trace gases and particles and evolution of ozone, reactive nitrogen, and organic aerosol. *Journal of Geophysical Research: Atmospheres*, *121*(12), 7383–7414. https://doi.org/10.1002/2016jd025040

Majluf, F. Y., Krechmer, J. E., Daube, C., Knighton, W. B., Dyroff, C., Lambe, A. T., et al. (2022). Mobile near-field measurements of biomass burning volatile organic compounds: Emission ratios and factor analysis. *Environmental Science and Technology Letters*, *9*(5), 383–390. https://doi.org/10.1021/acs.estlett.2c00194

Manfred, K. M., Washenfelder, R. A., Wagner, N. L., Adler, G., Erdesz, F., Womack, C. C., et al. (2018). Investigating biomass burning aerosol morphology using a laser imaging nephelometer. *Atmospheric Chemistry and Physics*, *18*(3), 1879–1894. https://doi.org/10.5194/acp-18-1879-2018

May, A. A., Levin, E. J. T., Hennigan, C. J., Riipinen, I., Lee, T., Collett, J. L., Jr., et al. (2013). Gas-particle partitioning of primary organic aerosol emissions: 3. Biomass burning. *Journal of Geophysical Research: Atmospheres*, *118*(19), 11327–11338. https://doi.org/10.1002/jgrd.50828

May, A. A., McMeeking, G. R., Lee, T., Taylor, J. W., Craven, J. S., Burling, I., et al. (2014). Aerosol emissions from prescribed fires in the United States: A synthesis of laboratory and aircraft measurements. *Journal of Geophysical Research: Atmospheres*, *119*(20), 11826–11849. https://doi.org/10.1002/2014jd021848

McCarty, J. L., Korontzi, S., Justice, C. O., & Loboda, T. (2009). The spatial and temporal distribution of crop residue burning in the contiguous United States. *Science of the Total Environment*, *407*(21), 5701–5712. https://doi.org/10.1016/j.scitotenv.2009.07.009

McCourt, M. L., McMillan, W. W., Ackerman, S., Holz, R., Revercomb, H. E., & Tobin, D. (2004). Using the "blue spike" to characterize biomass-burning sites during southern African regional science initiative (SAFARI) 2000. *Journal of Geophysical Research*, *109*(D20), D20307. https://doi.org/10.1029/2004jd004805

McGill, M., Hlavka, D., Hart, W., Scott, V. S., Spinhirne, J., & Schmid, B. (2002). Cloud physics lidar: Instrument description and initial measurement results. *Applied Optics*, *41*(18), 3725–3734. https://doi.org/10.1364/ao.41.003725

McManus, J. B., Zahniser, M. S., Nelson, D. D., Shorter, J. H., Herndon, S. C., Jervis, D., et al. (2015). Recent progress in laser-based trace gas instruments: Performance and noise analysis. *Applied Physics B*, *119*(1), 203–218. https://doi.org/10.1007/s00340-015-6033-0

McMeeking, G. R., Kreidenweis, S. M., Baker, S., Carrico, C. M., Chow, J. C., Collett, J. L., et al. (2009). Emissions of trace gases and aerosols during the open combustion of biomass in the laboratory. *Journal of Geophysical Research*, *114*(D19), D19210. https://doi.org/10.1029/2009jd011836

Melvin, M. A. (2018). National prescribed fire use survey report Technical Report 03-18, Coalition of Prescribed Fire Councils. Retrieved from https://www.stateforesters.org/wp-content/uploads/2018/2012/2018-Prescribed-Fire-Use-Survey-Report-2011.pdf

Melvin, M. A. (2020). National prescribed fire use survey report Technical Report 04-20, Coalition of Prescribed Fire Councils. Retrieved from https://www.stateforesters.org/wp-content/uploads/2020/2012/2020-Prescribed-Fire-Use-Report.pdf

Miller, D. D., Bajracharya, A., Dickinson, G. N., Durbin, T. A., McGarry, J. K., Moser, E. P., et al. (2022). Diffusive uptake rates for passive air sampling: Application to volatile organic compound exposure during FIREX-AQ campaign. *Chemosphere*, *287*, 131808. https://doi.org/10.1016/j.chemosphere.2021.131808

Min, K. E., Washenfelder, R. A., Dube, W. P., Langford, A. O., Edwards, P. M., Zarzana, K. J., et al. (2016). A broadband cavity enhanced absorption spectrometer for aircraft measurements of glyoxal, methylglyoxal, nitrous acid, nitrogen dioxide, and water vapor. *Atmospheric Measurement Techniques*, *9*(2), 423–440. https://doi.org/10.5194/amt-9-423-2016

Moore, R. H., Wiggins, E. B., Ahern, A. T., Zimmerman, S., Montgomery, L., Campuzano Jost, P., et al. (2021). Sizing response of the ultra-high sensitivity aerosol spectrometer (UHSAS) and laser aerosol spectrometer (LAS) to changes in submicron aerosol composition and refractive index. *Atmospheric Measurement Techniques*, *14*(6), 4517–4542. https://doi.org/10.5194/amt-14-4517-2021

Müller, M., Anderson, B. E., Beyersdorf, A. J., Crawford, J. H., Diskin, G. S., Eichler, P., et al. (2016). In situ measurements and modeling of reactive trace gases in a small biomass burning plume. *Atmospheric Chemistry and Physics*, *16*(6), 3813–3824. https://doi.org/10.5194/acp-16-3813-2016

Müller, M., Mikoviny, T., Feil, S., Haidacher, S., Hanel, G., Hartungen, E., et al. (2014). A compact PTR-ToF-MS instrument for airborne measurements of volatile organic compounds at high spatiotemporal resolution. *Atmospheric Measurement Techniques*, *7*(11), 3763–3772. https://doi.org/10.5194/amt-7-3763-2014

Mutch, R. W. (1994). Fighting fire with prescribed fire - a return to ecosystem health. *Journal of Forestry*, *92*(11), 31–33.

Nance, J. D., Hobbs, P. V., Radke, L. F., & Ward, D. E. (1993). Airborn measurements of gases and particles from an Alaskan Wildfire. *Journal of Geophysical Research*, *98*(D8), 14873–14882. https://doi.org/10.1029/93jd01196

Ng, N. L., Herndon, S. C., Trimborn, A., Canagaratna, M. R., Croteau, P. L., Onasch, T. B., et al. (2011). An Aerosol Chemical Speciation Monitor (ACSM) for routine monitoring of the composition and mass concentrations of ambient aerosol. *Aerosol Science and Technology*, *45*(7), 780–794. https://doi.org/10.1080/02786826.2011.560211

Nowell, H. K., Holmes, C. D., Robertson, K., Teske, C., & Hiers, J. K. (2018). A new picture of fire extent, variability, and drought interaction in prescribed fire landscapes: Insights from Florida government records. *Geophysical Research Letters*, *45*(15), 7874–7884. https://doi.org/10.1029/2018gl078679

Ogren, J. A. (2010). Comment on "Calibration and intercomparison of filter-based measurements of visible light absorption by aerosols". *Aerosol Science and Technology*, *44*(8), 589–591. https://doi.org/10.1080/02786826.2010.482111

Ogren, J. A., Wendell, J., Andrews, E., & Sheridan, P. J. (2017). Continuous light absorption photometer for long-term studies. *Atmospheric Measurement Techniques*, *10*(12), 4805–4818. https://doi.org/10.5194/amt-10-4805-2017

Onasch, T. B., Trimborn, A., Fortner, E. C., Jayne, J. T., Kok, G. L., Williams, L. R., et al. (2012). Soot particle aerosol mass spectrometer: Development, validation, and initial application. *Aerosol Science and Technology*, *46*(7), 804–817. https://doi.org/10.1080/02786826.2012.663948

Pagonis, D., Campuzano-Jost, P., Guo, H., Day, D. A., Schueneman, M. K., Brown, W. L., et al. (2021). Airborne extractive electrospray mass spectrometry measurements of the chemical composition of organic aerosol. *Atmospheric Measurement Techniques*, *14*(2), 1545–1559. https://doi.org/10.5194/amt-14-1545-2021

Palm, B. B., Peng, Q., Fredrickson, C. D., Lee, B. H., Garofalo, L. A., Pothier, M. A., et al. (2020). Quantification of organic aerosol and brown carbon evolution in fresh wildfire plumes. *Proceedings of the National Academy of Sciences of the United States of America*, *117*(47), 29469–29477. https://doi.org/10.1073/pnas.2012218117

Palmer, P. I., Parrington, M., Lee, J. D., Lewis, A. C., Rickard, A. R., Bernath, P. F., et al. (2013). Quantifying the impact of BOReal forest fires on tropospheric oxidants over the Atlantic using aircraft and satellites (BORTAS) experiment: Design, execution and science overview. *Atmospheric Chemistry and Physics*, *13*(13), 6239–6261. https://doi.org/10.5194/acp-13-6239-2013

Pankow, J. F., Luo, W., Melnychenko, A. N., Barsanti, K. C., Isabelle, L. M., Chen, C., et al. (2012). Volatilizable biogenic organic compounds (VBOCs) with two dimensional gas chromatography-time of flight mass spectrometry (GC x GC-TOFMS): Sampling methods, VBOC complexity, and chromatographic retention data. *Atmospheric Measurement Techniques*, *5*(2), 345–361. https://doi.org/10.5194/amt-5-345-2012

Park, R. J., Jacob, D. J., & Logan, J. A. (2007). Fire and biofuel contributions to annual mean aerosol mass concentrations in the United States. *Atmospheric Environment*, *41*(35), 7389–7400. https://doi.org/10.1016/j.atmosenv.2007.05.061

Permar, W., Wang, Q., Selimovic, V., Wielgasz, C., Yokelson, R. J., Hornbrook, R. S., et al. (2021). Emissions of trace organic gases from western US Wildfires based on WE-CAN aircraft measurements. *Journal of Geophysical Research: Atmospheres*, *126*(11). https://doi.org/10.1029/2020jd033838

Peterson, D. A., Campbell, J. R., Hyer, E. J., Fromm, M. D., Kablick, G. P., Cossuth, J. H., & DeLand, M. T. (2018). Wildfire-driven thunderstorms cause a volcano-like stratospheric injection of smoke. *NPJ Climate and Atmospheric Science*, *1*, 30. https://doi.org/10.1038/s41612-018-0039-3

Peterson, D. A., Fromm, M. D., McRae, R. H. D., Campbell, J. R., Hyer, E. J., Taha, G., et al. (2021). Australia's Black Summer pyrocumulonimbus super outbreak reveals potential for increasingly extreme stratospheric smoke events. *NPJ Climate and Atmospheric Science*, *4*(1), 38. https://doi.org/10.1038/s41612-021-00192-9

Peterson, D. A., Fromm, M. D., Solbrig, J. E., Hyer, E. J., Surratt, M. L., & Campbell, J. R. (2017). Detection and inventory of intense pyroconvection in Western North America using GOES-15 daytime infrared data. *Journal of Applied Meteorology and Climatology*, *56*(2), 471–493. https://doi.org/10.1175/jamc-d-16-0226.1

Peterson, D. A., Hyer, E. J., Campbell, J. R., Fromm, M. D., Hair, J. W., Butler, C. F., & Fenn, M. A. (2015). THE 2013 RIM FIRE implications for predicting extreme fire spread, pyroconvection, and smoke emissions. *Bulletin of the American Meteorological Society*, *96*(2), 229–247. https://doi.org/10.1175/bams-d-14-00060.1

Peterson, D. A., Hyer, E. J., Campbell, J. R., Solbrig, J. E., & Fromm, M. D. (2017). A conceptual model for development of intense pyrocumulonimbus in Western North America. *Monthly Weather Review*, *145*(6), 2235–2255. https://doi.org/10.1175/mwr-d-16-0232.1

Peterson, D. A., Thapa, L. H., Saide, P. E., Soja, A. J., Gargulinski, E. M., Hyer, E. J., et al. (2022). Measurements from inside a thunderstorm driven by wildfire: The 2019 FIREX-AQ field experiment. *Bulletin of the American Meteorological Society*. https://doi.org/10.1175/bams-d-21-0049.1

Potter, C. (2020). Snowmelt timing impacts on growing season phenology in the northern range of Yellowstone National Park estimated from MODIS satellite data. *Landscape Ecology*, *35*(2), 373–388. https://doi.org/10.1007/s10980-019-00951-3

Pouliot, G., Rao, V., McCarty, J. L., & Soja, A. (2017). Development of the crop residue and rangeland burning in the 2014 National Emissions Inventory using information from multiple sources. *Journal of the Air & Waste Management Association*, *67*(5), 613–622. https://doi.org/10.1080/10962247.2016.1268982

Radeloff, V. C., Helmers, D. P., Kramer, H. A., Mockrin, M. H., Alexandre, P. M., Bar-Massada, A., et al. (2018). Rapid growth of the US wildland-urban interface raises wildfire risk. *Proceedings of the National Academy of Sciences*, *115*(13), 3314–3319. https://doi.org/10.1073/pnas.1718850115

Ramo, R., Roteta, E., Bistinas, I., van Wees, D., Bastarrika, A., Chuvieco, E., & van der Werf, G. R. (2021). African burned area and fire carbon emissions are strongly impacted by small fires undetected by coarse resolution satellite data. *Proceedings of the National Academy of Sciences of the United States of America*, *118*(9). https://doi.org/10.1073/pnas.2011160118

Rappold, A. G., Stone, S. L., Cascio, W. E., Neas, L. M., Kilaru, V. J., Carraway, M. S., et al. (2011). Peat bog wildfire smoke exposure in rural North Carolina is associated with cardiopulmonary emergency department visits assessed through syndromic surveillance. *Environmental Health Perspectives*, *119*(10), 1415–1420. https://doi.org/10.1289/ehp.1003206

Reid, C. E., Brauer, M., Johnston, F. H., Jerrett, M., Balmes, J. R., & Elliott, C. T. (2016). Critical review of health impacts of wildfire smoke exposure. *Environmental Health Perspectives*, *124*(9), 1334–1343. https://doi.org/10.1289/ehp.1409277

Ridley, B. A., Grahek, F. E., & Walega, J. G. (1992). A small, high-sensitivity, medium-response ozone detector suitable for measurements from light aircraft. *Journal of Atmospheric and Oceanic Technology*, *9*(2), 142–148. https://doi.org/10.1175/1520-0426(1992)009<0142:ashsmr>2.0.co;2

Roberts, G. C., & Nenes, A. (2005). A continuous-flow streamwise thermal-gradient CCN chamber for atmospheric measurements. *Aerosol Science and Technology*, *39*(3), 206–221. https://doi.org/10.1080/027868290913988

Roberts, J. M., Stockwell, C. E., Yokelson, R. J., de Gouw, J., Liu, Y., Selimovic, V., et al. (2020). The nitrogen budget of laboratory-simulated western US wildfires during the FIREX 2016 Fire Lab study. *Atmospheric Chemistry and Physics*, *20*(14), 8807–8826. https://doi.org/10.5194/acp-20-8807-2020

Robinson, M. A., Decker, Z. C. J., Barsanti, K. C., Coggon, M. M., Flocke, F. M., Franchin, A., et al. (2021). Variability and time of day dependence of ozone photochemistry in Western wildfire plumes. *Environmental Science & Technology*, *55*(15), 10280–10290. https://doi.org/10.1021/acs.est.1c01963

Rogers, H. M., Ditto, J. C., & Gentner, D. R. (2020). Evidence for impacts on surface-level air quality in the northeastern US from long-distance transport of smoke from North American fires during the Long Island Sound Tropospheric Ozone Study (LISTOS) 2018. *Atmospheric Chemistry and Physics*, *20*(2), 671–682. https://doi.org/10.5194/acp-20-671-2020

Rollins, A. W., Rickly, P. S., Gao, R. S., Ryerson, T. B., Brown, S. S., Peischl, J., & Bourgeois, I. (2020). Single-photon laser-induced fluorescence detection of nitric oxide at sub-parts-per-trillion mixing ratios. *Atmospheric Measurement Techniques*, *13*(5), 2425–2439. https://doi.org/10.5194/amt-13-2425-2020

Rollins, A. W., Thornberry, T. D., Ciciora, S. J., McLaughlin, R. J., Watts, L. A., Hanisco, T. F., et al. (2016). A laser-induced fluorescence instrument for aircraft measurements of sulfur dioxide in the upper troposphere and lower stratosphere. *Atmospheric Measurement Techniques*, *9*(9), 4601–4613. https://doi.org/10.5194/amt-9-4601-2016

Ryerson, T. B., Williams, E. J., & Fehsenfeld, F. C. (2000). An efficient photolysis system for fast-response NO2 measurements. *Journal of Geophysical Research*, *105*(D21), 26447–26461. https://doi.org/10.1029/2000jd900389

Sachse, G. W., Collins, J. E., Hill, G. F., Wade, L. O., Burney, L. G., & Ritter, J. A. (1991). Airborne tunable diode-laser sensor for high-precision concentartion and flux measurements of carbon-monoxide and methane. In *Conference on measurement of atmospheric gases*.

Sahu, L. K., Kondo, Y., Moteki, N., Takegawa, N., Zhao, Y., Cubison, M. J., et al. (2012). Emission characteristics of black carbon in anthropogenic and biomass burning plumes over California during ARCTAS-CARB 2008. *Journal of Geophysical Research*, *117*(D16). https://doi.org/10.1029/2011jd017401

Saide, P. E., Peterson, D. A., da Silva, A., Anderson, B., Ziemba, L. D., Diskin, G., et al. (2015). Revealing important nocturnal and day-to-day variations in fire smoke emissions through a multiplatform inversion. *Geophysical Research Letters*, *42*(9), 3609–3618. https://doi.org/10.1002/2015gl063737

Saide, P. E., Thapa, L. H., Ye, X., Pagonis, D., Campuzano-Jost, P., Guo, H., et al. (2022). Understanding the evolution of smoke mass extinction efficiency using field campaign measurements. *Geophysical Research Letters*, *49*(18), e2022GL099175. https://doi.org/10.1029/2022GL099175

Scheuer, E., Dibb, J. E., Twohy, C., Rogers, D. C., Heymsfield, A. J., & Bansemer, A. (2010). Evidence of nitric acid uptake in warm cirrus anvil clouds during the NASA TC4 campaign. *Journal of Geophysical Research*, *115*, D00J03. https://doi.org/10.1029/2009jd012716

Schill, G. P., Froyd, K. D., Bian, H., Kupc, A., Williamson, C., Brock, C. A., et al. (2020). Widespread biomass burning smoke throughout the remote troposphere. *Nature Geoscience*, *13*(6), 422–427. https://doi.org/10.1038/s41561-020-0586-1

Schoennagel, T., Balch, J. K., Brenkert-Smith, H., Dennison, P. E., Harvey, B. J., Krawchuk, M. A., et al. (2017). Adapt to more wildfire in western North American forests as climate changes. *Proceedings of the National Academy of Sciences of the United States of America*, *114*(18), 4582–4590. https://doi.org/10.1073/pnas.1617464114

Schroeder, P., Brewer, W. A., Choukulkar, A., Weickmann, A., Zucker, M., Holloway, M. W., & Sandberg, S. (2020). A compact, flexible, and robust micropulsed Doppler lidar. *Journal of Atmospheric and Oceanic Technology*, *37*(8), 1387–1402. https://doi.org/10.1175/jtech-d-19-0142.1

Schwarz, J. P., Gao, R. S., Spackman, J. R., Watts, L. A., Thomson, D. S., Fahey, D. W., et al. (2008). Measurement of the mixing state, mass, and optical size of individual black carbon particles in urban and biomass burning emissions. *Geophysical Research Letters*, *35*(13), L13810. https://doi.org/10.1029/2008gl033968

Sedlacek, A. J., III., Buseck, P. R., Adachi, K., Onasch, T. B., Springston, S. R., & Kleinman, L. (2018). Formation and evolution of tar balls from northwestern US wildfires. *Atmospheric Chemistry and Physics*, *18*(15), 11289–11301. https://doi.org/10.5194/acp-18-11289-2018

Sekimoto, K., Koss, A. R., Gilman, J. B., Selimovic, V., Coggon, M. M., Zarzana, K. J., et al. (2018). High- and low-temperature pyrolysis profiles describe volatile organic compound emissions from western US wildfire fuels. *Atmospheric Chemistry and Physics*, *18*(13), 9263–9281. https://doi.org/10.5194/acp-18-9263-2018

Selimovic, V., Yokelson, R. J., McMeeking, G. R., & Coefield, S. (2019). In situ measurements of trace gases, PM, and aerosol optical properties during the 2017 NW US wildfire smoke event. *Atmospheric Chemistry and Physics*, *19*(6), 3905–3926. https://doi.org/10.5194/acp-19-3905-2019

Selimovic, V., Yokelson, R. J., McMeeking, G. R., & Coefield, S. (2020). Aerosol mass and optical properties, smoke influence on O3, and High NO3 production rates in a Western U.S. City impacted by wildfires. *Journal of Geophysical Research: Atmospheres*, *125*(16), e2020JD032791. https://doi.org/10.1029/2020JD032791

Selimovic, V., Yokelson, R. J., Warneke, C., Roberts, J. M., de Gouw, J., Reardon, J., & Griffith, D. W. T. (2018). Aerosol optical properties and trace gas emissions by PAX and OP-FTIR for laboratory-simulated western US wildfires during FIREX. *Atmospheric Chemistry and Physics*, *18*(4), 2929–2948. https://doi.org/10.5194/acp-18-2929-2018

Simpson, I. J., Blake, D. R., Blake, N. J., Meinardi, S., Barletta, B., Hughes, S. C., et al. (2020). Characterization, sources and reactivity of volatile organic compounds (VOCs) in Seoul and surrounding regions during KORUS-AQ. *Elementa-Science of the Anthropocene*, *8*. https://doi.org/10.1525/elementa.434

Sinclair, D., & Hoopes, G. S. (1975). A continuous flow condensation nucleus counter. *Journal of Aerosol Science*, *6*(1), 1–7. https://doi.org/10.1016/0021-8502(75)90036-1

Singh, H. B., Cai, C., Kaduwela, A., Weinheimer, A., & Wisthaler, A. (2012). Interactions of fire emissions and urban pollution over California: Ozone formation and air quality simulations. *Atmospheric Environment*, *56*, 45–51. https://doi.org/10.1016/j.atmosenv.2012.03.046

Sinyuk, A., Holben, B. N., Eck, T. F., Giles, D. M., Slutsker, I., Korkin, S., et al. (2020). The AERONET Version 3 aerosol retrieval algorithm, associated uncertainties and comparisons to Version 2. *Atmospheric Measurement Techniques*, *13*(6), 3375–3411. https://doi.org/10.5194/amt-13-3375-2020

Smirnov, A., Holben, B. N., Slutsker, I., Giles, D. M., McClain, C. R., Eck, T. F., et al. (2009). Maritime aerosol network as a component of aerosol robotic network. *Journal of Geophysical Research*, *114*(D6), D06204. https://doi.org/10.1029/2008jd011257

Soja, A. J., Cofer, W. R., Shugart, H. H., Sukhinin, A. I., Stackhouse, P. W., McRae, D. J., & Conard, S. G. (2004). Estimating fire emissions and disparities in boreal Siberia (1998-2002). *Journal of Geophysical Research*, *109*(D14), D14S06. https://doi.org/10.1029/2004jd004570

Soja, A. J., Al-Saadi, J. A., Giglio, L., Randall, D., Kittaka, C., Pouliot, G. A., et al. (2009). Assessing satellite-based fire data for use in the National Emissions Inventory. *Journal of Applied Remote Sensing*, *3*(1), 031504. https://doi.org/10.1117/1.3148859

Stein, A. F., Draxler, R. R., Rolph, G. D., Stunder, B. J. B., Cohen, M. D., & Ngan, F. (2015). NOAA'S HYSPLIT atmospheric transport and dispersion modeling system. *Bulletin of the American Meteorological Society*, *96*(12), 2059–2077. https://doi.org/10.1175/bams-d-14-00110.1

Stephens, S. L., McIver, J. D., Boerner, R. E. J., Fettig, C. J., Fontaine, J. B., Hartsough, B. R., et al. (2012). The effects of forest fuel-reduction treatments in the United States. *BioScience*, *62*(6), 549–560. https://doi.org/10.1525/bio.2012.62.6.6

Stockwell, C. E., Bela, M. M., Coggon, M. M., Gkatzelis, G. I., Wiggins, E., Gargulinski, E. M., et al. (2022). Airborne emission rate measurements validate remote sensing observations and emission inventories of Western U.S. Wildfires. *Environmental Science & Technology*, *56*(12), 7564–7577. https://doi.org/10.1021/acs.est.1c07121

Stockwell, C. E., Veres, P. R., Williams, J., & Yokelson, R. J. (2015). Characterization of biomass burning emissions from cooking fires, peat, crop residue, and other fuels with high-resolution proton-transfer-reaction time-of-flight mass spectrometry. *Atmospheric Chemistry and Physics*, *15*(2), 845–865. https://doi.org/10.5194/acp-15-845-2015

Stockwell, C. E., Yokelson, R. J., Kreidenweis, S. M., Robinson, A. L., DeMott, P. J., Sullivan, R. C., et al. (2014). Trace gas emissions from combustion of peat, crop residue, domestic biofuels, grasses, and other fuels: Configuration and Fourier transform infrared (FTIR) component of the fourth fire lab at Missoula experiment (FLAME-4). *Atmospheric Chemistry and Physics*, *14*(18), 9727–9754. https://doi.org/10.5194/acp-14-9727-2014

Sumlin, B., Fortner, E., Lambe, A., Shetty, N. J., Daube, C., Liu, P., et al. (2021). Diel cycle impacts on the chemical and light absorption properties of organic carbon aerosol from wildfires in the western United States. *Atmospheric Chemistry and Physics*, *21*(15), 11843–11856. https://doi.org/10.5194/acp-21-11843-2021

Swap, R. J., Annegarn, H. J., Suttles, J. T., Haywood, J., Helmlinger, M. C., Hely, C., et al. (2002). The southern African regional science initiative (SAFARI 2000): Overview of the dry season field campaign. *South African Journal of Science*, *98*(3–4), 125–130.

Tang, W., Emmons, L. K., Buchholz, R. R., Wiedinmyer, C., Schwantes, R. H., He, C., et al. (2022). Effects of fire diurnal variation and plume rise on U.S. Air quality during FIREX-AQ and WE-CAN Based on the multi-scale infrastructure for chemistry and aerosols (MUSICAv0). *Journal of Geophysical Research: Atmospheres*, *127*(16), e2022JD036650. https://doi.org/10.1029/2022JD036650

Taylor, J., Best, F., Ciganovich, N., Dutcher, S., Ellington, S., Garcia, R., et al. (2005). Performance of an infrared sounder on several airborne platforms: The scanning high resolution interferometer sounder (S-HIS). *Proceedings of SPIE - The International Society for Optical Engineering*, *5882*(1), 588214–588212. https://doi.org/10.1117/12.618081

Thapa, L. H., Ye, X., Hair, J. W., Fenn, M. A., Shingler, T., Kondragunta, S., et al. (2022). Heat flux assumptions contribute to overestimation of wildfire smoke injection into the free troposphere. *Communications Earth & Environment*, *3*(1), 236. https://doi.org/10.1038/s43247-022-00563-x

Thelen, B., French, N. H. F., Koziol, B. W., Billmire, M., Owen, R. C., Johnson, J., et al. (2013). Modeling acute respiratory illness during the 2007 San Diego wildland fires using a coupled emissions-transport system and generalized additive modeling. *Environmental Health*, *12*(1), 94. https://doi.org/10.1186/1476-069X-12-94

Tomsche, L., Piel, F., Mikoviny, T., Nielsen, C. J., Guo, H., Campuzano-Jost, P., et al. (2022). Measurement report: Emission factors of NH3 and NHx for wildfires and agricultural fires in the United States. *EGUsphere*, *2022*, 1–16. https://doi.org/10.5194/egusphere-2022-879

Toon, O. B., Maring, H., Dibb, J., Ferrare, R., Jacob, D. J., Jensen, E. J., et al. (2016). Planning, implementation, and scientific goals of the studies of emissions and atmospheric composition, clouds and climate coupling by regional Surveys (SEAC(4)RS) field mission. *Journal of Geophysical Research: Atmospheres*, *121*(9), 4967–5009. https://doi.org/10.1002/2015jd024297

University of Maryland. (2020). VIIRS/NPP active fires 6-min L2 swath 375m NRT. In NASA (Ed.). https://doi.org/10.5067/VIIRS/VNP14IMG_NRT.002

van Harten, G., Diner, D. J., Daugherty, B. J. S., Rheingans, B. E., Bull, M. A., Seidel, F. C., et al. (2018). Calibration and validation of airborne multiangle spectropolarimetric imager (AirMSPI) polarization measurements. *Applied Optics*, *57*(16), 4499–4513. https://doi.org/10.1364/ao.57.004499

Veres, P. R., Neuman, J. A., Bertram, T. H., Assaf, E., Wolfe, G. M., Williamson, C. J., et al. (2020). Global airborne sampling reveals a previously unobserved dimethyl sulfide oxidation mechanism in the marine atmosphere. *Proceedings of the National Academy of Sciences of the United States of America*, *117*(9), 4505–4510. https://doi.org/10.1073/pnas.1919344117

Wang, S. Y., Coggon, M. M., Gkatzelis, G. I., Warneke, C., Bourgeois, I., Ryerson, T., et al. (2021). Chemical Tomography in a fresh wildland fire plume: A large eddy simulation (LES) study. *Journal of Geophysical Research: Atmospheres*, *126*(18). https://doi.org/10.1029/2021jd035203

Ward, D. E., Susott, R. A., Kauffman, J. B., Babbitt, R. E., Cummings, D. L., Dias, B., et al. (1992). Smoke and fire characteristics for cerado and deforestation burns in Brazil - BASE-B experiment. *Journal of Geophysical Research*, *97*(D13), 14601–14619. https://doi.org/10.1029/92jd01218

Warneke, C., Bahreini, R., Brioude, J., Brock, C. A., de Gouw, J. A., Fahey, D. W., et al. (2009). Biomass burning in Siberia and Kazakhstan as an important source for haze over the Alaskan arctic in April 2008. *Geophysical Research Letters*, *36*(2), L02813. https://doi.org/10.1029/2008gl036194

Warneke, C., de Gouw, J. A., Stohl, A., Cooper, O. R., Goldan, P. D., Kuster, W. C., et al. (2006). Biomass burning and anthropogenic sources of CO over New England in the summer 2004. *Journal of Geophysical Research*, *111*(D23), D23S15. https://doi.org/10.1029/2005JD006878

Warneke, C., Froyd, K. D., Brioude, J., Bahreini, R., Brock, C. A., Cozic, J., et al. (2010). An important contribution to springtime Arctic aerosol from biomass burning in Russia. *Geophysical Research Letters*, *37*(1), L01801. https://doi.org/10.1029/2009gl041816

Washenfelder, R. A., Attwood, A. R., Brock, C. A., Guo, H., Xu, L., Weber, R. J., et al. (2015). Biomass burning dominates brown carbon absorption in the rural southeastern United States. *Geophysical Research Letters*, *42*(2), 653–664. https://doi.org/10.1002/2014gl062444

Washenfelder, R. A., Azzarello, L., Ball, K., Brown, S. S., Decker, Z. C. J., Franchin, A., et al. (2022). Complexity in the evolution, composition, and spectroscopy of brown carbon in aircraft measurements of wildfire plumes. *Geophysical Research Letters*, *49*(9), e2022GL098951. https://doi.org/10.1029/2022GL098951

Weibring, P., Richter, D., Walega, J. G., & Fried, A. (2007). First demonstration of a high performance difference frequency spectrometer on airborne. *Optics Express*, *15*(21), 13476–13495. https://doi.org/10.1364/oe.15.013476

Welton, E. J., Campbell, J. R., Spinhirne, J. D., & Scott, V. S. (2000). Global monitoring of clouds and aerosols using a network of micro-pulse lidar systems. In *Conference on lidar remote sensing for industry and environment monitoring*.

Wentworth, G. R., Aklilu, Y.-A., Landis, M. S., & Hsu, Y.-M. (2018). Impacts of a large boreal wildfire on ground level atmospheric concentrations of PAHs, VOCs and ozone. *Atmos. Environ.*, *178*, 19–30. https://doi.org/10.1016/j.atmosenv.2018.01.013

Westerling, A. L. (2016). Increasing western US forest wildfire activity: Sensitivity to changes in the timing of spring. *Philosophical Transactions of the Royal Society B: Biological Sciences*, *371*(1696), 20150178. https://doi.org/10.1098/rstb.2015.0178

Westerling, A. L., Hidalgo, H. G., Cayan, D. R., & Swetnam, T. W. (2006). Warming and earlier spring increase western US forest wildfire activity. *Science*, *313*(5789), 940–943. https://doi.org/10.1126/science.1128834

Westphal, D. L., & Toon, O. B. (1991). Simulations of microphysical, radiative and dynamic processes in a continental-scale forest-fire smoke plume. *Journal of Geophysical Research*, *96*(D12), 22379–22400. https://doi.org/10.1029/91jd01956

Wiggins, E. B., Anderson, B. E., Brown, M. D., Campuzano-Jost, P., Chen, G., Crawford, J., et al. (2021). Reconciling assumptions in bottom-up and top-down approaches for estimating aerosol emission rates from wildland fires using observations from FIREX-AQ. *Journal of Geophysical Research: Atmospheres*, *126*(24). https://doi.org/10.1029/2021jd035692

Wiggins, E. B., Soja, A. J., Gargulinski, E., Halliday, H. S., Pierce, R. B., Schmidt, C. C., et al. (2020). High temporal resolution satellite observations of fire radiative power reveal link between fire behavior and aerosol and gas emissions. *Geophysical Research Letters*, *47*(23). https://doi.org/10.1029/2020gl090707

Xu, L., Crounse, J. D., Vasquez, K. T., Allen, H., Wennberg, P. O., Bourgeois, I., et al. (2021). Ozone chemistry in western US wildfire plumes. *Science Advances*, *7*(50). https://doi.org/10.1126/sciadv.abl3648

Yacovitch, T. I., Herndon, S. C., Roscioli, J. R., Floerchinger, C., McGovern, R. M., Agnese, M., et al. (2014). Demonstration of an ethane spectrometer for methane source identification. *Environmental Science & Technology*, *48*(14), 8028–8034. https://doi.org/10.1021/es501475q

Yates, E. L., Iraci, L., Singh, H., Tanaka, T., Roby, M., Hamill, P., et al. (2016). Airborne measurements and emission estimates of greenhouse gases and other trace constituents from the 2013 California Yosemite Rim wildfire. *Atmos. Environ.*, *127*, 293–302. https://doi.org/10.1016/j.atmosenv.2015.12.038

Ye, X., Arab, P., Ahmadov, R., James, E., Grell, G. A., Pierce, B., et al. (2021). Evaluation and intercomparison of wildfire smoke forecasts from multiple modeling systems for the 2019 Williams Flats fire. *Atmos. Chem. Phys.*, *21*(18), 14427–14469. https://doi.org/10.5194/acp-21-14427-2021

Ye, X., Saide, P. E., Hair, J., Fenn, M., Shingler, T., Soja, A., et al. (2022). Assessing vertical allocation of wildfire smoke emissions using observational constraints from airborne lidar in the Western U.S. *Journal of Geophysical Research: Atmospheres*, *127*(21), e2022JD036808. https://doi.org/10.1029/2022JD036808

Yokelson, R. J., Burling, I. R., Gilman, J. B., Warneke, C., Stockwell, C. E., de Gouw, J., et al. (2013). Coupling field and laboratory measurements to estimate the emission factors of identified and unidentified trace gases for prescribed fires. *Atmos. Chem. Phys.*, *13*(1), 89–116. https://doi.org/10.5194/acp-13-89-2013

Yokelson, R. J., Burling, I. R., Urbanski, S. P., Atlas, E. L., Adachi, K., Buseck, P. R., et al. (2011). Trace gas and particle emissions from open biomass burning in Mexico. *Atmos. Chem. Phys.*, *11*(14), 6787–6808. https://doi.org/10.5194/acp-11-6787-2011

Yokelson, R. J., Crounse, J. D., DeCarlo, P. F., Karl, T., Urbanski, S., Atlas, E., et al. (2009). Emissions from biomass burning in the Yucatan. *Atmos. Chem. Phys.*, *9*(15), 5785–5812. https://doi.org/10.5194/acp-9-5785-2009

Yokelson, R. J., Goode, J. G., Ward, D. E., Susott, R. A., Babbitt, R. E., Wade, D. D., et al. (1999). Emissions of formaldehyde, acetic acid, methanol, and other trace gases from biomass fires in North Carolina measured by airborne Fourier transform infrared spectroscopy. *Journal of Geophysical Research*, *104*(D23), 30109–30125. https://doi.org/10.1029/1999jd900817

Yu, P. F., Toon, O. B., Bardeen, C. G., Bucholtz, A., Rosenlof, K. H., Saide, P. E., et al. (2016). Surface dimming by the 2013 Rim Fire simulated by a sectional aerosol model. *Journal of Geophysical Research: Atmospheres*, *121*(12), 7079–7087. https://doi.org/10.1002/2015jd024702

Yuan, B., Koss, A. R., Warneke, C., Coggon, M., Sekimoto, K., & de Gouw, J. A. (2017). Proton-transfer-reaction mass spectrometry: Applications in atmospheric sciences. *Chemical Reviews*, *117*(21), 13187–13229. https://doi.org/10.1021/acs.chemrev.7b00325

Zarzana, K. J., Min, K. E., Washenfelder, R. A., Kaiser, J., Krawiec-Thayer, M., Peischl, J., et al. (2017). Emissions of glyoxal and other carbonyl compounds from agricultural biomass burning plumes sampled by aircraft. *Environ. Sci. Technol.*, *51*(20), 11761–11770. https://doi.org/10.1021/acs.est.7b03517

Zeng, L., Dibb, J., Scheuer, E., Katich, J. M., Schwarz, J. P., Bourgeois, I., et al. (2022). Characteristics and evolution of brown carbon in western United States wildfires. *Atmos. Chem. Phys.*, *22*(12), 8009–8036. https://doi.org/10.5194/acp-22-8009-2022

Zeng, L., Sullivan, A. P., Washenfelder, R. A., Dibb, J., Scheuer, E., Campos, T. L., et al. (2021). Assessment of online water-soluble brown carbon measuring systems for aircraft sampling. *Atmos. Meas. Tech.*, *14*(10), 6357–6378. https://doi.org/10.5194/amt-14-6357-2021

Zhang, Y. J., Tang, L. L., Wang, Z., Yu, H. X., Sun, Y. L., Liu, D., et al. (2015). Insights into characteristics, sources, and evolution of submicron aerosols during harvest seasons in the Yangtze River delta region, China. *Atmos. Chem. Phys.*, *15*(3), 1331–1349. https://doi.org/10.5194/acp-15-1331-2015

Zheng, W., Flocke, F. M., Tyndall, G. S., Swanson, A., Orlando, J. J., Roberts, J. M., et al. (2011). Characterization of a thermal decomposition chemical ionization mass spectrometer for the measurement of peroxy acyl nitrates (PANs) in the atmosphere. *Atmos. Chem. Phys.*, *11*(13), 6529–6547. https://doi.org/10.5194/acp-11-6529-2011

Zhou, D. K., Smith, W. L., Li, J., Howell, H. B., Cantwell, G. W., Larar, A. M., et al. (2002). Thermodynamic product retrieval methodology and validation for NAST-1. *Applied Optics*, *41*(33), 6957–6967. https://doi.org/10.1364/ao.41.006957

Zhou, D. K., Smith, W. L., Liu, X., Larar, A. M., Huang, H. L. A., Li, J., et al. (2005). Thermodynamic and cloud parameter retrieval using infrared spectral data. *Geophysical Research Letters*, *32*(15), L15805. https://doi.org/10.1029/2005gl023211

Zhou, S., Collier, S., Jaffe, D. A., Briggs, N. L., Hee, J., Sedlacek, A. J., et al. (2017). Regional influence of wildfires on aerosol chemistry in the western US and insights into atmospheric aging of biomass burning organic aerosol. *Atmos. Chem. Phys.*, *17*(3), 2477–2493. https://doi.org/10.5194/acp-17-2477-2017

Zhu, J., Crozier, P. A., Ercius, P., & Anderson, J. R. (2014). Derivation of optical properties of carbonaceous aerosols by monochromated electron energy-loss spectroscopy. *Microscopy and Microanalysis*, *20*(3), 748–759. https://doi.org/10.1017/S143192761400049X

References From the Supporting Information

Akherati, A., He, Y., Coggon, M. M., Koss, A. R., Hodshire, A. L., Sekimoto, K., et al. (2020). Oxygenated aromatic compounds are important precursors of secondary organic aerosol in biomass-burning emissions. *Environ. Sci. Technol.*, *54*(14), 8568–8579. https://doi.org/10.1021/acs.est.0c01345

Baylon, P., Jaffe, D. A., Hall, S. R., Ullmann, K., Alvarado, M. J., & Lefer, B. L. (2018). Impact of biomass burning plumes on photolysis rates and ozone formation at the mount bachelor observatory. *Journal of Geophysical Research: Atmospheres*, *123*(4), 2272–2284. https://doi.org/10.1002/2017jd027341

Baylon, P., Jaffe, D. A., Wigder, N. L., Gao, H., & Hee, J. (2015). Ozone enhancement in western US wildfire plumes at the Mt. Bachelor Observatory: The role of NOx. *Atmos. Environ*, *109*, 297–304. https://doi.org/10.1016/j.atmosenv.2014.09.013

Briggs, N. L., Jaffe, D. A., Gao, H., Hee, J. R., Baylon, P. M., Zhang, Q., et al. (2016). Particulate matter, ozone, and nitrogen species in aged wildfire plumes observed at the mount bachelor observatory. *Aerosol and Air Quality Research*, *16*(12), 3075–3087. https://doi.org/10.4209/aaqr.2016.03.0120

Cappa, C. D., Lim, C. Y., Hagan, D. H., Coggon, M., Koss, A., Sekimoto, K., et al. (2020). Biomass-burning-derived particles from a wide variety of fuels - Part 2: Effects of photochemical aging on particle optical and chemical properties. *Atmos. Chem. Phys.*, *20*(14), 8511–8532. https://doi.org/10.5194/acp-20-8511-2020

Chai, J. J., Miller, D. J., Scheuer, E., Dibb, J., Selimovic, V., Yokelson, R., et al. (2019). Isotopic characterization of nitrogen oxides (NOx), nitrous acid (HONO), and nitrate (pNO(3)(-)) from laboratory biomass burning during FIREX. *Atmospheric Measurement Techniques*, *12*(12), 6303–6317. https://doi.org/10.5194/amt-12-6303-2019

Chandra, B. P., McClure, C. D., Mulligan, J., & Jaffe, D. A. (2020). Optimization of a method for the detection of biomass-burning relevant VOCs in Urban areas using thermal desorption gas chromatography mass spectrometry. *Atmosphere*, *11*(3), 276. https://doi.org/10.3390/atmos11030276

Collier, S., Zhou, S., Onasch, T. B., Jaffe, D. A., Kleinman, L., Sedlacek, A. J., et al. (2016). Regional influence of aerosol emissions from wildfires driven by combustion efficiency: Insights from the BBOP campaign. *Environ. Sci. Technol.*, *50*(16), 8613–8622. https://doi.org/10.1021/acs.est.6b01617

Decker, Z. C. J., Zarzana, K. J., Coggon, M., Min, K. E., Pollack, I., Ryerson, T. B., et al. (2019). Nighttime chemical transformation in biomass burning plumes: A box model analysis initialized with aircraft observations. *Environ. Sci. Technol.*, *53*(5), 2529–2538. https://doi.org/10.1021/acs.est.8b05359

de Gouw, J. A., & Warneke, C. (2007). Measurements of volatile organic compounds in the Earths atmosphere using proton-transfer-reaction mass spectrometry. *Mass Spectrometry Reviews*, *26*(2), 223–257. https://doi.org/10.1002/mas.20119

Hatch, L. E., Jen, C. N., Kreisberg, N. M., Selimovic, V., Yokelson, R. J., Stamatis, C., et al. (2019). Highly speciated measurements of terpenoids emitted from laboratory and mixed-conifer forest prescribed fires. *Environ. Sci. Technol.*, *53*(16), 9418–9428. https://doi.org/10.1021/acs.est.9b02612

Hatch, L. E., Rivas-Ubach, A., Jen, C. N., Lipton, M., Goldstein, A. H., & Barsanti, K. C. (2018). Measurements of I/SVOCs in biomass-burning smoke using solid-phase extraction disks and two-dimensional gas chromatography. *Atmos. Chem. Phys.*, *18*(24), 17801–17817. https://doi.org/10.5194/acp-18-17801-2018

Jen, C. N., Liang, Y., Hatch, L. E., Kreisberg, N. M., Stamatis, C., Kristensen, K., et al. (2018). High hydroquinone emissions from burning manzanita. *Environmental Science & Technology Letters*, *5*(6), 309–314. https://doi.org/10.1021/acs.estlett.8b00222

Laskin, A., Lin, P., Laskin, J., Fleming, L. T., & Nizkorodov, S. (2018). Molecular characterization of atmospheric brown carbon. In S. W. Hunt, A. Laskin, & S. A. Nizkorodov (Eds.), *Multiphase environmental chemistry in the atmosphere* (pp. 261–274).

Li, H., Lamb, K. D., Schwarz, J. P., Selimovic, V., Yokelson, R. J., McMeeking, G. R., & May, A. A. (2019). Inter-comparison of black carbon measurement methods for simulated open biomass burning emissions. *Atmos. Environ.*, *206*, 156–169. https://doi.org/10.1016/j.atmosenv.2019.03.010

Lim, C. Y., Hagan, D. H., Coggon, M. M., Koss, A. R., Sekimoto, K., de Gouw, J., et al. (2019). Secondary organic aerosol formation from the laboratory oxidation of biomass burning emissions. *Atmos. Chem. Phys.*, *19*(19), 12797–12809. https://doi.org/10.5194/acp-19-12797-2019

Lin, P., Fleming, L. T., Nizkorodov, S. A., Laskin, J., & Laskin, A. (2018). Comprehensive molecular characterization of atmospheric Brown carbon by high resolution mass spectrometry with electrospray and atmospheric pressure photoionization. *Anal. Chem.*, *90*(21), 12493–12502. https://doi.org/10.1021/acs.analchem.8b02177

Lyman, S. N., Gratz, L. E., Dunham-Cheatham, S. M., Gustin, M. S., & Luippold, A. (2020). Improvements to the accuracy of atmospheric oxidized mercury measurements. *Environmental Science & Technology*, *54*(21), 13379–13388. https://doi.org/10.1021/acs.est.0c02747

McClure, C. D., & Jaffe, D. A. (2018). Investigation of high ozone events due to wildfire smoke in an urban area. *Atmos. Environ.*, *194*, 146–157. https://doi.org/10.1016/j.atmosenv.2018.09.021

McClure, C. D., Lim, C. Y., Hagan, D., Kroll, J. H., & Cappa, C. D. (2020). Biomass-burning-derived particles from a wide variety of fuels - Part 1: Properties of primary particles. *Atmos. Chem. Phys.*, *20*(3), 1531–1547. https://doi.org/10.5194/acp-20-1531-2020

Ren, X., Luke, W. T., Kelley, P., Cohen, M. D., Olson, M. L., Walker, J., et al. (2020). Long-term observations of atmospheric speciated mercury at a coastal site in the Northern Gulf of Mexico during 2007-2018. *Atmosphere*, *11*(3), 268. https://doi.org/10.3390/atmos11030268

Santin, C., Doerr, S. H., Jones, M. W., Merino, A., Warneke, C., & Roberts, J. M. (2020). The Relevance of pyrogenic carbon for carbon budgets from fires: Insights from the FIREX experiment. *Global Biogeochemical Cycles*, *34*(9). https://doi.org/10.1029/2020gb006647

Stockwell, C. E., Kupc, A., Witkowski, B., Talukdar, R. K., Liu, Y., Selimovic, V., et al. (2018). Characterization of a catalyst-based conversion technique to measure total particulate nitrogen and organic carbon and comparison to a particle mass measurement instrument. *Atmospheric Measurement Techniques*, *11*(5), 2749–2768. https://doi.org/10.5194/amt-11-2749-2018

Tomaz, S., Cui, T. Q., Chen, Y. Z., Sexton, K. G., Roberts, J. M., Warneke, C., et al. (2018). Photochemical cloud processing of primary wildfire emissions as a potential source of secondary organic aerosol. *Environ. Sci. Technol.*, *52*(19), 11027–11037. https://doi.org/10.1021/acs.est.8b03293

Womack, C. C., Manfred, K. M., Wagner, N. L., Adler, G., Franchin, A., Lamb, K. D., et al. (2021). Complex refractive indices in the ultraviolet and visible spectral region for highly absorbing non-spherical biomass burning aerosol. *Atmos. Chem. Phys.*, *21*(9), 7235–7252. https://doi.org/10.5194/acp-21-7235-2021

Zarzana, K. J., Selimovic, V., Koss, A. R., Sekimoto, K., Coggon, M. M., Yuan, B., et al. (2018). Primary emissions of glyoxal and methylglyoxal from laboratory measurements of open biomass burning. *Atmos. Chem. Phys.*, *18*(20), 15451–15470. https://doi.org/10.5194/acp-18-15451-2018

Zhang, Q., Zhou, S., Collier, S., Jaffe, D., Onasch, T., Shilling, J., et al. (2018). Understanding composition, formation, and aging of organic aerosols in wildfire emissions via combined mountain top and airborne measurements. In S. W. Hunt, A. Laskin, & S. A. Nizkorodov (Eds.), *Multiphase environmental chemistry in the atmosphere* (pp. 363–385).

Zhou, S., Collier, S., Jaffe, D. A., Briggs, N. L., Hee, J., Sedlacek, A. J., III, et al. (2017). Regional influence of wildfires on aerosol chemistry in the western US and insights into atmospheric aging of biomass burning organic aerosol. *Atmos. Chem. Phys.*, *17*(3), 2477–2493. https://doi.org/10.5194/acp-17-2477-2017